NOTE TO USERS

ION CHANNELS IN GLOSSOPHARYNGEAL NEURONS

ELECTROPHYSIOLOGICAL PROPERTIES, PO_2- AND ATP-SENSITIVITY OF PARAGANGLION NEURONS OF THE RAT GLOSSOPHARYNGEAL NERVE

By

VERONICA A. CAMPANUCCI

A Thesis

Submitted to the school of Graduate Studies

In Partial Fulfilment of the Requirements for the Degree

DOCTOR OF PHILOSOPHY

McMaster University

DOCTOR OF PHILOSOPHY (2004) McMASTER UNIVERSITY

(Department of Biology) Hamilton, Ontario

TITLE: Electrophysiological properties, PO_2- and ATP-sensitivity of paraganglion neurons of the rat glossopharyngeal nerve.

AUTHOR: Verónica A. Campanucci, *Licenciada* in Biology (University of Buenos Aires, Argentina)

SUPERVISOR: Professor Colin A. Nurse

NUMBER OF PAGES: xxi, 240

ABSTRACT

Paraganglion neurons within the rat glossopharyngeal nerve (GPN) are part of a nitric oxide synthase (nNOS)-synthesizing plexus of nerve fibers that innervate a chemosensory organ, the carotid body (CB). This thesis focused on the anatomical, biophysical, pharmacological, and immunocytochemical characterization of these GPN neurons with a view towards understanding their role in efferent CB inhibition. GPN neurons were grouped in two distinct populations, a proximal one near the bifurcation with the carotid sinus nerve, and a more distal one concentrated further along the GPN. Both neuronal populations shared similar passive membrane properties and expressed voltage-dependent Na^+, K^+, and a broad spectrum of Ca^{2+} channels which included L-, N-, P/Q-, R- and T- types. In addition, they expressed a novel O_2-sensitive K^+ conductance, mediated via voltage-independent background or 'leak' K^+ channels. Hypoxia depolarized and/or increased excitability in GPN neurons via inhibition of these 'leak' K^+ channels, whose pharmacology suggested involvement of the tandem pore domain, halothane inhibited K^+ (THIK) channel family. Indeed, when THIK-1 channels were heterologously expressed in HEK 293 cells, the resulting K^+ currents were found to be reversibly inhibited by hypoxia. GPN neurons were also sensitive to several neurotransmitters including acetylcholine, dopamine, serotonin and importantly, ATP, acting via multiple ionotropic P2X receptors. Pharmacological and confocal immunofluorescence studies suggested that these P2X receptors consisted of at least

heteromeric P2X2-P2X3, homomeric P2X4 and homomeric P2X7 receptors. In co-cultures of GPN neurons and CB chemoreceptor (type I) cell clusters, activation of P2X receptors on adjacent GPN neurons caused NO-dependent hyperpolarization of type I cells. Taken together these findings suggest key roles for hypoxia and ATP in the activation of GPN neurons, leading to Ca^{2+} entry, NOS activation, and NO-mediated inhibition of carotid body function.

Acknowledgements

Firstly, I would like to thank my supervisor, Dr. Colin Nurse, for his excellent guidance and encouragement and for giving me the opportunity of working on a fascinating project. I would also like to thank him for his 'contagious' passion for science and research, which I hope will accompany me throughout my whole research career. I always will be grateful for his understanding, that allowed my much-needed re-energizing escapades to Argentina. I am thankful for having learned, worked and shared these years with Cathy Vollmer, who offers to everybody in the lab, a balanced mix of motherhood/friendship that even from the very beginning made me feel 'at home' so far away from home. Also, without her excellent technical assistance the daily, smooth functioning of the lab would not be possible. Her friendship, yearly newsletter and tiramisu will be deeply missed. My gratitude goes out to the past and present lab members, Roger Thompson, Suzie Farragher, Mike Jonz, Ian Fearon, Jing Jing Liu, Joe Buttigieg, and specially, to Min Zhang, to whom I am grateful for his teaching skills on the 'secrets' of patch-clamping of neurons and for sharing with me litres and litres of the most beautiful varieties of Chinese tea, which I hope keep me cleansed and young for many years. I would also like to thank the members of my Committee, Dr. Chris Wood and Dr. Mike O'Donnell for their valuable criticism and encouragement. My thanks goes out to Pat Hayward, for all the help and advice, and to Barb Reuter for her always helpful, attentive and kind predisposition.

I would like to deeply thank my family members, 'mamá', 'papá', Silvia, Mateo, Alejo, Sergio and 'abuela' Isabel for their neverending love and support and for being always with me even when we are living in opposite parts of the world. I want to also thank all my friends Pato, Fer, Guille, Na, Xime, Tom, Carlos, Claudia and Santosh, among many others, for all the good shared moments. Lastly, the most special thanks to Juan for his love and support, for understanding me, for spoiling me and for making me happy. Without him this thesis would not have been possible.

TABLE OF CONTENTS

LIST OF FIGURES AND TABLES

CHAPTER 1

CHAPTER 2

CHAPTER 3

CHAPTER 4

LIST OF ABBREVIATIONS

α,β-MeATP	α,β-methylene ATP
ω-agatx	ω-agatoxin IVA
ω-ctx	ω-conotoxin GVIA
4-AP	4- aminopyridine
5-HT	5-hydroxytryptamine (serotonin)
AA	arachidonic acid
ACh	acetylcholine
AN	anadamide
ATP	adenosine triphosphate
BBG	brilliant blue G
BzATP	2'- & 3'-O-(4 benzoylbenzoyl)-ATP
CB	carotid body
C_{in}	input capacitance
CNS	central nervous system
cPTIO	2-(4-carboxyphenyl)-4,4,5,5-tetramethyl-imidazoline-1- oxyl-3-oxide potassium or carboxy-PTIO
CSN	carotid sinus nerve
D289	styryl pyridinium dye (4-Di-2-ASP)
DA	dopamine

EC_{50}	concentration of agonist causing half maximal activation
GAP-43	growth-associated protein 43
GPN	glossopharyngeal nerve
h	steady state inactivation
Hal	halothane
Hox	hypoxia
HVA	high voltage activated Ca^{2+} channels
IbTx	iberiotoxin
IC_{50}	concentration of antagonist causing half maximal inhibition
I_{Ca}	calcium current
I_K	potassium current
IKO_2	oxygen-sensitive K^+ current
I_{Na}	sodium current
I_p	peak current (i.e. I_{Na} or I_{Ca})
IVM	ivermectin
JGPN neuron	'juxtaposed' GPN neuron
L-NAME	L-NG-nitroarginine methylester (L-NAME)
LVA	low voltage activated Ca^{2+} channels
NF	neurofilament
NG	nodose ganglion
NO	nitric oxide
NOS	nitric oxide synthase

Nox	normoxia
OxATP	oxidized-ATP
P2X	ionotropic purinergic receptor
P2Y	metabotropic purinergic receptor
PBS	phosphate-buffered saline
PCO_2	partial pressure of carbon dioxide
PG	petrosal ganglion
PO_2	partial pressure of oxygen
Quid	quinidine
RCB	red blood cell
Rec	recovery
R_{in}	input resistance
Rot	rotenone
RR	ruthenium red
Rs	series resistance
$S_{1/2}$	slope factor at $V_{1/2}$
TASK	tandem 2 pore domain acid sensitive K^+ channel
TEA	tetraethylammonium
TH	tyrosine hydroxylase
THIK	tandem 2 pore domain halothane inhibited K^+ channel
TTX	tetrodotoxin
$V_{1/2}$	holding potential where I_p was half-maximal

VAChT	vesicular acetylcholine transporter
Vm	resting potential

CHAPTER 1

General Introduction

Oxygen (O_2) is absolutely required for support of most life forms due to its central role as the final acceptor of electrons in the mitochondrial respiratory chain, making possible the synthesis of energy molecules, e.g. adenosine triphosphate (ATP), by oxidative phosphorylation. Various living organisms, from bacteria to mammals, have the capability of generating adaptive responses to conditions of low oxygen (hypoxia), which help minimize the deleterious effects of O_2 deficiency. These responses to hypoxia can be acute (occurring over a time scale of seconds to minutes) or chronic (over a time course of hours to days). Survival of mammals in acute hypoxia is critically linked with appropriate changes in the cardiovascular and respiratory systems to maintain oxygen delivery to tissues (López-Barneo, 2003). When that need is not met, even transient localized O_2 deficits can produce irreversible cellular damage, leading to stroke, myocardial infarction, chronic lung disease and sudden infant death syndrome (SIDS), as

well as reperfusion injury of transplanted organs. The main O_2 chemosensor that triggers acute responses to low blood O_2 (hypoxemia) is the carotid body (CB). Stimulation of this organ during hypoxia leads to a compensatory reflex increase in ventilation so as to maintain the partial pressure of O_2 (PO_2) in arterial blood. This reflex critically involves activation of an *afferent* sensory pathway from the CB, via nerve fibers in the carotid sinus (CSN) and glossopharyngeal (GPN) nerves. However, the overall fine control of CB function also includes an *efferent* inhibitory pathway (Neil and O'Regan, 1969, 1971; Fidone and Sato, 1970; Prabhakar *et al.* 1993; Wang *et al.* 1993, 1994a,b, 1995a,b; Prabhakar 1999), which involves groups of autonomic neurons located within the GPN nerve and their projections to the CB. The cellular physiology of these autonomic GPN neurons is poorly understood, as are the stimuli that normally regulate their activity, especially during hypoxic stress. A major goal of this thesis is to provide a detailed understanding of the anatomical distribution, connectivity, and neurophysiological mechanisms that control activity in these GPN neurons, and help clarify their role in the general control of respiration via their efferent inputs to the CB. First, the relevant background on our current understanding of CB chemoreception is considered below.

Carotid body: the main peripheral O_2-chemosensor

The carotid body (CB), which is strategically located at the bifurcation of the common carotid artery (Fig. 1), is a bilateral organ containing groups of glomus (type I) cells, enveloped by glial-like sustentacular (type II) cells (Fig. 2). Glomus cells act as chemoreceptors and are innervated by afferent (sensory) fibers (Fig. 2), which relay

sensory information to the Nucleus Tractus Solitarius (NTS) in the brainstem (Jordan, 1994). The parent cell bodies of these afferent fibers are located in the petrosal ganglion. The chemosensory units, consisting of glomus cell clusters innervated by a sensory nerve fiber, sense arterial PO_2 and during hypoxia initiate the arterial chemoreflex by increasing sensory discharge in the carotid sinus nerve (CSN), a branch of the glossopharyngeal nerve (Eyzaguirre and Zapata, 1984; González *et al.* 1994; López-Barneo *et al.* 2001). This leads to hyperventilation and restoration of blood PO_2. In addition, the CB can also sense a variety of other natural stimuli in the blood including PCO_2, pH, temperature and osmolality (Eyzaguirre and Zapata, 1984; González *et al.* 1994), and more recent studies suggest it is also a low-glucose sensor (Koyama *et al.* 2000; López-Barneo, 2001, 2003; Bin-Jaliah *et al.* 2004). The cellular mechanisms underlying hypoxia-induced responses in glomus cells involve a PO_2-dependent inhibition of K^+ channels, as originally proposed by López-Barneo *et al.* (1988) in the rabbit, though debate continues as to whether or not it is an essential step (Donnelly, 1999). Various K^+ conductances appear to be modulated by hypoxia in these cells and there are also marked species differences among the individual K^+ channel types (González *et al.* 1994; Peers and Buckler, 1995; Peers, 1997; Prabhakar, 2000; López -Barneo, 2001). For example, in the rat at least two types of K^+ conductances have been reported to be modulated by hypoxia: a large conductance Ca^{2+}-activated K^+ conductance (BK_{Ca}; Peers, 1990; Wyatt and Peers, 1995; López-López *et al.* 1997) and a background, voltage-insensitive TASK-1-like K^+ conductance (Buckler, 1999; Buckler *et al.* 2000). Inhibition of this background conductance may play an important role in quiescent glomus cells at voltages close to

resting potential, leading to depolarization and increased excitability. On the other hand, inhibition of BK_{Ca} channels may be more important in spontaneously active cells, though there is evidence from secretory studies on glomus cells in culture (Jackson and Nurse, 1998) and CB tissue slices (Pardal *et al.* 2000) that these channels are open in resting cells under normoxic conditions. Though the molecular identity of the PO_2 sensor in the CB is unknown, and even controversial (Prabhakar, 2000; López-Barneo *et al.* 2001), a reduction of K^+ conductance during hypoxia appears to be an important signal that triggers glomus cell depolarization, Ca^{2+} entry, and secretion of neurotransmitters. Of these, dopamine (DA) is the best studied (González *et al.* 1994), but appears not to be essential for hypoxic chemotransmission (Donnelly, 1996). However, there has been long-standing interest in acetylcholine (ACh) as an important excitatory transmitter in both cat (Fitzgerald, 2000) and rat (Nurse and Zhang, 1999; Zhang *et al.* 2000; Zhang and Nurse, 2004) CB, but the evidence here is controversial. More recently ATP, acting via postsynaptic purinergic P2X receptors, has emerged as a key excitatory neurotransmitter in CB chemosensory function (Zhang *et al.* 2000; Rong *et al.* 2003). One current model proposes that co-release of ACh and ATP is the main mechanism mediating fast excitatory chemotransmission in the rat CB (Zhang *et al.* 2000; Zhang and Nurse, 2004), though other neurotransmitters, e.g. substance P, may be important in other species (Prabhakar, 2000). These events are thought to occur in the direction glomus cell- to-petrosal ending, and there is morphological evidence for reciprocal synapses between these two elements (Fig. 2; McDonald, 1981). Additionally, local autocrine-paracrine mechanisms at glomus cell clusters appear to modulate chemoreceptor function by both

positive and negative feedback pathways (González *et al.* 1994), and involve other neurotransmitters/ neuromodulators such as dopamine, 5-HT and GABA (Benot and López-Barneo, 1990; Fearon *et al.* 2003; Zhang *et al.* 2003). Of particular relevance to this thesis is yet another modulatory pathway involving efferent inhibitory connections to the CB, that is dependent on the release of the gaseous neurotransmitter/ neuromodulator, nitric oxide (NO). The relevant background on the role of NO in carotid body chemoreceptor inhibition is considered next.

Nitric oxide and carotid body chemoreceptor inhibition

In the central and peripheral nervous systems, nitric oxide (NO) acts as a membrane-permeant diffusible neurotransmitter that can signal between distant synapses and cells. NO is synthesized from L -arginine in a reaction that is catalysed by a family of enzymes, the NO synthases (NOSs; Fig. 3). Three NOS isoforms have been identified and named according to the cell type or conditions in which they were first described: endothelial NOS (eNOS), neuronal NOS (nNOS) and inducible or inflammatory NOS (iNOS). These enzymes share ~ 50% sequence homology and catalyse the NADPH- and O_2 -dependent oxidation of L-arginine to NO and citrulline, with N^{ω}-hydroxy-L-arginine formed as an intermediate. NOSs are flavohaem enzymes that are active only as dimers. Each monomer has a carboxy-terminal diflavin-reductase domain and an amino-terminal oxygenase domain. Dimerization is thought to activate the enzyme by sequestering iron, generating high-affinity binding sites for arginine and the essential cofactor tetrahydrobiopterin (BH_4), and allowing electron transfer from the reductase-domain

flavins to the oxygenase-domain haem. Activity is also dependent on bound calmodulin. In iNOS, calmodulin is tightly bound, whereas in eNOS and nNOS, calmodulin binding is dependent on calcium, and enzyme activity is therefore calcium dependent. Bound calmodulin is thought to enhance the rates of electron transfer through the reductase domain to the oxygenase domain (for reviews see Lancaster and Stuehr, 1996; Stuehr, 1997; Macmicking *et al.* 1997; Mayer and Hemmens, 1997; Förstermann *et al.* 1998; Stuehr, 1999; Vallance and Leiper, 2002). NO has been implicated in many diverse functions, such as neuronal development, synaptic transmission, synaptic plasticity, and in both neuroprotection and neurotoxicity (Lipton *et al.* 1994; Schuman and Madison, 1994; Jaffrey and Snyder, 1995; Holscher, 1997).

In the last decade, NO has emerged as a major inhibitory signal in carotid body (CB) chemoreceptor function. Immunocytochemical and histochemical studies in the rat (Höhler *et al.* 1994; Grimes *et al.* 1994) and cat (Prabhakar *et al.* 1993; Wang *et al.* 1993, 1994a,b, 1995a,b) have revealed a plexus of nNOS-positive nerve fibers associated with clusters of CB chemosensory glomus cells, as well as with the CB vasculature. As illustrated in Fig. 2, nNOS-positive fibers were reported to originate from: (1) autonomic neurons located in the CB and distributed along the carotid sinus (CSN) and glossopharyngeal (GPN) nerves, with terminations mainly on CB blood vessels, and (2) unipolar sensory neurons of the petrosal ganglion. Many studies have demonstrated that CSN fibers mediate a so-called 'efferent inhibition' of CB chemoreceptors, however, the underlying mechanisms are not completely understood. Since the early 1990's, NO was proposed as 'the inhibitory neurotransmitter' in the CB (Prabhakar *et al.* 1993; Wang *et*

al. 1993, 1994a,b, 1995a,b). First, the CB was recognized as a site of NO synthesis since incubation with the NO precursor, L-arginine, yielded detectable co-production of ^{3}H-citrulline and NO. Second, electrical stimulation of the CSN or exposure of the CB to hypoxia, caused an elevation in ^{3}H-citrulline formation, which was prevented by the specific NOS antagonist, L-NAME. Third, these effects of NO seemed to be mediated by cyclic GMP (cGMP), consistent with the known ability of NO to activate a soluble form of guanylate cyclase (Wang *et al.* 1995a,b). Fourth, NO donors were reported to inhibit the chemosensory responses to hypoxia, induced chemically by sodium cyanide in the cat CB (Alcayaga *et al.* 1997, 1999), as well as inhibit L-type Ca^{2+} currents in chemoreceptor glomus cells of the rabbit CB, via both cGMP-dependent and -independent mechanisms (Summers *et al.* 1999). Fifth, though both eNOS and nNOS isoforms are localized in the CB, nNOS mutant mice display augmented ventilatory responses to hypoxia, while eNOS mutants show the opposite effect (Kline *et al.* 1998, 2000; Kline and Prabhakar, 2000).

Since nNOS immunoreactivity was present in both sensory and autonomic ganglion cells innervating the cat CB, it has been suggested that two neural mechanisms may be involved in the inhibitory neural regulation of carotid chemoreceptors. Thus, while sensory C-fibers would interact with chemoreceptor glomus cells, autonomic microganglia neurons would control CB blood flow by acting on the vasculature (Wang *et al.* 1995b). Nevertheless, the question still remained as to how the NOS-positive nerve fibers became activated, so as to synthesize and release NO during natural CB chemoexcitation. Previous reports suggested that acute hypoxia inhibited NO synthase activity in CB extracts, while chronic hypoxia upregulated mRNA encoding nNOS

(Prabhakar, 1999). In this thesis (Chapters 2 and 3), I tested the hypothesis that acute hypoxia itself, in addition to being a well-known CB chemoexcitant, was also a direct chemostimulus for nNOS-positive neurons of the GPN nerve. At the time these studies began, there was little or no evidence for direct 'hypoxia-sensing' mechanisms in peripheral neurons, though the sensitivity of neurons in the central nervous system (CNS) to hypoxia was well recognized. The relevant literature on this topic is reviewed in the following section.

O_2-sensing in central neurons

Hypoxia-induced inhibition of central neuron activity

In general, most neurons respond to hypoxia by decreasing their metabolic demands and thus their need to generate ATP through oxidative phosphorylation. Energy derived from ATP is mostly spent in maintaining ion gradients, a cost that is directly related to the level of neuronal activity. Consequently, most neurons reduce their metabolic requirements by decreasing their activity (Haddad and Jiang, 1997). One important mechanism leading to such decrease in neuronal activity involves regulation of Na^+ channels. Voltage-gated Na^+ channels play a crucial role in neuronal function in the central nervous system. These channels generate and propagate action potentials, which are essential for communication between neurons, and are thought to play a role in pathophysiological events such as hypoxia (Urenjak and Obrenovitch, 1996). Studies have shown that reducing Na^+ channel activity (e.g., by application of tetrodotoxin) attenuates neuronal hypoxic responses and reduces hypoxia-induced neuronal injury and

death *in vitro* (Weber and Taylor, 1994) and *in vivo* (Prenen *et al.* 1988). For example, hypoxia was reported to cause inhibition of voltage-gated Na^+ channels in the adult neocortex and hippocampus (Cummins *et al.* 1991, 1993). It has been suggested that these inhibitory effects on Na^+ channels during hypoxia may be an adaptive response enhancing neuronal tolerance to a low-oxygen environment and may delay hypoxia-induced neuronal injury and death (Cummins *et al.* 1991, 1993). Furthermore, it has been reported that anoxia-related cell death in hippocampal neurons could be prevented by removal of extracellular Na^+ ions (Friedman and Haddad, 1994), and more recently, that activation of voltage-activated Na^+ channels leads to apoptosis in cultured neocortical neurons (Banasiak *et al.* 2004). Thus, inhibition of Na^+ channels by low PO_2 in central neurons seems to play an important role in increasing their survival during hypoxic stress conditions.

Another mechanism of decreasing neuronal activity during hypoxia is by modulation of K^+ channels, which play a variety of important roles in setting neuronal resting potential, the recovery phase of the action potential, and influencing neuronal excitability. For example, Jiang and co-workers (1994) reported that oxygen deprivation activates ATP-sensitive K^+ channels in neurons from the susbtantia nigra. Thus, a reduction in ATP production releases the inhibition that ATP causes on these K^+ channels, leading to K^+ efflux and membrane hyperpolarization.

Hypoxia-induced activation of central neurons

Although most of brain function decreases during hypoxic conditions (see above), not all neurons reduce their activity during O_2 deprivation. There are populations of neurons in the brain that act in a way analogous to classical oxygen chemosensors. Central O_2-sensitive sites that direct respiratory and sympathetic activity have been identified in the thalamus, hypothalamus, pons, and medulla (Dawes *et al.* 1983; Horn and Waldrop, 1997; Koos *et al.* 1998, Martin-Body and Johnston, 1988; Solomon *et al.* 2000; Sun and Reis, 1994). Activation of these oxygen-sensitive sites leads to increased sympathetic and respiratory activity or, in the fetus, in which increasing respiratory efforts would be counterproductive, decreased respiratory activity.

Inhibition of K^+ channels: As discussed above for specialized O_2-chemoreceptors in the carotid body (CB), hypoxic inhibition of K^+ channels has been reported in some central neurons. In particular, Haddad and colleagues have described a K^+ channel, from rat neocortex and substantia nigra, that is regulated by intracellular Ca^{2+}, ATP and pH and is also reversibly inhibited by hypoxia (Jiang and Haddad, 1994a,b; reviewed by Haddad and Jiang, 1997). Hypoxia modulates this channel by causing a slow reduction in channel open state probability. More recently, tandem-pore domain or 'background' K^+ channels have been reported in central neurons (Millar *et al.* 2000; Brickley *et al.* 2001), and their lack of voltage sensitivity suggests that they control cell resting membrane potential and excitability. TASK-1 channels, a type of background K^+ channels that are closely related to the O_2-sensitive ones in carotid body glomus cells of the rat (Buckler, 1999; Buckler *et*

al. 2000), have been identified in cerebellar granular neurons (Millar *et al.* 2000; Brickley *et al.* 2001). Interestingly, as in the case of glomus cells, the TASK-1 channels were reported to be O_2-sensitive in these neurons and their inhibition by hypoxia led to membrane depolarization and increased excitability (Plant *et al.* 2002). Another example of this PO_2-dependent modulation of neuronal activity via K^+ channels is seen in the excitation of hypoxia-chemosensitive neurons in the rat rostral ventrolateral medulla, where chemical hypoxia (induced by sodium cyanide) was also associated with a reduced K^+ conductance (Wang *et al.* 2001).

Activation of cation channels. Voltage-gated Ca^{2+} channels are the primary means of Ca^{2+} influx into excitable cells and hence are critical for the wide variety of cellular functions that are Ca^{2+} dependent. However, activation of Ca^{2+} channels by stressful conditions, e.g. hypoxia, may lead to deleterious consequences as in the case of Na^+ channels. In general, the activation of these Ca^{2+} channels is regulated by changes in membrane potential, mediated principally by changes in K^+ channel activity or neurotransmitters that depolarize the neuron. In brainstem neurons, hypoxia causes activation of L-type Ca^{2+} channels via hypoxia-induced glutamate release (Mironov and Richter, 1998). Similar effects were reported in rat hippocampal neurons, where hypoxia caused potentiation of L- and N-type Ca^{2+} currents (Lukyanetz *et al.* 2003). Interestingly, L-type calcium channel blockers significantly attenuated the neuronal injury induced by oxygen deprivation in cultured hippocampal neurons (Kimura *et al.* 1998). In contrast, in other studies hypoxia was reported to cause blockade (> 95%) of L-type channels CA1 and

CA3 neurons in submerged hippocampal slices. These contrasting data on the effects of hypoxia on Ca^{2+} channels may be due to differences in experimental conditions.

Effects of hypoxia on peripheral neurons

Despite numerous studies concerning the effects of hypoxia on central neurons, there are few reports on the actions of low PO_2 on peripheral neurons. Lukyanetz and colleagues (2003) have recently reported that hypoxia causes a rise in intracellular Ca^{2+} ions in dorsal root ganglion (DRG) neurons. This hypoxia-induced effect could be almost completely prevented by application of the blocker, nifedipine, which blocks L-type calcium channels, the predominant type expressed in DRG neurons. However, as mentioned above, these effects on Ca^{2+} channels could be related to the deleterious effects of hypoxia. Aside from the data presented in Chapters 2 and 3 of this thesis, there are no reports on the mechanisms involved in the physiological responses of peripheral neurons to hypoxia.

Electrophysiological techniques

All electrophysiological data presented in this thesis were obtained with the aid of the patch clamp technique. This technique was developed by Neher and Sakmann (1976) and allows the recording of ionic currents or membrane potential from live cells. The technique emerged as a complement to the classical voltage-clamp methods used by Hodgkin and Huxley (1952) on the squid giant axon, and importantly, permitted reliable voltage-clamp recordings from small, fragile cells. Before then, fine-tip glass

microelectrodes were used for impaling cells, but the damage introduced by the electrode made recording from small cells (< 15 μm) unreliable. In contrast, the patch clamp technique uses a single electrode to pass current and record voltage simultaneously, but most importantly, the shunt between electrode and cell membrane is drastically reduced. Following application of slight suction within a fresh pipette (~ 1 μm tip diameter), a high resistance seal, i.e. 'gigaseal', can be formed between the glass and membrane (Hamill *et al.* 1981), resulting in the ability to resolve tiny currents above background noise. These gigaseals are mechanically stable, allowing patches to be withdrawn from the cell and studied in isolation (Hamill *et al.* 1981). Various configurations have been developed to study single channel activity, including cell-attached, inside-out and outside-out patches (Hamill *et al.* 1981; Jones, 1990). In addition, it is also possible to obtain recordings as a result of activation of macroscopic currents flowing across the whole-cell membrane. The whole-cell configuration is achieved by rupturing the patch after gigaseal formation and this results in access to the cell interior and the ability to record whole-cell currents. Alternatively, this configuration also allows the recording of changes in membrane potential (current-clamp mode), due to some physiological response of a cell (Penner, 1995). Although the whole-cell method has the advantage of controlling the intracellular medium by replacing it with the pipette solution of known ionic composition, it also causes dialysis of normal cytoplasmic components when the patch is ruptured (Marty and Neher, 1995). This is particularly important since ion channels can be regulated by second messengers, ATP, and regulatory proteins (e.g. via phosphorylation), which may be lost through dialysis in the traditional whole-cell

configuration. To overcome this experimental limitation, Horn and Marty (1988) developed a variation of the technique known as 'perforated-patch' recording, which was used in the majority of electrophysiological experiments in this thesis. In this variation, electrical continuity between pipette and cytoplasm is achieved not by rupturing the membrane, but by incorporation of a channel-forming substance inside the pipette so as to create a low resistance access to the cell interior. This method does not cause 'washout' of larger, critical diffusing molecules since these newly formed 'perforations' in the membrane patch are permeable to monovalent, but not divalent cations, and to a lesser extent, anions (Kleinberg and Finkelstein, 1984). The main disadvantage of the perforated-patch technique is that the series resistance (R_s), which is a sum of the pipette and the membrane patch resistances, is ~ 3 fold higher than that in traditional whole-cell recordings and can introduce substantial voltage errors (Jones, 1990). However, if care is taken to compensate the majority of R_s, and if the input resistance of the cell is high (> 1 GΩ), as in the case of GPN neurons investigated in this thesis, these voltage errors are minimal (Jones, 1990).

Goals and organization of thesis

The primary goal of this thesis was to perform an anatomical, immunocytochemical, pharmacological, and electrophysiological characterization of paraganglion neurons from the rat glossopharyngeal nerve (GPN), with particular emphasis on possible physiological mechanisms by which these neurons are activated, leading to efferent inhibition of carotid body chemoreceptors. The end result is a novel

interpretation and broader view of the role played by GPN neurons in carotid body chemoreceptor function during hypoxia.

The main body of this thesis is written in a 'sandwich' style, comprising a series of three papers that are either published in peer-reviewed journals, or are in preparation for submission. Some of the papers are multi-authored, so a short preface appears at the beginning of each paper that describes my contribution.

Chapter 1 comprises background knowledge about O_2-sensing mechanisms in peripheral chemoreceptors and central neurons, as well as an introduction to the patch-clamp technique which was extensively used in this thesis for the recording of ionic currents and membrane potential from isolated neurons from the GPN. Chapter 2 is an electrophysiological characterization of the passive and active membrane properties of isolated GPN neurons, with emphasis on the different types of voltage-gated cation channels expressed. It also includes an introduction to the O_2-sensing properties of these neurons. Chapter 3 contains an immunocytochemical and anatomical characterization of GPN neurons and their projections to the carotid body, including the identification of a previously-unrecognized 'distal' population along the GPN. A major component involves the study of O_2-sensitivity in GPN neurons, including a detailed biophysical and pharmacological characterization of the O_2-sensitive K^+ channels expressed in these neurons and their role in generation of the 'receptor potential' during hypoxia. Chapter 4 concerns the study of the physiological responses of GPN neurons to ATP, a pharmacological and immunocytochemical identification of the multiple purinergic receptor subunits involved, and their potential role in CB chemoreceptor function.

Chapter 5 is a general discussion of the results presented in the previous chapters and of possible future directions that emerged from my work during this thesis. Finally, the contents of the Appendices describe: (1) hypoxic inhibition of heterologously expressed THIK-1 (Kcnk13) background K^+ channels in HEK 293 cells; these data validate our hypothesis raised in Chapter 3 about the molecular identity of the O_2-sensitive K^+ channels in GPN neurons; (2) the effects of a variety of neurotransmitters (i.e., acetylcholine, dopamine and serotonin) on membrane properties of isolated GPN neurons; (3) preliminary data which test the potential involvement of the mitochondrion as the O_2-sensor in GPN neurons; and (4) preliminary data suggesting a hypoxia-induced augmentation of Ca^{2+} currents in GPN neurons.

Figure 1. Schematic diagram of the anatomical localization of the rat carotid body (CB). Diagram shows the relationship of the rat CB to adjacent nerve, ganglia, and arteries. It shows the egg-shaped CB located at the bifurcation of the common carotid arteries, adjacent to the superior cervical ganglion (SCG; not shown clearly in diagram) and nodose ganglion (NG). The CB is innervated by carotid sinus nerve (CSN), a branch of the IXth cranial or glossopharyngeal nerve (GPN), as well as by sympathetic nerves. Another branch of the GPN innervates the tongue and pharyngeal structures. The blood supply of the CB arises from the external carotid artery (modified from McDonald and Mitchell, 1975).

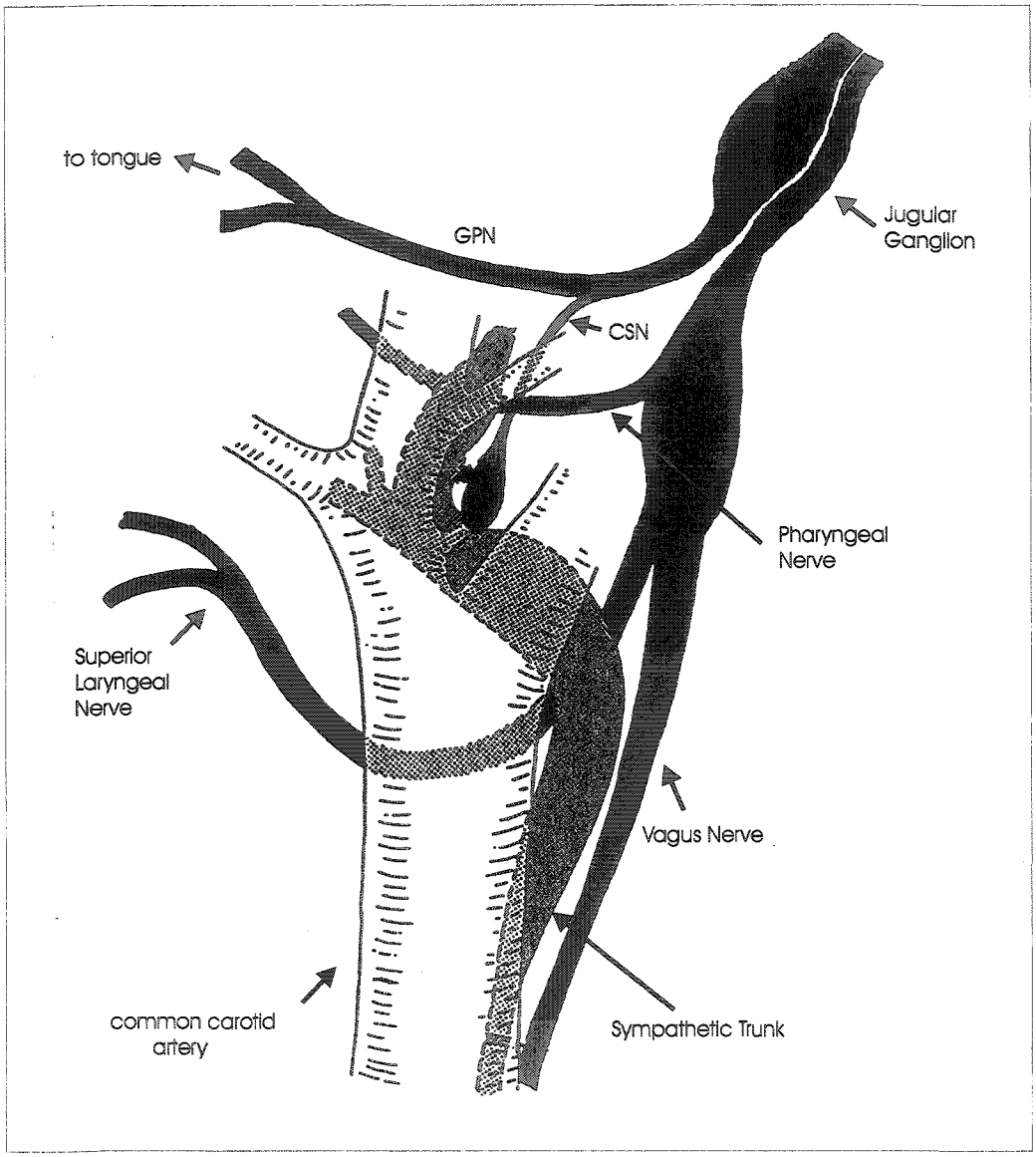
to tongue
GPN
Jugular Ganglion
CSN
Pharyngeal Nerve
Superior Laryngeal Nerve
Vagus Nerve
common carotid artery
Sympathetic Trunk

Figure 2. Schematic diagram of a carotid body (CB) chemoreceptor unit. These units are formed by clusters of chemoreceptor glomus (type I) cells, enveloped by glial-like sustentacular (type II) cells. The CB is a highly vascularized organ, allowing the glomus cells to sense arterial PO_2, PCO_2, pH and glucose (Pardal and López-Barneo, 2001). In a given cell cluster, glomus cells are electrically coupled by gap junctions. When these cells are activated by a chemosensory stimulus (e.g., low PO_2 or hypoxia) they depolarize, causing Ca^{2+} influx and neurotransmitter release onto sensory nerve endings. Glomus cells receive sensory innervation from petrosal ganglion (PG) nerve endings, and reciprocal synaptic connections form between the two elements (McDonald, 1981; González *et al.* 1994). In addition, CB chemoreceptor units are in close proximity to nNOS-expressing efferent fibers from the PG and glossopharyngeal nerve, and some fibers may originate from within the CB itself. These nNOS-expressing nerve endings are thought to be involved in CB efferent inhibition (Prabhakar *et al.* 1993; Wang *et al.* 1993, 1994a,b, 1995a,b).

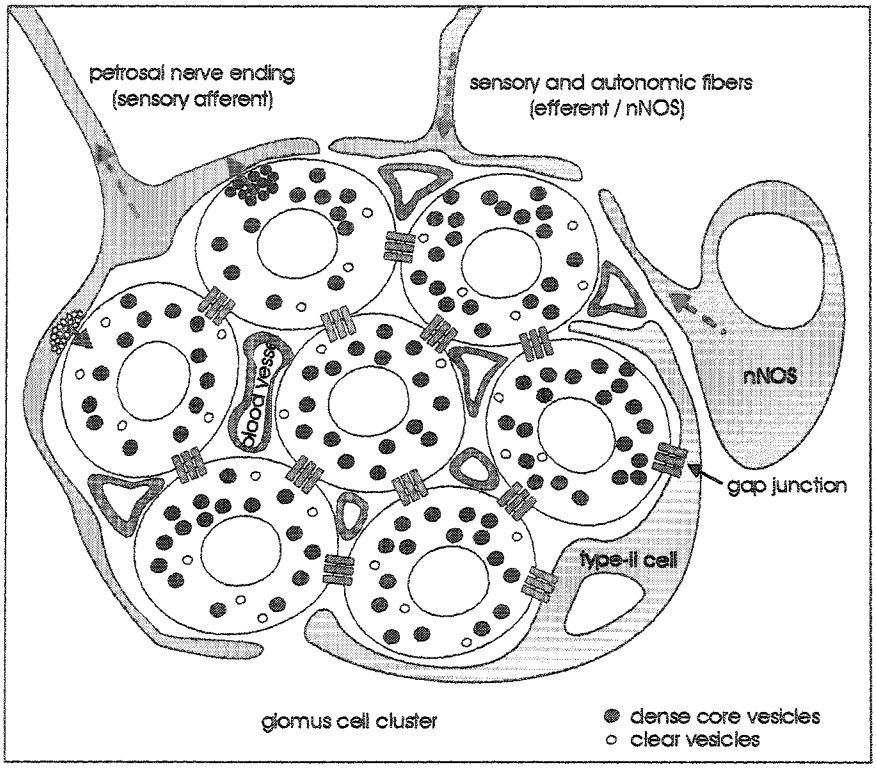
petrosal nerve ending
(sensory afferent)
sensory and autonomic fibers
(efferent / nNOS)
blood vessel
nNOS
gap junction
type-II cell
glomus cell cluster
dense core vesicles
clear vesicles

Figure 3. The nNOS pathway. For enzymatic activity, the neuronal nitric oxide synthase (nNOS) enzymes must dimerize and bind the cofactors tetrahydrobiopterin (BH_4), haem, flavin mononucleotide (FMN) and flavin adenine dinucleotide (FAD). On binding Ca^{2+}-calmodulin (CaM), the active enzyme catalyses the oxidation of L-arginine to citrulline and nitric oxide (NO), and requires molecular oxygen (O_2) and NADPH as co-substrates. Each NOS dimer co-ordinates a single zinc (Zn^{2+}) atom (modified from Vallance and Leiper, 2002).

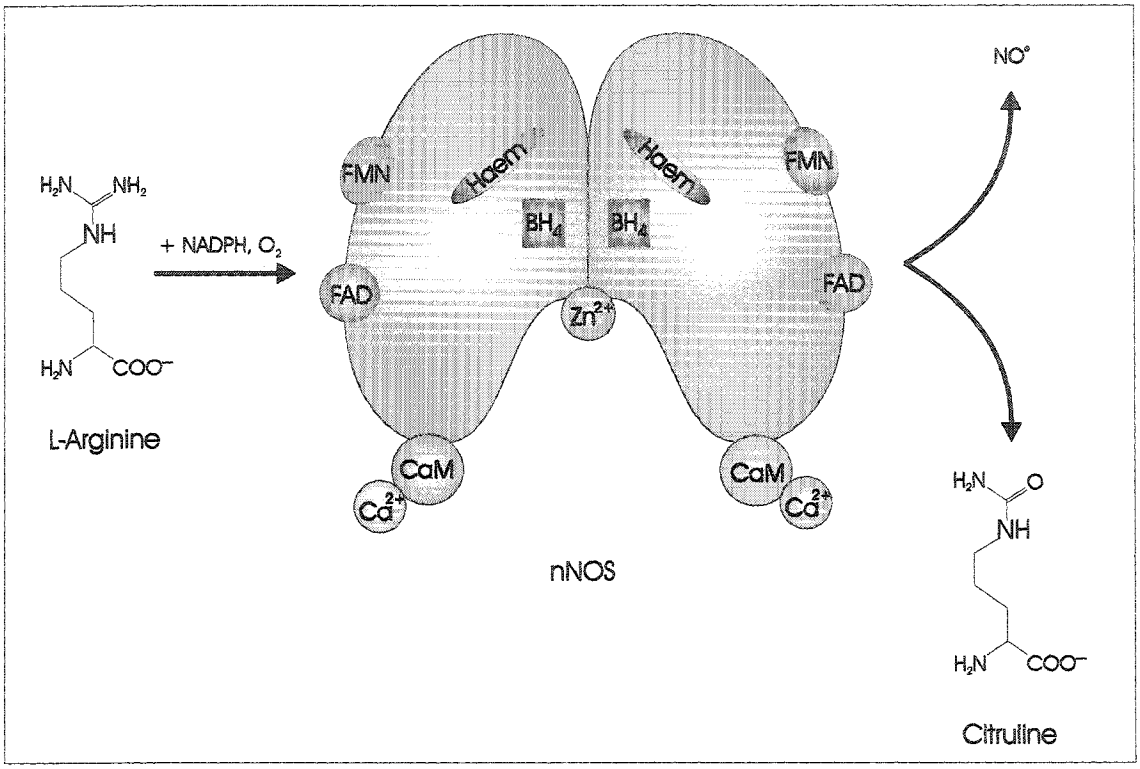
NO°
FMN
Haem
Haem
FMN
BH4
BH4
+ NADPH, O2
FAD
FAD
Zn2+
CaM
CaM
Ca2+
Ca2+
L-Arginine
nNOS
Citruline

CHAPTER 2

Biophysical characterization of whole-cell currents in O_2-sensitive neurons from the rat glossopharyngeal nerve

The work in this chapter will be submitted to the journal *Neuroscience*

The authors are: Verónica A. Campanucci and Colin A. Nurse

I was responsible for performing experiments, data analysis and preparation of the manuscript.

ABSTRACT

In this study we use whole-cell and nystatin perforated recordings to characterize the biophysical properties of two populations of O_2-sensitive paraganglion neurons from the rat glossopharyngeal nerve (GPN). This nerve contains neuronal nitric oxide synthase (nNOS)-synthesizing fibers that are thought to be involved in NO-mediated efferent inhibition of carotid body chemoreceptors. GPN neurons were visualized in whole mounts by vital staining with the styryl pyridinium dye, 4-Di-2-ASP (D289), and confirmed to be distributed along the nerve in two anatomically separate groups, one at the carotid sinus nerve bifurcation (proximal) and the other, at a more distal location (distal). The passive membrane properties of proximal (n = 40) and distal (n = 178) GPN neurons were respectively: mean input resistance of 1.5 and 1.6 GΩ; mean input capacitance of 25.0 and 27.4 pF and mean resting potential of -53.9 and -53.3 mV. All neurons had similar voltage-dependent macroscopic currents composed of: tetrodotoxin (TTX)-sensitive Na^+ currents, prolonged and transient Ca^{2+} currents, and delayed rectifier-type K^+ currents. Threshold activation for the Na^+ currents was approximately -30 mV and they were inactivated within 10 ms. TTX inhibited Na^+ currents in a dose-dependent manner with an IC_{50} of ~ 0.2 μM. Pharmacological dissection of the different channels contributing to the inward Ca^{2+} currents revealed the presence of nifedipine-sensitive L-type, ω-agatoxin IVA-sensitive P/Q-type, ω-conotoxin GVIA-sensitive N-type, SNX-482-sensitive R-type, and Ni^{2+}-sensitive, but SNX-482-insensitive, T-type channels. The outward currents were carried largely by voltage-dependent, delayed rectifier, K^+ channels sensitive to tetraethylammonium (TEA; 10 mM) and 4-

aminopyridine (4-AP; 2 mM). Exposure to a chemosensory stimulus, hypoxia (PO_2 range: 80 - 5 Torr), caused a dose-dependent decrease in K^+ current which persisted in the presence of TEA and 4-AP, consistent with the involvement of background K^+ channels. GPN neurons generated TTX-sensitive, Na^+-dependent action potentials, and in spontaneously active neurons, hypoxia caused membrane depolarization and an increase in firing frequency. These properties endow GPN neurons with an exquisite ability to regulate carotid body chemoreceptor function during hypoxia, via Ca^{2+}-dependent activation of NOS and release of NO.

INTRODUCTION

The carotid bodies (CB) are the main mammalian peripheral O_2-chemoreceptor organs, which are involved in the control of breathing. The CB chemoreceptor (type I) cells lie in synaptic opposition with petrosal sensory nerve endings and help monitor blood levels of PO_2, PCO_2 and pH (González *et al.* 1994). Thus, during hypoxia the CB can initiate compensatory reflexes in order to maintain blood PO_2 homeostasis via the control of ventilation (González *et al.* 1994; López-Barneo *et al.* 2001). The first step in this reflex response is depolarization of type I receptor cells, which leads to Ca^{2+}-dependent neurotransmitter release (e.g., ACh, ATP and catecholamines) and excitation of petrosal sensory nerve endings (González *et al.* 1994; Fitzgerald, 2000; Prabhakar, 2000; Zhang *et al.* 2000). The result is an increase in afferent discharge in the carotid sinus nerve (CSN), leading to the hyperventilatory reflex (González *et al.* 1994).

Chemoreceptor inhibition is the mechanism by which the CB responses are reduced during chemical stimulation, leading to an inhibition of chemoreceptor discharge. Autonomic neurons of the glossopharyngeal nerve (GPN) are thought to contribute to this inhibition via release of NO. These neurons give rise to an extensive plexus of neuronal nitric oxide synthase (nNOS)-containing nerve fibers that project to the CB of adult rats (Höhler *et al.* 1994; Grimes *et al.* 1994). The cell bodies of some of the neurons involved in this plexus are located at the branchpoint of the GPN and the CSN. Though previous studies have suggested that NO is an important neurotransmitter or neuromodulator involved in the efferent inhibition of CB chemoreceptors (Prabhakar *et al.* 1993; Wang *et al.* 1993, 1994a,b, 1995a,b; Höhler *et al.* 1994; Grimes *et al.* 1994;

Prabhakar 1999), the physiological properties of these nNOS-containing neurons are poorly understood. In the rat, we recently demonstrated that these neurons are found in two groups, one located at the CSN bifurcation and the other concentrated at a more distal region along the GPN (Campanucci *et al.* 2003a). Retrograde labeling techniques demonstrated that both populations innervated the CB, and electrophysiological experiments showed that they were hypoxia-sensitive (Campanucci *et al.* 2003a).

In the present study, we focused on the biophysical characterization of the membrane properties of these nNOS-expressing GPN neurons, with the expectation that this knowledge will contribute to our understanding of the physiological events underlying carotid body chemoreceptor inhibition during hypoxia.

METHODS

Cell culture. Wistar rat pups (9-10 days old, Charles River Laboratory, St. Constant, QC, Canada) were first stunned by a blow to the head that rendered them unconscious, and then killed by decapitation before removing the carotid bifurcation, surrounding ganglia and attached nerves. All procedures for animal handling were carried out according to the guidelines of the Canadian Council on Animal Care (CCAC). Since proximal and distal neurons from the glossopharyngeal nerve (GPN) were morphologically similar, the two populations were cultured separately. First, sections of the GPN, extending from its intersection with the carotid sinus nerve (CSN) to a region ~ 5 mm distal to the intersection, were dissected and then divided into two segments to separate the proximal from the distal group of GPN neurons. The segments were placed in L-15 plating medium (Gibco/Invitrogen Canada Inc., Burlington, ON, Canada) containing 0.3 % glucose (Sigma Chemical Co., St Louis, MO, USA) and 1 % penicillin/streptomycin (Gibco). Then, the segments were separately pooled and digested with enzyme (0.1 % Collagenase, Invitrogen; 0.1 % trypsin, Sigma; and 0.01 % DNase, Invitrogen), and mechanically dissociated to produce dispersed GPN neurons. The neurons were pelleted by centrifugation and resuspended in F-12 nutrient medium containing: 10 % Cosmic Calf Serum (HyClone, South Logan, UT, USA), 3 % glucose (Sigma), 2 mM L-glutamine (Gibco), 3 μg/ml insulin (Sigma) and 1 % penicillin/streptomycin (Gibco). The cell suspension was plated onto a thin layer of collagen or Matrigel (Collaborative Research, Bedford, MA, USA) that was previously applied to the central wells of 35 mm tissue culture dishes. Cultures were fed with fresh medium the following day and grown

at 37 °C in a humidified atmosphere of 95 % air-5 % CO_2. They were used either for patch-clamp experiments or immunofluorescence studies ~ 24-48 hr following isolation.

Electrophysiology. Membrane potential (current clamp) and ionic currents (voltage clamp) were monitored in GPN neurons using the nystatin perforated-patch technique, which preserves cytoplasmic integrity (Horn and Marty, 1988). Some experiments (e.g. measurements of Ca^{2+} currents) were carried out using conventional whole-cell recording that resulted in intracellular dialysis (Hamill *et al.* 1981). Patch pipettes were made from Corning #7052 glass (A-M Systems Inc., Carlsborg, WA, USA) or borosilicate glass (WPI, Sarasota, FL, USA) using a vertical puller (PP 83; Narishige Scientific Instrument Lab., Tokyo, Japan) and were fire-polished. When filled with intracellular recording solution, micropipettes had a resistance of 5-10 MΩ and formed gigaseals between 2 and 12 GΩ. Approximately 80 % of the series resistance (range, 20-40 MΩ in perforated-patch recording) was compensated. Ca^{2+} current data were corrected for changes in junction potentials in different extracellular solutions using pClamp 9.0 software. Whole-cell currents were recorded at 22-25 °C using an Axopatch 1D Amplifier (Axon Instruments Inc., Union City, CA, USA) equipped with a 1 GΩ headstage feedback resistor. All currents and membrane potential measurements were recorded at a frequency of 10 kHz. Signals were filtered at 1 kHz and stored on a Pentium II PC with the aid of a Digidata 1200A/B computer interface and pClamp 9.0 software (Axon Instruments) for data acquisition and analysis. I-V plots are leak unsubtracted. Hypoxia (PO_2 range: 5-80 Torr) was generated by bubbling 100 % N_2 into the perfusion reservoir and PO_2

measurements were obtained with the aid of a carbon-fiber electrode (5 μm diameter, Dagan Corporation, Minneapolis, MN, USA) and a VA-10 NPI Amplifier (NPI Electronic, Hauptstrasse, Tamm, Germany). Control experiments were performed by bubbling the extracellular recording solution with compressed air instead of N_2 gas. The solution in the recording chamber (volume, 0.75-1 ml) was exchanged by perfusion under gravity and simultaneous removal by suction at a rate of ~ 6 ml min^{-1} (Thompson and Nurse, 1998). The effects of hypoxia were examined in time-series studies, during which cells were voltage clamped at -60 mV and currents were evoked using voltage ramps from -100 to +60 mV over one second, followed by step potentials to +30 and +60 mV for 50 ms each.

During studies on threshold activation of Na^+ currents, 0.5 μM TTX was applied to avoid clamping artifacts related to limitations of the patch amplifier to counteract the fast activation and large magnitude of the Na^+ currents. Steady-state inactivation curves for transient Na^+ and Ca^{2+} currents were generated from the peak inward currents elicited by voltage steps to 0 mV (for Na^+) or -10 mV (for Ca^{2+}) from various holding potentials between -100 to +20 mV. These data were fitted with smooth curves according to a modified version of the Boltzmann equation (Clark *et al.* 1990):

$$h = \frac{I_p(V_m)}{I_{p\,max}} = \frac{1}{\exp\dfrac{(V_m + V_{1/2})}{S_{1/2}} + 1}$$

where h is the steady state inactivation determined by dividing the peak current I_p (i.e. I_{Na} or I_{Ca}) at each holding potential (V_m) by the max I_{Na} or I_{Ca} recorded. The variables $V_{1/2}$ (holding potential where I_p was half-maximal) and $S_{1/2}$ (slope factor at $V_{1/2}$) were adjusted for best fit of the curve to the observed data.

Solutions. Experiments were performed using extracellular solution of the following composition (mM): NaCl 135, KCl 5, Hepes 10, glucose 10, $CaCl_2$ 2, $MgCl_2$ 2, pH adjusted to 7.4 with NaOH at room temperature. Patch pipettes were filled with intracellular recording solution of the following composition (mM): K-gluconate 110, KCl 25, Hepes 10, NaCl 5, $CaCl_2$ 2, pH adjusted to 7.2 with KOH, plus 500 μg/ml nystatin. All solutions were filtered through a 0.2 μm millipore filter before use. During recordings, the culture was continuously perfused under gravity flow and removal of excess fluid by suction ensured that the fluid level in the recording chamber remained relatively constant. For the isolation of Ca^{2+} currents in GPN neurons, both Na^+ and K^+ currents were blocked using extracellular solution of the following composition (mM): NaCl 110, CsCl 5, $CaCl_2$ 5, $MgCl_2$ 2, Hepes 10, glucose 10, tetraethylamonium (TEA) 20, tetrodotoxin (TTX) 0.001; pH was adjusted to 7.4 with NaOH. The pipette solution for conventional whole-cell recording contained (mM): CsCl 105, NaCl 10, TEA 25, EGTA 11, $CaCl_2$ 2, MgATP 2, Hepes 10; pH was adjusted to 7.2 with CsOH.

Drugs. K^+ currents were blocked using tetraethylammonium (TEA, 10 mM) and 4-aminopyridine (4-AP, 2 mM) (both obtained from Sigma). To block voltage-dependent

Na^+ currents, tetrodotoxin (TTX, Alomone Labs, Ltd., Jerusalem, Israel) was added to the bathing solution. In addition, the calcium channel types present in GPN neurons were investigated with the aid of specific blockers. Nifedipine (L-type) and Ni^{2+} (T- and R-type) were obtained from Sigma; ω-conotoxin GIVA (N-type), SNX-482 (R-type) and ω-agatoxin IVA (P/Q-type) were obtained from Alomone. EC_{50} and IC_{50} values were obtained by the best fit of the data using the Hill function.

Styryl pyridinium dye staining. Rat pups (9-10 days old) received an intraperitonial injection of 10-15 mg/kg of 4-(4-(diethylamino)styryl)-*N*- methylpyridinium iodide or 4-Di-2-ASP (D289; Molecular Probes Inc., Eugene, OR, USA) 18-20 hr before examination of the tissue (Nurse and Farraway, 1989). Pups were first stunned by a blow to the head that rendered them unconscious, and then killed by decapitation before removing the petrosal ganglion (PG), and the attached glossopharyngeal (GPN) and carotid sinus (CSN) nerves. All procedures for animal handling were carried out according to the guidelines of the Canadian Council on Animal Care (CCAC). Samples were mounted in phosphate-buffered saline (PBS) and viewed with a confocal microscope (BIO RAD Microradiance 2000) equipped with an argon (used at 488 nm) laser. Lasersharp software was used for image acquisition and CorelDraw 9 for image processing and manipulation.

Statistics. Current densities (pA/pF) and current ratios were compared using two-tailed student *t*-test and non-parametric Mann-Whitney tests, respectively. In addition, mean

current densities recorded during time series protocols were compared by repeated measurements ANOVA. The level of significance was set at $P < 0.05$.

RESULTS

Styryl pyridinium staining of GPN neurons

In previous studies (Campanucci *et al.* 2003a), retrograde labeling and immunocytochemical techniques were used to identify two anatomically distinct populations of autonomic neurons along the rat glossopharyngeal nerve (GPN), that project to the carotid body. One group of GPN neurons was dispersed around the branch point with the carotid sinus nerve (CSN; proximal group), whereas the other was concentrated at a more distal bifurcation of the GPN (distal group). In the present study, we found that the styryl dye 4-Di-2-ASP (D289) conveniently labeled both populations of GPN neurons after overnight (18-20 hr) administration in 9-10 day-old rat pups (see Methods). A typical confocal image from a whole-mount containing petrosal ganglion (PG), GPN and CSN after vital staining with D289 is shown in Fig. 1 (n = 5), and reveals the relative distribution of the two groups of GPN neurons. The simplicity of this method should prove useful for locating other autonomic neurons associated with laryngeal and pharyngeal nerves.

Passive membrane properties of GPN neurons

Glossopharyngeal (GPN) neurons survived in culture for up to one week. Figure 2A shows a representative example of a GPN neuron after 24 hr in culture, i.e. the conditions used for patch-clamp experiments. The following results are based on conventional whole-cell and nystatin perforated patch recordings from ~ 150 GPN neurons. The passive membrane properties of both populations of neurons are

summarized in Table 1. For the proximal (n = 40) and distal (n = 178) groups, the mean input resistance (R_{in}) was 1.5 ± 0.2 GΩ and 1.6 ± 0.1 GΩ (range: 0.3 to 4 GΩ) respectively; the mean input capacitance (C_{in}) was 25.0 ± 1.2 pF and 27.4 ± 0.7 pF (range: 8.5 to 43 pF). The mean resting potential (V_m) was -53.9 ± 1.2 mV and –53.3 ± 0.6 mV (range: from –40 to –80 mV) respectively. Both groups of neurons had similar passive and active (see later) membrane properties, making them indistinguishable from each other in culture, unless they were plated separately.

Whole-cell voltage-activated currents

All neurons studied had similar types of voltage-activated currents as determined by voltage clamp analysis. In normal external and internal (pipette) solutions, depolarization steps from a holding potential of –60 mV to approximately –30 mV and higher elicited a fast transient inward current followed by a prolonged outward current (Fig. 2 B, C). As described below these voltage-dependent currents included a fast transient inward Na^+, a transient and a slow prolonged inward Ca^{2+}, and outward K^+ currents as determined by application of ion channel blockers and various voltage clamp protocols.

Voltage-gated Na^+ currents

In order to isolate Na^+ currents from the total macroscopic inward currents, Ca^{2+} currents were first blocked by adding either 200 μM Cd^{2+} or by substituting half of the extracellular Ca^{2+} with 1 mM Ni^{2+}. Maximum Na^+ currents were elicited after application

of a pre-step voltage to –100 mV for 100 ms to remove Na^+ inactivation. The threshold for activation of the Na^+ current was approximately –30 mV for both populations of GPN neurons (Fig. 3 A; n = 5), and the current was inactivated within 10 ms (Fig. 3 A, see example traces). In general, there were no significant differences in the activation properties of Na^+ currents between proximal and distal GPN neurons, and for both groups the maximum Na^+ current was evoked at step potentials near 0 mV. Confirmation that the fast transient component of the inward current was carried by Na^+ ions was obtained in experiments using tetrodotoxin (TTX). As illustrated in Figure 3 B, TTX caused a dose-dependent inhibition of the inward current with an IC_{50} of 0.2 ± 0.1 and 0.1 ± 0.0 μM (n = 5) for proximal and distal neurons respectively. At a concentration of 1 μM TTX, the Na^+ current was inhibited by ~ 80 %, suggesting that most of the Na^+ channels were TTX-sensitive.

Steady-state inactivation curves for the Na^+ current were regenerated for groups of 5 proximal and 5 distal GPN neurons, and fitted by the Boltzmann equation (see Methods; Fig. 3 C; r^2 was 0.99 for both groups of data). The holding potential where I_{Na} was half-maximal, $V_{1/2}$, was –33.3 ± 1.3 and –25.0 ± 1.0 mV for the proximal and distal groups, respectively; the corresponding slope factor $S_{1/2}$ was 7.8 ± 0.6 and 9.1 ± 0.6 respectively. In general, the magnitude of the currents and current density (Fig. 3 A) in the distal group were smaller than those recorded from the proximal group, at the same test potentials. In these experiments, neurons were studied no latter than 18-24 hr after isolation, before significant neurite extension (Fig. 2 A), to minimize voltage errors due

to inadequate space-clamp. However, such errors could not be completely excluded since these cells develop processes during the first few days in culture.

Pharmacological properties of voltage-gated Ca^{2+} currents

Voltage-gated Ca^{2+} currents in GPN neurons were investigated by first blocking inward Na^+ currents with TTX, and outward K^+ currents by substituting Cs^+ and TEA for K^+, in both the intracellular (pipette) and extracellular solutions (see Methods). In addition, to increase the magnitude of these currents the extracellular Ca^{2+} concentration was raised from 2 mM to 5 mM. To remove inactivation, a conditioning or pre-step voltage to –100 mV for 100 ms was applied, and subsequent step depolarizations evoked transient and prolonged inward Ca^{2+} currents that were reversibly blocked by 200 μM Cd^{2+} (n = 5). A representative example of this effect is shown in Fig. 4 A.

In order to dissect the different types of Ca^{2+} currents present, various Ca^{2+} channel blockers were used. The N-type channel blocker, ω-conotoxin GVIA (ω-ctx, 1 μM; Fig. 4 B; n = 6), caused irreversible inhibition of the sustained component of the Ca^{2+} current, but had relatively little effect on the fast transient component. Interestingly, while most (~ 70 %) of the sustained component was sensitive to ω-ctx, a small residual component (~ 30 %) persisted in the presence of the drug (Fig. 4 B), suggesting the presence of a sustained Ca^{2+} current that was not N-type. Application of 100 μM Ni^{2+}, a known blocker of T-type and R-type Ca^{2+} channels (Elmslie, 2004), caused a reversible inhibition (~ 60 %) of the transient component of the Ca^{2+} current that persisted in the presence of ω-ctx (Fig. 5 A; n = 8). These data suggest that most of the transient current

is carried by T- or R-type channels. To determine whether R-type Ca^{2+} channels were present, SNX-482 (50-100 nM), a selective R-type Ca^{2+} channel blocker (Newcomb *et al.* 1998), was used. SNX-482 caused a reversible inhibition (~ 32 %) of the transient Ca^{2+} current in 4/5 neurons tested (Fig. 5 B). These data suggest that most GPN neurons express R-type Ca^{2+} channels, sensitive to both Ni^{2+} and SNX-482. Additionally, T-type Ca^{2+} channels that are sensitive to 100 μM Ni^{2+}, but insensitive to 50-100 nM SNX-482, also appear to be present.

The persistence of a small, sustained component of Ca^{2+} current in the presence of ω-ctx (Fig. 4 B) raised the possibility that L-type Ca^{2+} channels were also present in GPN neurons. To test this idea we used the L-type Ca^{2+} channel blocker, nifedipine. As exemplified in Fig. 6 A, nifedipine (50 μM; n = 8) caused a reversible inhibition of the prolonged inward Ca^{2+} current. In most cases, however, recovery of Ca^{2+} current after nifedipine application was incomplete (~ 78 %). We also tested for the presence of P/Q-type Ca^{2+} channels using the selective blocker, ω-agatoxin IVA (ω-agatx). As shown in Fig. 6 B, 50 nM ω-agatx inhibited whole-cell Ca^{2+} current by ~ 25 % (n = 3), and the effect was still present in neurons pre-treated with ω-ctx (1 μM) to block N-type Ca^{2+} channels (n = 3; not shown). In all cases the effects of ω-agatx were poorly reversible. From a total of 8 GPN neurons tested, ω-agatx inhibited Ca^{2+} currents in 6 cases, suggesting that most neurons expressed P- and/or Q-type Ca^{2+} channels; in the two remaining cases (one proximal and one distal neuron) ω-agatx had no detectable effect on Ca^{2+} current. Since the same variability was observed in the expression of Ca^{2+} channel

subtypes among the proximal and distal populations of GPN neurons, results obtained from both populations were pooled to simplify data presentation in Figs. 4-6.

Steady-state inactivation of transient Ca^{2+} currents

A steady-state inactivation curve was obtained for the transient component of the Ca^{2+} current in a group of 3 distal GPN neurons (Fig. 7). In these experiments the transient component was first isolated from the long-lasting component of the Ca^{2+} current by pre-treatment with ω-ctx (1 μM) and nifedipine (50 μM) to block N- and L-type currents respectively. Steady-state inactivation data for the transient Ca^{2+} current were fitted by Boltzmann equation (r^2 was 0.99), and the estimated values of $V_{1/2}$ was – 56.6 ± 0.5 mV and $S_{1/2}$ was 10.9 ± 0.5 (see Fig. 7). These data imply that at the resting potential of GPN neurons (i.e. ~ -54 mV, see Table 1), approximately one-half of the transient population of Ca^{2+} channels are available for carrying current, though at least two subtypes (i.e. T- and R-types) appear to contribute. As explained for Na^+ currents (see above), neurons were studied no later than 18-24 hr after isolation to minimize clamping errors. Attempts to obtain inactivation curves for the prolonged component of Ca^{2+} currents were unsuccessful, due to 'run down' of these currents over time.

Voltage-gated K^+ currents

Application of depolarizing step potentials caused activation of outward currents in GPN neurons (Fig. 8 A; n = 6 and 11, for proximal and distal neurons respectively). These outward currents were carried predominantly by K^+ ions, since they were blocked

in a dose-dependent manner by classical K^+ channel blockers, such as TEA (IC_{50} ~ 7.9 mM; Fig. 8 B, n = 5) and 4-AP (Fig. 8 C, n = 5). GPN neurons were particularly sensitive to 4-AP since concentrations as low as 10^{-4} M caused ~ 35 % inhibition of the outward current at a step potential of +30 mV (Fig. 8 C). Furthermore, we recently reported that application of 200 μM Cd^{2+}, an indirect blocker of Ca^{2+}-dependent K^+ currents, caused ~ 10-15 % inhibition of the outward currents in GPN neurons (Campanucci *et al.* 2003a). Therefore, these data taken together suggest that most of the outward K^+ current present in these neurons is carried by delayed rectifier-type and Ca^{2+}-activated K^+ channels, though the latter are iberiotoxin- and apamin-insensitive (Campanucci *et al.* 2003a).

Action potential generation in GPN neurons

GPN neurons elicited action potentials upon injection of near-threshold or suprathreshold depolarizing current pulses (Fig. 9). These action potentials were due mainly to Na^+ ions since they were abolished by 0.1 μM TTX (Fig. 9). Table 2 summarizes data from proximal and distal GPN neurons on various action potential parameters including amplitude, duration (at 0 mV), threshold voltage, and overshoot. In addition, some GPN neurons (n = 10, Fig. 11 C) were spontaneously active in culture. Though not studied in detail, it appeared that spontaneous activity was more common when bicarbonate buffer was used in the extracellular solution and the temperature was raised to ~ 35 °C.

GPN neurons and O_2-sensing

As recently described (Campanucci *et al.* 2003a), GPN neurons were sensitive to moderate-to-severe hypoxia (PO_2 ~ 15 Torr), resulting in inhibition of a background K^+ current that showed outward rectification in physiological K^+ solutions. In the present study, O_2 sensitivity of outward K^+ current in GPN neurons was compared over a broader range of PO_2 using ramp depolarizations, or step depolarizations to +30 mV (Fig. 10 B), a potential within the range of spiking GPN neurons (Fig. 9, 11). As illustrated in Fig. 10 A-C, lowering PO_2 from 150 Torr (normoxia) to 80 and 5 Torr resulted in a dose-dependent inhibition of the outward K^+ current (at +30 mV) in a group of 7 distal GPN neurons. Furthermore, this response was unaltered by the presence of classical K^+ channel blockers, i.e. 4-AP (2 mM) and TEA (10 mM), and was observed in both proximal and distal GPN neurons (Fig. 10 D, E; n = 5 for each population). The relation between PO_2 and percent K^+ current inhibition is summarized in Fig. 10 F, which includes data from our previous study (Campanucci *et al.* 2003a). To determine whether O_2 sensitivity of GPN neurons required an intact cytoplasm, we compared data from perforated-patch recording (Fig. 10 A-E), with those using conventional whole-cell recording from 'dialysed' cells. As exemplified in Fig. 10 G, hypoxic inhibition of K^+ currents was absent in dialysed cells (n = 5), suggesting that cytoplasmic factors are required for mediating O_2 sensitivity in GPN neurons.

The effect of hypoxia on membrane excitability was also studied under current clamp conditions in GPN neurons that were quiescent or spontaneously active. As exemplified in Fig. 11 A-B (n = 10), hypoxia depolarized and increased the probability of

cell firing in neurons that were initially quiescent (see also Campanucci *et al.* 2003a,b). This is consistent with our recent report that hypoxia caused depolarization of the neuronal resting potential, which in some cases led to action potential generation (Campanucci *et al.* 2003a). In neurons that were spontaneously active, hypoxia caused membrane depolarization and an increase in the probability of firing (Fig. 11 C-D; n = 3). A comparison of action potential duration revealed that the effects of hypoxia were accompanied by a broadening of the action potential (see Fig. 11 D), consistent with the inhibition of K^+ channels. In addition, in spontaneously active neurons a decrease in spike amplitude during hypoxia was observed (Fig. 11 C-D), possibly due to inactivation of Na^+ channels during the sustained depolarization.

DISCUSSION

In this study we characterized the biophysical properties of two populations of neurons within the rat glossopharyngeal nerve (GPN), which provide efferent innervation to a chemosensory organ, the carotid body. Activation of this efferent pathway is thought to lead to chemoreceptor inhibition, which contributes to the regulation of breathing in mammals (Prabhakar *et al.* 1993; Wang *et al.* 1993; 1994a; 1995a, Prabhakar 1999, 2000). These neurons are located in two populations, one dispersed around the bifurcation of the GPN and carotid sinus nerve, and the other concentrated more distally along the GPN (Campanucci *et al.* 2003a). Both populations had similar passive membrane properties and, as discussed below, a variety of voltage-dependent Na^+, Ca^{2+} and K^+ channels. A unique population of O_2-sensitive voltage-independent, background K^+ channels has been previously identified in these cells (Campanucci *et al.* 2003a; see chapter 3). In the present study, we made the novel observation that the vital styryl dye, 4-Di-2-ASP (D289), provided a convenient and simple method of labeling both populations of GPN neurons in living tissue. While the mechanism underlying this dye labeling remains unclear, styryl dyes have proved useful for vital staining of a variety of sensory cells, nerve fibers, and cells expressing purinergic P2X receptors (Lichtman *et al.* 1987; Magrassi *et al.* 1987; Nurse and Farraway, 1989; Meyers *et al.* 2003). The method should prove useful in future studies for routine identification of other autonomic ganglion neurons associated with visceral nerve fibers.

Voltage-dependent currents in glossopharyngeal neurons

Na^+ currents: Sodium currents in GPN neurons were mostly TTX-sensitive, since 80 % of these currents was inhibited by low doses of TTX (< 1 μM). Interestingly, the Na^+-inactivation curve for GPN neurons was shifted to more positive potentials compared to neighboring petrosal (Stea and Nurse, 1992; Cummins *et al.* 2002) and other (Herzog *et al.* 2003a,b; Black *et al.* 2004) sensory neurons. Thus the $V_{1/2}$ for GPN neurons was –33.3 ± 1.3 and –25.0 ± 1.0 mV for the proximal and distal groups respectively, compared to -53.5 mV for petrosal neurons (Stea and Nurse, 1992) and -73.8 mV for dorsal root ganglion neurons (Black *et al.* 2004). It has been reported that some chimeric Na^+ channels (Na(v)1.2 + Na(v)1.5) display $V_{1/2}$ at more depolarized potentials than those of the separate recombinant Na^+ channels (Mantegazza *et al.* 2001). Furthermore, there is evidence that Na^+ channel gating and inactivation properties can be modulated by the expression of different β subunits (Qu *et al.* 2001). The fact that several GPN neurons were spontaneously active, especially during recordings in bicarbonate buffer at ~ 35 °C, is consistent with the expression of Na^+ channels that are largely removed from inactivation at voltages close to the resting potential (~ -55 mV, see Table 1).

Ca^{2+} currents: GPN neurons were found to express a wide variety of voltage-gated Ca^{2+} channels. The individual components were distinguished on the basis of their pharmacological properties and, to some extent, their voltage-dependent gating. Evidence was obtained for the expression of at least five Ca^{2+}-current components, i.e. L-, N-, P and/or Q-, T- and R-type currents. Most of the currents may be categorized as high

voltage-activated (HVA), although the T-types are considered low voltage-activated (LVA). Of the five types of Ca^{2+}currents expressed, the predominant N-type or ω-conotoxin GVIA-sensitive current was activated at ~ -20 mV and peaked at ~ 0 mV (see Fig. 4 B). The nifedipine-sensitive (L-type) and the ω-agatoxin IVA-sensitive (P/Q-type) currents appeared as smaller components and were activated at potentials ~ -30 mV and ~ -10 mV, respectively (see Fig. 6 A, B). On the other hand, the transient component of the Ca^{2+} current was Ni^{2+}-sensitive (T- and R-types), activating at ~ -40 mV and reaching peak values at ~ -10 mV (see Fig. 5 A). Use of the selective R-type Ca^{2+} channel blocker, SNX-482, permitted isolation of the residual (~ 75 %) T-type current from the overall transient component (Fig. 5 B). Thus, the Ni^{2+}-sensitive transient current in GPN neurons appeared to consist of both T- and R-components. Different Ca^{2+} channels have been proposed to have specific cellular functions. For example, N-type calcium channels have been proposed to initiate synaptic vesicle fusion on activation by action potentials that depolarize the pre-synaptic membrane (Wu and Saggau, 1994). In sensory neurons, both L-type and N-type Ca^{2+} channels appear to play a role in the regulation of neurotransmitter expression by activity-dependent mechanisms (Brosenitsch *et al.* 1998; Brosenitsch and Katz, 2001). Since T-type channels are activated at lower threshold voltages, they help transiently in action potential initiation and in the control of repetitive firing in neurons and other (e.g. cardiac) cells. Little is known about the role of R-type calcium channels in neuronal function, but recent evidence suggests that they are important in dendritic calcium entry and synaptic transmission (Wu and Saggau, 1994;

Wu *et al.* 1998). Thus, the degree of Ca^{2+} channel diversity observed in single GPN neurons allows Ca^{2+} influx to be regulated over a wide range of voltages.

K^+ currents: The voltage-dependent outward K^+ currents were mediated mainly by delayed rectifying K^+ channels, since they were strongly inhibited by 4-AP (2 mM) and TEA (10 mM). In addition, we recently reported that GPN neurons express a Ca^{2+}-activated K^+ current that was relatively insensitive to 100 nM iberiotoxin and 100 nM apamin (Campanucci *et al.* 2003a), blockers of large (BK) and small (SK) conductance Ca^{2+}-dependent K^+ channels respectively.

Physiological role of Ca^{2+} channels in GPN neurons

GPN neurons express an O_2-sensitive background K^+ conductance, which is inhibited in a dose-dependent manner by a decrease in PO_2 over the range 80-5 Torr (this study; Campanucci *et al.* 2003a). These findings, together with the observation that hypoxia depolarizes and increases firing frequency in spontaneously active GPN neurons, suggest that these cells are particularly well equipped for fine regulation of intracellular Ca^{2+} levels, via the wide diversity of Ca^{2+} channel types, i.e. L, T, N, P/Q and R, observed in this study. Together, these mechanisms allow for regulation of NO synthesis and release, dependent on O_2 availability. GPN neurons provide NO-mediated efferent inhibition to a chemosensory organ, i.e. carotid body (Wang *et al.* 1994a,b, 1995a,b), that is itself excited by hypoxia particularly over an arterial PO_2 range of 5-60 Torr (González *et al.* 1994). Therefore, this negative feedback efferent pathway should allow GPN

neuronal activity to provide exquisite control of carotid body function over a broad range of PO_2.

Acknowledgements

We thank Cathy Vollmer for expert technical assistance throughout this study, which was supported by a grant from the Canadian Institutes for Health Research to C.A.N. (MOP-57909), and CIHR scholarship to V.A.C.

Table 1. Passive membrane properties and resting potential in proximal and distal populations of GPN neurons. *Vm*, resting potential; C_{in}, input capacitance; R_{in}, input resistance; *n:* number of neurons tested.

GPN location	V_m *(mV)*	C_{in} *(pF)*	R_{in} *(GΩ)*	*n*
proximal	-53.9 ± 1.2	25.0 ± 1.2	1.5 ± 0.2	40
distal	-53.3 ± 0.6	27.4 ± 0.7	1.6 ± 0.1	178

Table 2. Action potential properties in proximal and distal populations of GPN neurons. *Amp*, action potential amplitude from resting potential- to- peak; *Duration*, action potential duration at 0 mV; *Threshold*, threshold voltage at which action potentials are generated; *Overshoot*, amplitude to peak from 0 mV; *n*, number of neurons tested. Data are expressed as mean ± s.e.m.,

GPN location	*Amp (mV)*	*Duration (ms)*	*Threshold (mV)*	*Overshoot (mV)*	*n*
proximal	114.8 ± 11.2	2.3 ± 0.1	-37.3 ± 2.1	62.2 ± 1.0	3
distal	125.5 ± 8.3	2.2 ± 0.3	-33.2 ± 0.9	62.9 ± 2.6	5

Figure 1. Styryl pyridinium dye (D289) staining of a whole-mount of the rat glossopharyngeal nerve. Dye was injected ~ 10 hr before the animal was sacrificed. Note D289-fluorescence in both populations (proximal and distal) of GPN neurons. Optical sections were sampled every 1.5 μm; sample depths were ~ 25 μm and ~ 21 μm for the proximal and distal populations respectively.

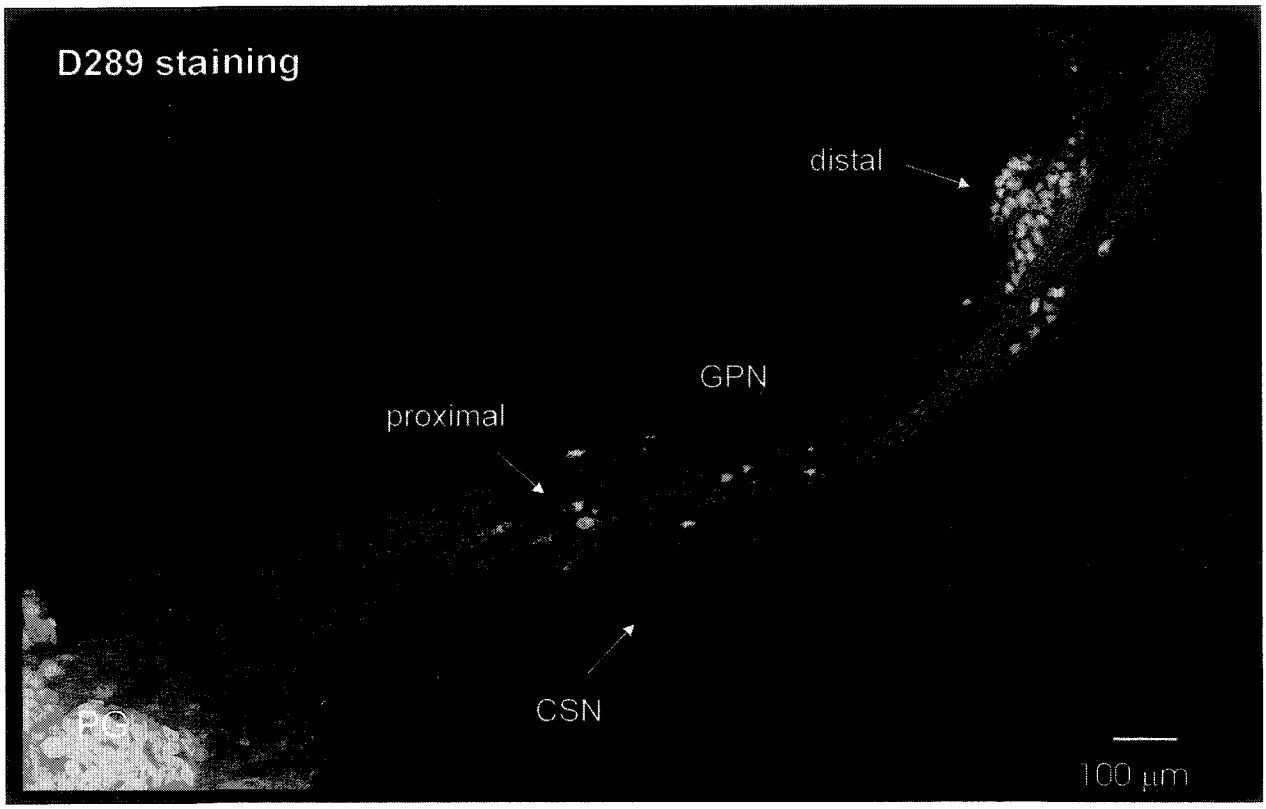
D289 staining
distal
GPN
proximal
CSN
PG
100 µm

Figure 2. Membrane currents and appearance of GPN neurons in culture. A, Differential interference contrast (DIC) image of a cultured (distal) GPN neuron 24 hr after isolation. Similar conditions were used for recording whole-cell currents by the perforated-patch technique as in B. C, I-V plots of the peak inward and outward currents shown in B.

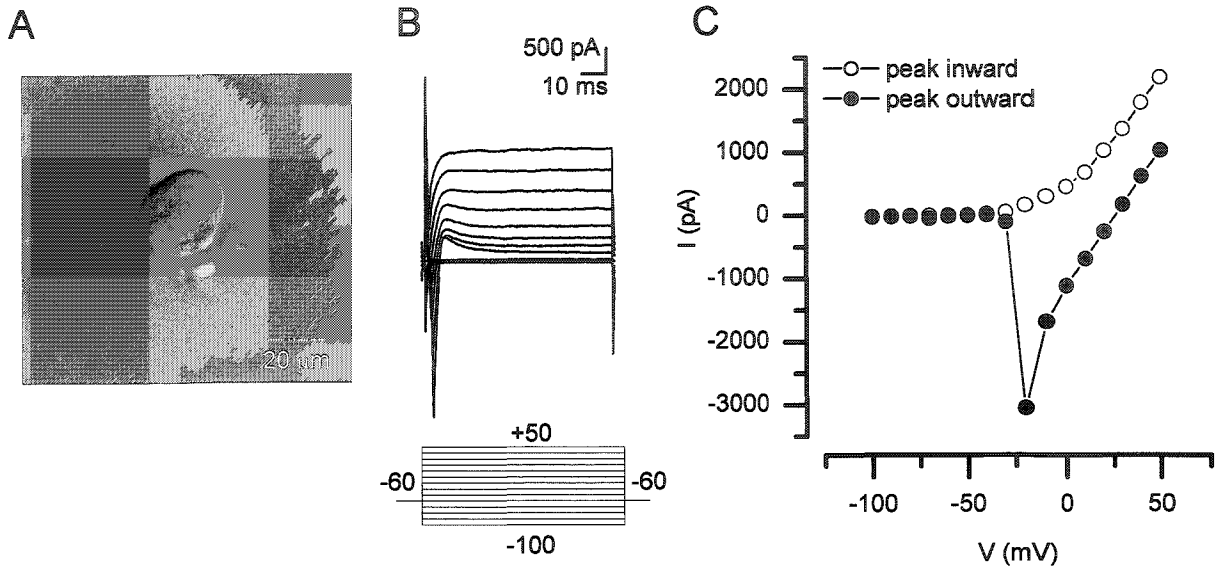
A
20 µm
B
500 pA
10 ms
+50
-60
-60
-100
C
peak inward
peak outward
2000
1000
0
-1000
-2000
-3000
I (pA)
-100
-50
0
50
V (mV)

Figure 3. Na^+ currents in GPN neurons. A, Na^+ currents were activated by application of test potentials from –100 to + 40 mV (increments of 10 mV) for a group of 5 proximal and 5 distal neurons. Current density or voltage plots are shown on right for both populations. Traces (left) show a representative example of current elicited during a step from –100 mV to –10 mV. B, Dose-dependent inhibition of Na^+ currents by TTX. Example traces (left) show the effect of increasing doses of TTX from 0.1 to 5 μM; dose-response curves for both populations (proximal and distal) are shown on right. For proximal and distal neurons the IC_{50} was 0.2 ± 0.1 and 0.1 ± 0.0 μM, respectively (n = 5 for each dose); the IC_{50} values were not significantly different. C, Steady-state inactivation curves for the Na^+ current generated by a single step to 0 mV from various pre-step holding potentials (left, example traces). Inactivation curves were fitted by the Boltzmann equation (see Methods, n = 5 for each group), with values of $V_{1/2}$ = –33.3 ± 1.3 and –25.0 ± 1.0 mV for proximal and distal populations respectively; the corresponding values for $S_{1/2}$ were 7.8 ± 0.6 and 9.1 ± 0.6 respectively.

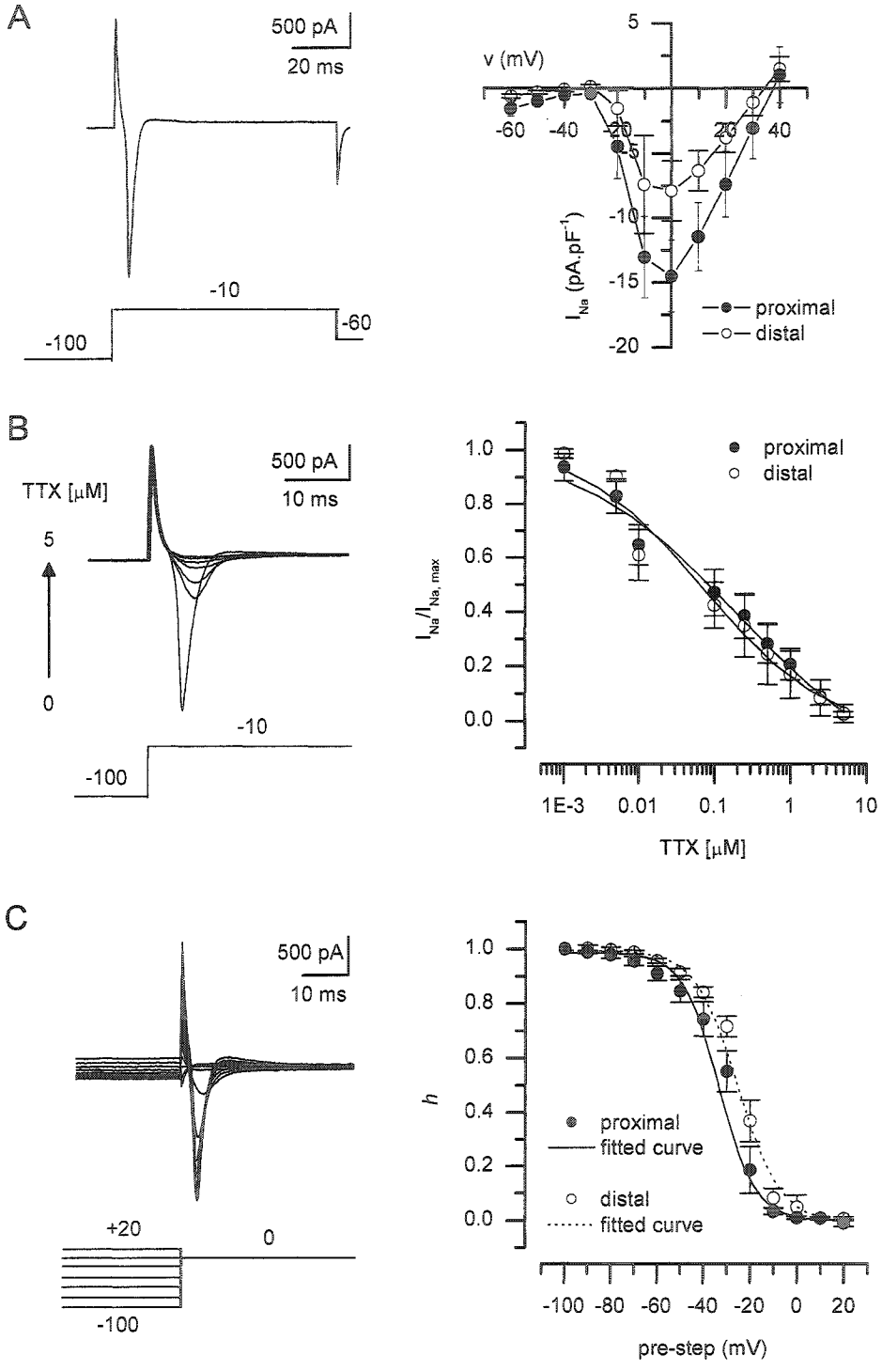
A
500 pA
20 ms
-10
-60
-100
v (mV)
5
-60
-40
-20
20
40
-5
-10
-15
-20
I_{Na} (pA.pF^{-1})
proximal
distal
B
TTX [μM]
5
0
500 pA
10 ms
-10
-100
1.0
0.8
0.6
0.4
0.2
0.0
$I_{Na}/I_{Na,\,max}$
proximal
distal
1E-3
0.01
0.1
1
10
TTX [μM]
C
500 pA
10 ms
+20
0
-100
h
proximal
fitted curve
distal
fitted curve
-100
-80
-60
-40
-20
0
20
pre-step (mV)

Figure 4. Sensitivity of Ca^{2+} current to cadmium (Cd^{2+}) and the N-type Ca^{2+} channel blocker, ω-conotoxin GVIA (ω-ctx). A, Example traces (left) and I-V plot (right) for Ca^{2+} currents recorded from a distal GPN neuron. Note that 200 μM Cd^{2+} completely inhibited Ca^{2+} currents. B, Irreversibly inhibition of prolonged component of voltage-activated Ca^{2+} current by ω-ctx (1 μM). Example traces (left) and I-V plot for a group of 6 neurons (right). The ω-ctx-sensitive 'difference' current is represented by gray triangles.

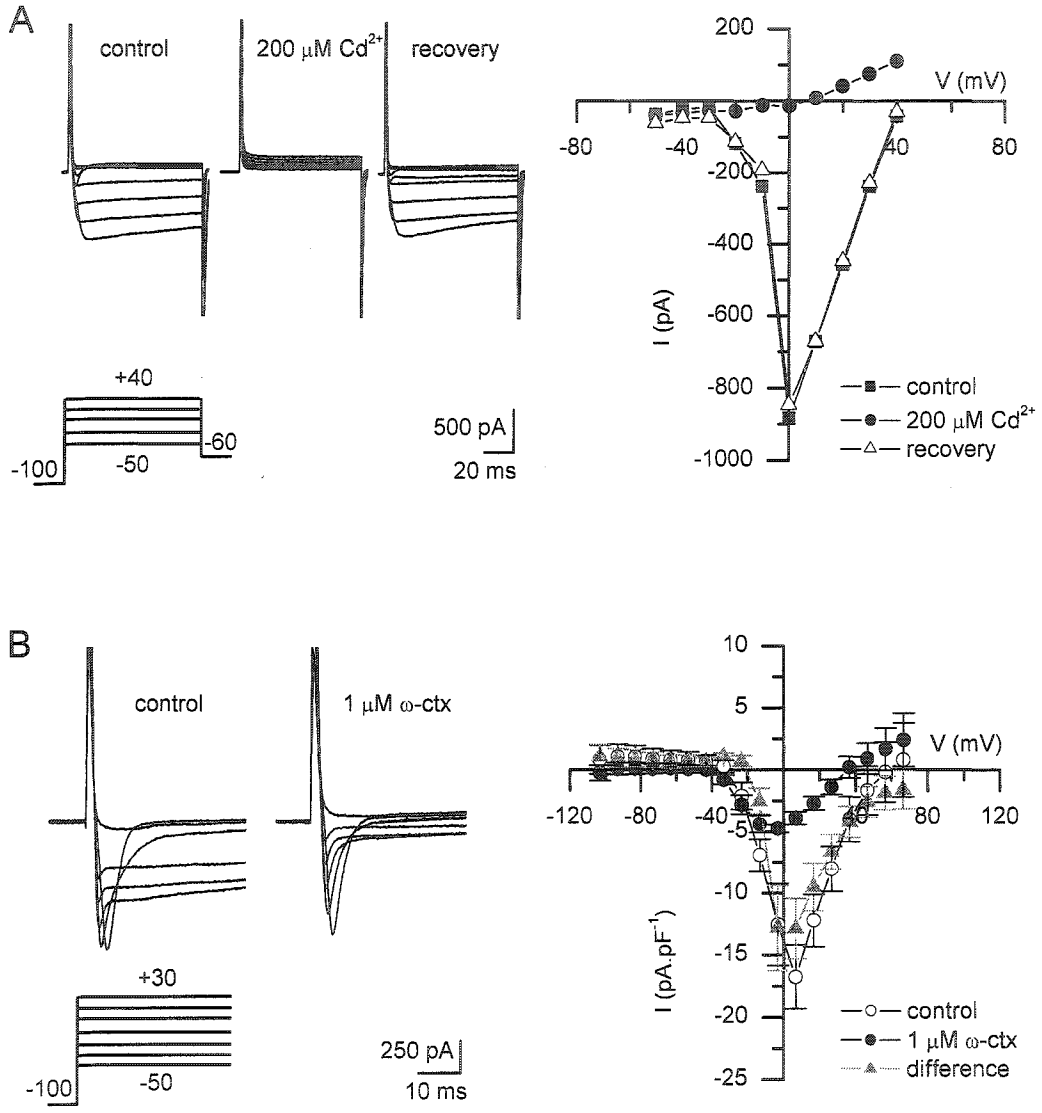
A
control
200 μM Cd2+
recovery
+40
-60
-100
-50
500 pA
20 ms
200
V (mV)
-80
-40
40
80
-200
-400
-600
-800
-1000
I (pA)
control
200 μM Cd2+
recovery
B
control
1 μM ω-ctx
+30
-100
-50
250 pA
10 ms
10
5
V (mV)
-120
-80
-40
80
120
-5
-10
-15
-20
-25
I (pA.pF-1)
control
1 μM ω-ctx
difference

Figure 5. Sensitivity of transient Ca^{2+} currents to nickel (Ni^{2+}) and the R-type Ca^{2+} channel blocker, SNX-482. To separate the transient component of the Ca^{2+} current from the prolonged component, the N-type Ca^{2+} channel blocker, ω-ctx (see also Fig. 4) and the L-type Ca^{2+} channel blocker, nifedipine (see also Fig. 6), were applied. A, Ni^{2+} (100 μM) reversibly inhibited ~ 50 % of the residual transient Ca^{2+} current. Figures show example traces (left) and I-V plot for a group of 8 neurons (right). Note the Ni^{2+}-sensitive 'difference' current in gray triangles. B, SNX-482 (50 nM) reversibly inhibited a component of the transient current. Figures show example traces (left) and I-V plot for a group of 4 neurons (right). Note the SNX-sensitive 'difference' current in gray triangles.

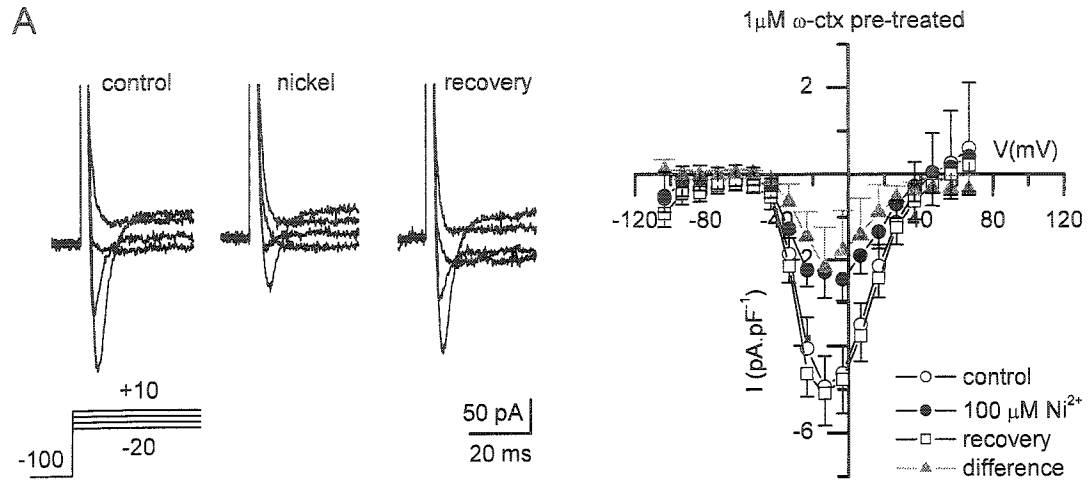
A
control
nickel
recovery
+10
-100
-20
50 pA
20 ms
1μM ω-ctx pre-treated
2
V(mV)
-120
-80
-40
40
80
120
I (pA.pF-1)
-6
control
100 μM Ni2+
recovery
difference

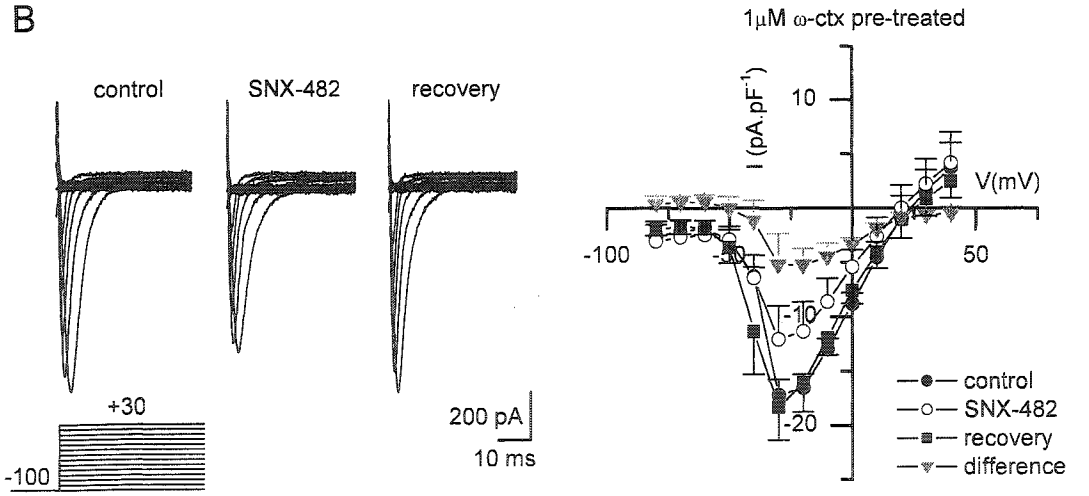
B
control
SNX-482
recovery
+30
-100
200 pA
10 ms
1μM ω-ctx pre-treated
I (pA.pF-1)
10
V(mV)
-100
50
-10
-20
control
SNX-482
recovery
difference

Figure 6. Sensitivity of the prolonged component of Ca^{2+} current to the L-type Ca^{2+} channel blocker, nifedipine, and the P/Q-type Ca^{2+} channel blocker, ω-agatoxin (ω-agatx). A, Nifedipine (50 μM) reversibly inhibited a small component of the prolonged Ca^{2+} current. Figures show example traces (left) and I-V plot for a group of 8 neurons (right). Note the nifedipine-sensitive 'difference' current in gray triangles. B, ω-agatx (50 nM) inhibited a small component of the prolonged Ca^{2+} current. Figures show example traces (left) and I-V plot for a group of 3 neurons (right). Note the ω-agatx-sensitive 'difference' current in gray triangles.

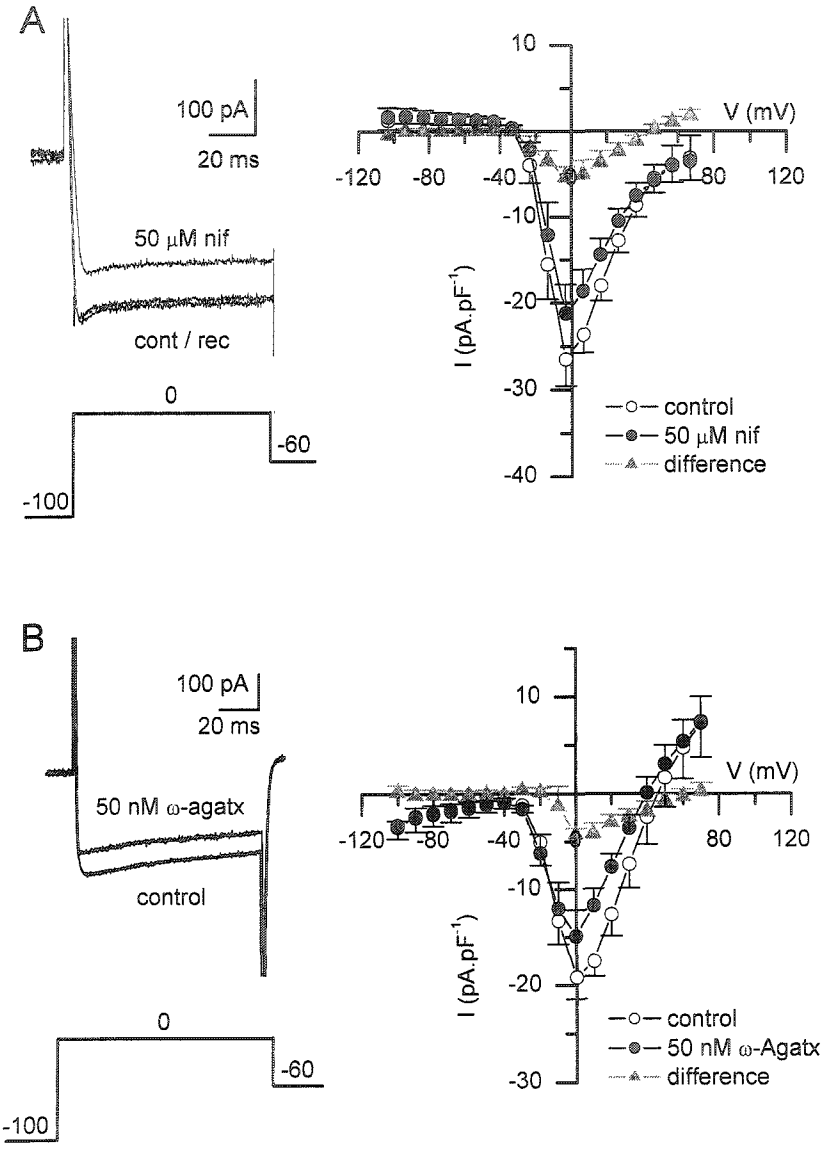
A
100 pA
20 ms
50 μM nif
cont / rec
0
-60
-100
10
V (mV)
-120
-80
-40
80
120
-10
-20
-30
-40
I (pA.pF-1)
control
50 μM nif
difference
B
100 pA
20 ms
50 nM ω-agatx
control
0
-60
-100
10
V (mV)
-120
-80
-40
80
120
-10
-20
-30
I (pA.pF-1)
control
50 nM ω-Agatx
difference

Figure 7. Steady-state inactivation curve for the transient Ca^{2+} current generated by a single step to -20 mV from various pre-step holding potentials (left, example traces). The inactivation curve was fitted by the Boltzmann equation (described in Methods, n = 3 distal neurons), with values of $V_{1/2}$ and $S_{1/2}$ of –56.6 ± 0.5 mV and 10.9 ± 0.5 respectively.

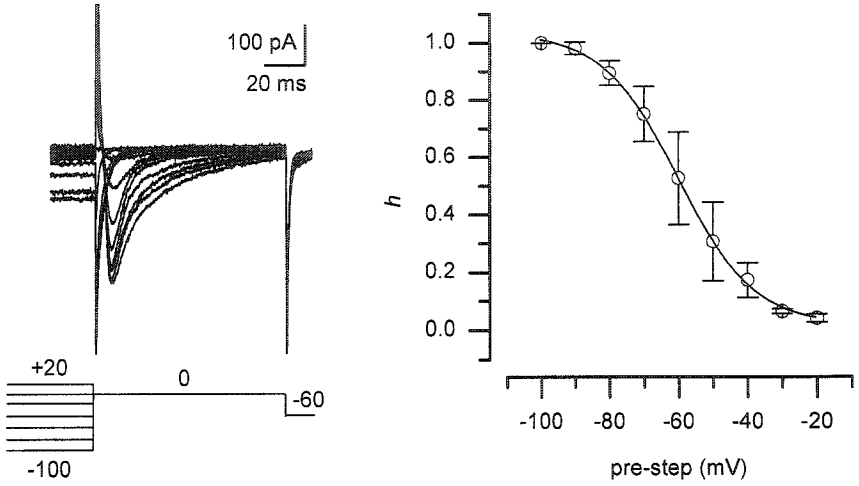
100 pA
20 ms
+20
0
-60
-100
h
1.0
0.8
0.6
0.4
0.2
0.0
-100
-80
-60
-40
-20
pre-step (mV)

Figure 8. Pharmacology of K^+ currents in GPN neurons. A, Application of depolarizing step potentials caused activation of outward currents in GPN neurons. Example traces (left) of outward currents were elicited by the voltage protocol shown below the traces. Current density I-V plots are shown on right for groups of 6 proximal and 11 distal neurons. B, An example of dose-dependent inhibition of outward current by increasing doses of TEA at a step potential of +30 mV. Dose-response curve is shown on right for a group of 5 distal neurons (IC_{50} = 7.9 mM). C, An example of dose-dependent inhibition of outward current by increasing doses 4-AP at a step potential of +30 mV. Dose-response curve is shown on right for a group of 5 distal neurons. In A-C, inward Na^+ currents were blocked by application of TTX (1 μM).

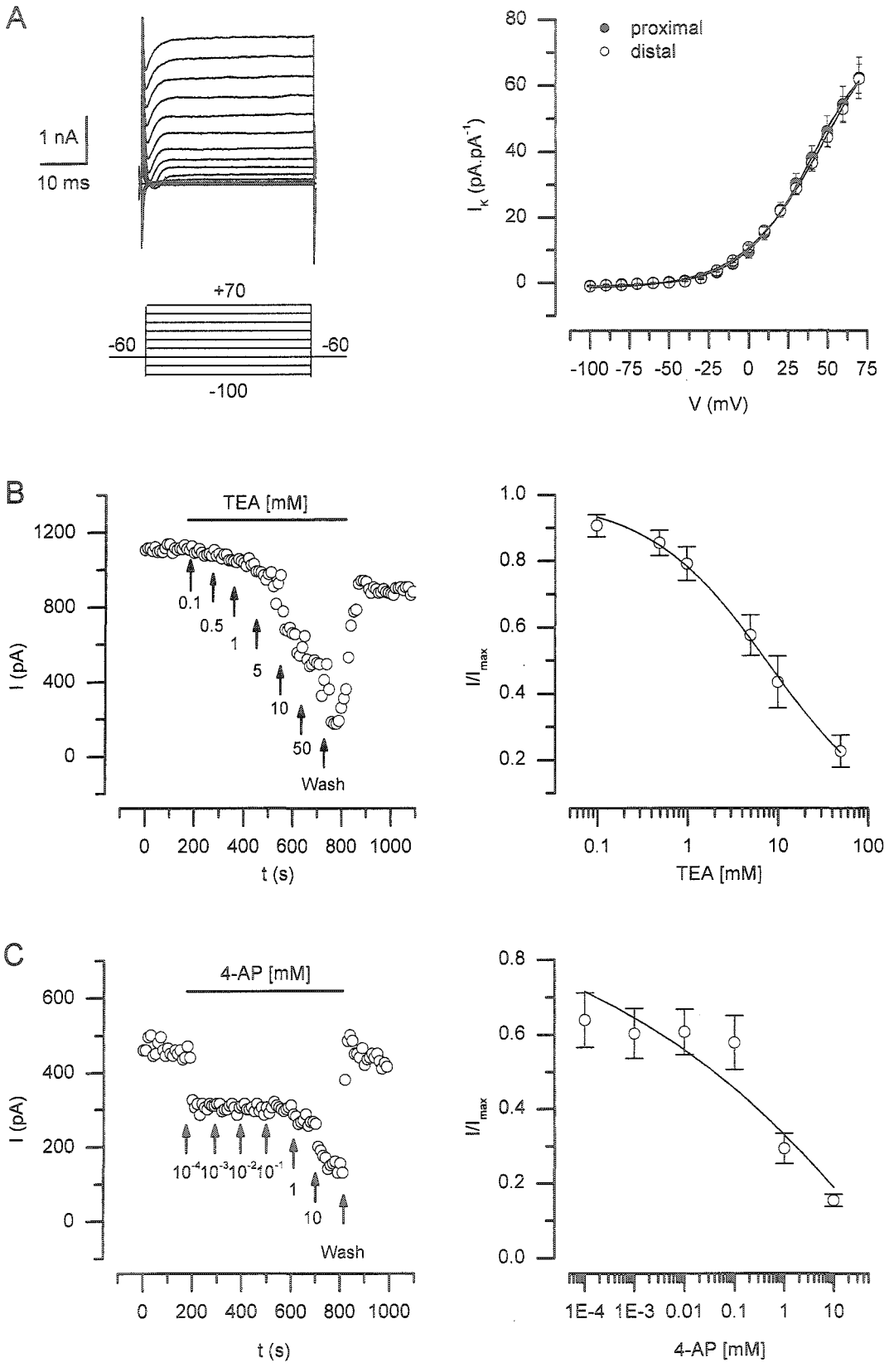
A
1 nA
10 ms
+70
-60
-60
-100
proximal
distal
I_K (pA.pA^{-1})
V (mV)
B
TEA [mM]
0.1
0.5
1
5
10
50
Wash
I (pA)
t (s)
I/I_{max}
TEA [mM]
C
4-AP [mM]
10^{-4} 10^{-3} 10^{-2} 10^{-1}
1
10
Wash
I (pA)
t (s)
I/I_{max}
4-AP [mM]

Figure 9. Action potential generation in GPN neurons. Action potentials were elicited upon injection of near-threshold depolarizing current pulses. Detailed traces (top; single pulse) show depolarization caused by injection of current for 350 ms in the absence and presence of TTX (0.1 μM). Note that TTX reversibly abolished spike activity (lower trace; repetitive pulses).

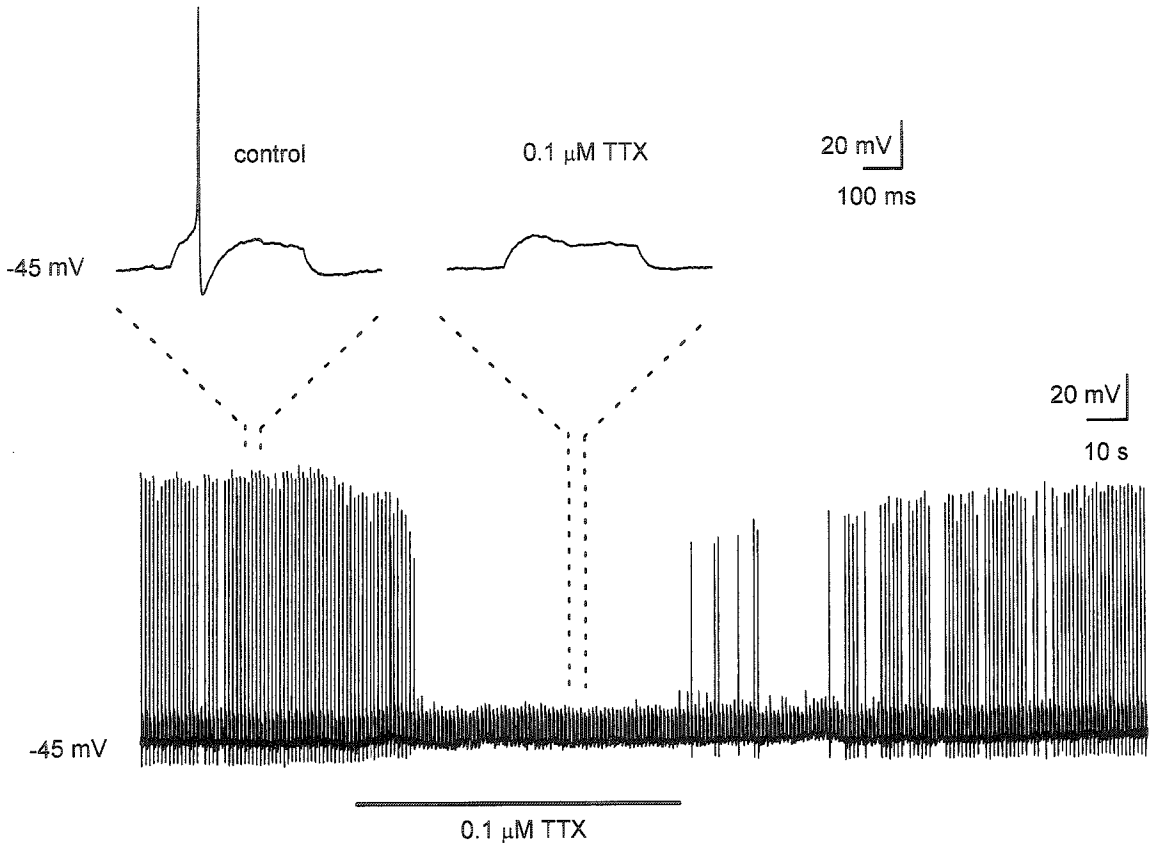
control
0.1 μM TTX
20 mV
100 ms
-45 mV
20 mV
10 s
-45 mV
0.1 μM TTX

Figure 10. O_2-sensitivity in GPN neurons. A, Effects of three levels of PO_2, ~ 150, ~ 80 and ~ 5 Torr, applied for a period of 3 min, on the outward current recorded at a step potential to +30 mV. Reduction in PO_2 from ~ 150 Torr caused a dose-dependent inhibition of the outward current. Trace in blue represents a mean of 3 amperometric measurements of PO_2 levels in the bathing solution. Note that PO_2 and current values were not simultaneously recorded. Current values were obtained from a group of 7 distal neurons. B, Representative example traces of data shown in A; normoxic (nox) PO_2 is defined arbitrarily as 150 Torr. C, Histogram compares the magnitude of the outward current density at +30 mV, at the three different PO_2; significant differences between paired groups are indicated by asterisk (*, $P < 0.05$). D, Effect of hypoxia (PO_2 ~ 15 Torr) in the presence and absence of classical K^+ channel blockers (4-AP and TEA; n = 5 for proximal (black circles) and distal (red circles) populations). Note that hypoxia-induced inhibition of outward current persisted in the presence of TEA and 4-AP (see Campanucci *et al.* 2003a). E, Example traces of the data shown in D. F, Dose-response curve for PO_2 vs percentage of maximum inhibition of outward K^+ current; maximum inhibition was chosen to correspond to that at a PO_2 of 5 Torr. Sample size n = 5 distal neurons. G, I-V plots of the effects of hypoxia (~ 15 Torr) on a group of 5 distal GPN neurons during recording with the conventional whole-cell technique. Note the lack of hypoxia-induced inhibition of K^+ current with this configuration of the patch clamp technique, possibly due to dialysis of key cytoplasmic components. In A-F, the perforated-patch variation of the technique was used, so as to preserve cytoplasmic integrity.

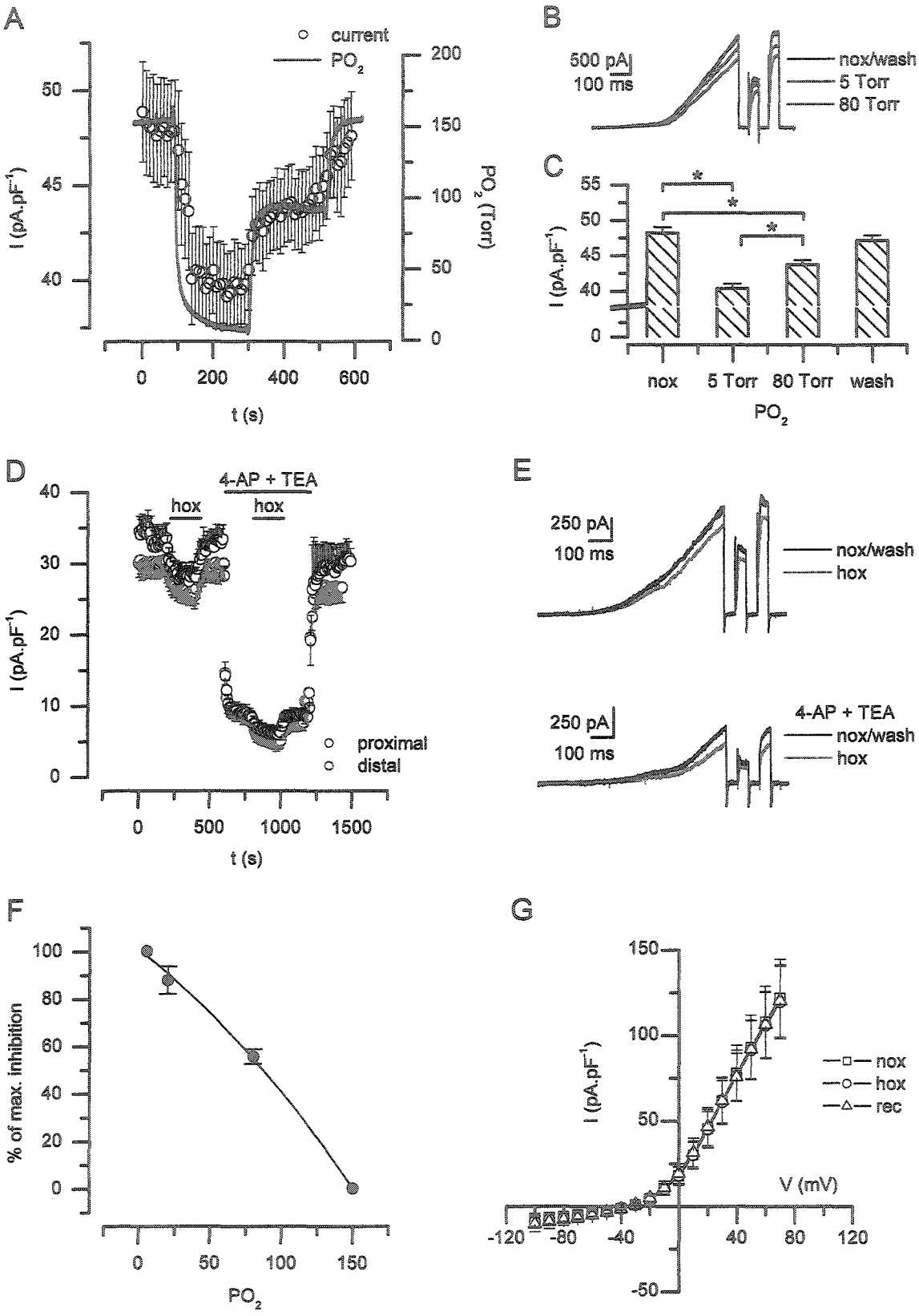
A
current
PO2
I (pA.pF-1)
PO2 (Torr)
t (s)
B
500 pA
100 ms
nox/wash
5 Torr
80 Torr
C
I (pA.pF-1)
nox
5 Torr
80 Torr
wash
PO2
D
4-AP + TEA
hox
hox
proximal
distal
I (pA.pF-1)
t (s)
E
250 pA
100 ms
nox/wash
hox
4-AP + TEA
F
% of max. inhibition
PO2
G
I (pA.pF-1)
V (mV)
nox
hox
rec

Figure 11. Effect of hypoxia on neuronal membrane potential and excitability. A, Effect of hypoxia (~ 15 Torr) on the probability of firing following repeated injections of constant near-threshold depolarizing current pulses. Note that hypoxia caused a small depolarization (seen more clearly in B) and increased the probability of cell firing (C). B, Expanded traces comparing the resting potential and action potential shape during normoxia (solid line) vs hypoxia (dotted line); note action potential broadening during hypoxia (inset). Arrow marks the start of the depolarizing step of 350 ms duration. C, Representative example of a spontaneously active distal GPN neuron, in which hypoxia caused depolarization and increased probability of firing. D, Comparison of the shape of single spontaneous action potentials generated in C during normoxia and hypoxia; note amplitude reduction and broadening of the spike during hypoxia (inset).

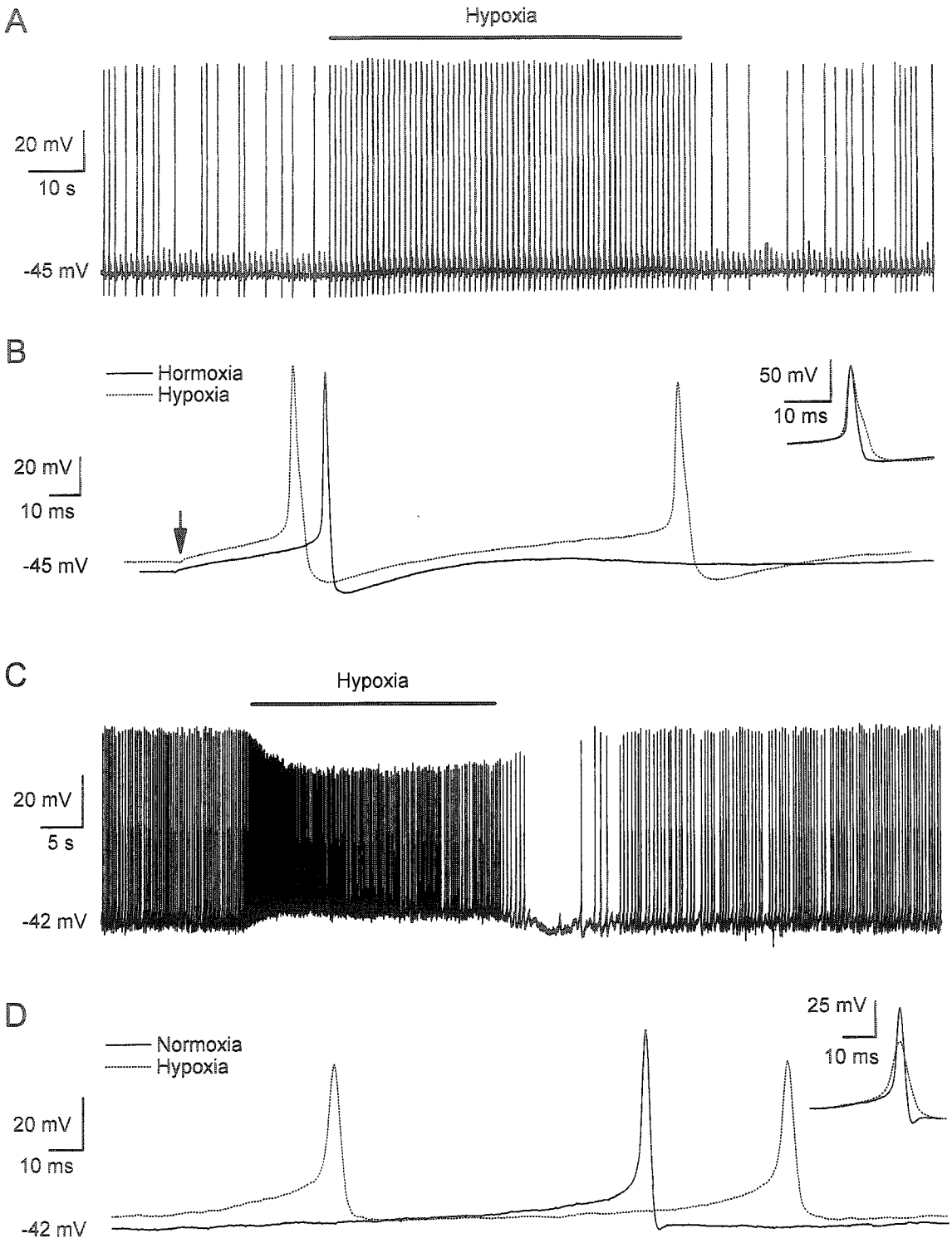
A
Hypoxia
20 mV
10 s
-45 mV
B
Hormoxia
Hypoxia
50 mV
10 ms
20 mV
10 ms
-45 mV
C
Hypoxia
20 mV
5 s
-42 mV
D
25 mV
10 ms
Normoxia
Hypoxia
20 mV
10 ms
-42 mV

CHAPTER 3

A novel O_2-sensing mechanism in glossopharyngeal neurons mediated by a halothane-inhibitable background K^+ conductance

This work has been previously published as:

Campanucci VA, Fearon IM, Nurse CA (2003) *Journal of Physiology,* 548:731-43.

I was responsible for performing all experiments, data analysis and preparation of the manuscript. Dr. Fearon was involved in the discussion of the data.

ABSTRACT

Modulation of K^+ channels by hypoxia is a common O_2-sensing mechanism in specialised cells. More recently, acid-sensitive TASK-like background K^+ channels, which play a key role in setting the resting membrane potential, have been implicated in O_2-sensing in certain cell types. Here, we report a novel O_2-sensitivity mediated by a weakly pH-sensitive background K^+ conductance in nitric oxide synthase (NOS)–positive neurons of the glossopharyngeal nerve (GPN). This conductance was insensitive to 30 mM TEA, 5 mM 4-AP, and 200 μM Cd^{2+}, but was reversibly inhibited by hypoxia (PO_2 = 15 mmHg), 2-5 mM halothane, 10 mM barium and 1 mM quinidine. Notably, the presence of halothane occluded the inhibitory effect of hypoxia. Under current clamp, these agents depolarised GPN neurons. In contrast, arachidonic acid (5-10 μM) caused membrane hyperpolarization and potentiation of the background K^+ current. This pharmacological profile suggests the O_2-sensitive conductance in GPN neurons is mediated by a class of background K^+ channels different from the TASK family; it appears more closely related to the THIK (tandem pore domain halothane-inhibited K^+) subfamily, or may represent a new member of the background K^+ family. Since GPN neurons are thought to provide NO-mediated efferent inhibition of the carotid body (CB), these channels may contribute to the regulation of breathing during hypoxia via negative feedback control of CB function, as well as to the inhibitory effect of volatile anesthetics (e.g. halothane) on respiration.

INTRODUCTION

Oxygen (O_2) plays a pivotal role in cell homeostasis and survival, and not surprisingly many organisms have evolved strategies for ensuring adequate supply of O_2 to the tissues. While all cells probably have some ability to sense O_2, over the last ~15 years there has been a major focus on the more specialised O_2-sensing cells, including carotid body chemoreceptors (González *et al.* 1994; Peers, 1997; López-Barneo *et al.* 2001; Prabhakar, 2000), pulmonary neuroepithelial bodies (Youngson *et al.* 1993; Fu *et al.* 2000), adrenal chromaffin cells (Thompson and Nurse, 1998), vascular smooth muscle cells (Archer *et al.* 1993, 1998; López-Barneo *et al.* 2001), and central neurons (Haddad and Jiang, 1993; 1997; Henrich *et al.* 2002; Plant *et al.* 2002). However, with the exception of pulmonary neuroepithelial bodies (Fu *et al.* 2000), the molecular identity of the PO_2 sensor is unclear though the transduction step in most cases involves modulation of various K^+ channel subtypes (Haddad and Jiang, 1997; Peers, 1997; López-Barneo *et al.* 2001; Plant *et al.* 2002).

In the last few years an emerging group of 'leak' or background potassium channels, called two-pore (2P) domain K^+ channels, has attracted special interest as targets for hypoxic modulation (Buckler 1997; Buckler *et al.* 2000; Hartness *et al.* 2001; Plant *et al.* 2002). These channels have subunits that contain four transmembrane regions surrounding two pore-forming loops in which lies the consensus sequence for the K^+ selectivity filter (Lesage and Lazdunski, 2000; Goldstein *et al.* 2001; Patel and Honoré, 2001b). In addition, these channels lack voltage-dependence and play a key role in setting the resting membrane potential and input resistance of the cell. A family of genes that

encode background K^+ channels has been recently identified, leading to the cloning and characetrization of a number of family members (Lesage and Lazdunski, 2000; Patel and Honoré, 2001a,b; Talley and Bayliss, 2002; Goldstein *et al.* 2001). The subfamilies include the acid-sensitive channels TASK-1 to TASK–5 (Duprat *et al.* 1997; Reyes *et al.* 1998; Kim *et al.* 2000; Ashmole *et al.* 2001; Decher *et al.* 2001; Vega-Sáenz *et al.* 2001), the mechanosensitive channels TREK-1, TREK-2 and TRAAK, the weak inward rectifiers TWIK-1 and TWIK-2 (Lesage and Lazdunski, 2000; Patel and Honoré, 2001a,b), TALK-1 (Girard *et al.* 2001), and the halothane-inhibited channels THIK-1 and THIK-2 (Rajan *et al.* 2001). The background channels differ from other major K^+ channel families (e.g. the voltage gated Kv channels), which consist of subunits with only a single pore-forming domain.

Interestingly, two members of the 2P K^+ channel family, TASK-1 (Kcnk3) and TASK-3 (Kcnk9), have been found to be O_2-sensitive in different tissues. A TASK-1-like conductance has been shown to be O_2-sensitive in rat carotid body chemoreceptors (Buckler *et al.* 2000) and cerebellar granule neurons (Plant *et al.* 2002), whereas TASK-3 appears to be O_2-sensitive in the lung carcinoma cell line H146, which are a model for pulmonary neuroepithelial bodies (Hartness *et al.* 2001).

In the present study we have characterised a novel O_2-sensing mechanism in neurons from the rat glossopharyngeal nerve (GPN). These autonomic neurons, together with a population of sensory neurons located in the petrosal ganglion, give rise to an extensive plexus of nitric oxide (NO)-synthesising nerve fibers that innervate the carotid body and are thought to play a key role in chemoreceptor adaptation to hypoxia

(Prabhakar *et al.* 1993; Wang *et al.* 1993, 1994a,b, 1995a,b; Höhler *et al.* 1994; Grimes *et al.* 1994). Interestingly, our electrophysiological and pharmacological characetrization of the O_2-sensitive K^+ conductance in GPN neurons revealed properties inconsistent with those of TASK-1 or TASK-3. Rather, the pharmacological profile suggested a new class of O_2-sensitive background K^+ channels that appear more closely related to the tandem pore domain, halothane-inhibited K^+ (THIK) channel family (Rajan *et al.* 2001), which are highly expressed in brain where their physiological function is unknown. Alternatively, the O_2-sensitive background K^+ channel expressed in GPN neurons may belong to a new subfamily not yet described, or to a new variant of one of the already described 2P domain members.

METHODS

Cell culture. A section of the glossopharyngeal nerve (GPN), extending from its intersection with the carotid sinus nerve (CSN) to a region ~ 5 mm distal to the intersection, was dissected from Wistar rat pups (10-14 days old, Charles River Laboratory, St. Constant, QC, Canada). Pups were first stunned by a blow to the head that rendered them unconscious, and then killed by decapitation before removing the carotid bifurcation, surrounding ganglia and attached nerves. All procedures for animal handling were carried out according to the guidelines of the Canadian Council on Animal Care (CCAC). The distal GPNs were pooled, digested with enzyme (0.1 % Collagenase, Invitrogen Canada Inc., Burlington, ON, Canada; 0.1 % trypsin, Sigma; and 0.01 % DNase, Invitrogen) and mechanically dissociated to produce dispersed GPN neurons that were grown on a thin layer of Matrigel (Collaborative Research, Bedford, MA, USA). The solutions and culture procedures were identical to those described elsewhere for the carotid body (Zhong *et al.* 1997). Cultures were grown at 37 °C in a humidified atmosphere of 95 % air-5 % CO_2, and used either for patch-clamp experiments or immunofluorescence studies ~ 24-48 hr following isolation.

NADPHd cytochemistry. GPN whole-mounts were rinsed in pre-warmed phosphate buffered saline (PBS) and fixed in 4 % para-formaldehyde overnight at 4 °C. After washing in PBS (3 × 5 min) the tissue was permeabilised in 0.5 % Triton X-100/TRIS-HCl overnight and incubated in NADPH (Sigma)/NBT/0.5 % Triton X-100/TRIS-HCl,

for 30 min at 37 °C in the dark. Whole-mounts were examined under brightfield optics after rinsing (3 × 5 min) with TRIS-HCl.

Immunofluorescence. Whole-mounts of the GPN or cultured GPN neurons were fixed in 4 % para-formaldehyde overnight at 4 °C or for 15 min at room temperature (RT), respectively. After washing in PBS (3 × 5 min) whole-mounts were incubated for 72 hr at 4 °C with primary antibody; an overnight incubation was used for cultures. Primary antibodies were: polyclonal rabbit anti-rat neuronal nitric oxide synthase (nNOS; 1:200; ImmunoStar Inc., Hudson, WI, USA) or monoclonal mouse anti-rat nNOS (1:200; Sigma), and anti-neurofilament, a monoclonal antibody against NF68kDa (1:5 dilution; Boehringer Mannheim, Montreal, QC, Canada), and a polyclonal antibody against vesicular ACh transporter (VAChT) raised in goat (1:200; Chemicon International, Temecula, CA). The primary antiserum was diluted in PBS containing 1 % BSA and 0.5 % Triton X-100. After incubation, the samples were washed in PBS (3 × 5 min) and incubated in the dark for 1 hr at room temperature with the secondary antibody conjugated to Alexa 594 (1:500, Molecular Probes, OR, USA), Cy3 (1:50; Jackson ImmunoResearch Laboratories Inc., West Grove, PA, USA) or FITC (1:50; Cappel, Malvern, PA, USA). The secondary antiserum was diluted in PBS containing 1 % BSA and 0.5 % Triton X-100. Samples were covered with a photobleaching reagent (Vectashield; Vector Laboratories, Burlingame, CA, USA) and viewed with a confocal microscope (BIO RAD Microradiance 2000) equipped with argon (2 lines, 488 and 514 nm) and helium/neon (543 nm) lasers. Lasersharp software was used for image

acquisition. In control experiments incubation with secondary antibody alone resulted in complete abolition of staining.

DiI retrograde labeling. Whole-mounts of the carotid bifurcation were washed with pre-warmed PBS and fixed overnight in 4 % paraformaldehyde at 4 °C. After washing (3 × 5 min each) in 0.1 M phosphate buffer, the tissue was attached by stainless steel minutien pins (Fine Science Tools Inc., Austria) to a petri dish coated with a sylgard bed. After immersion in PBS, an opening was made in the carotid body and a small crystal of DiI (1,1'-dioctadecyl-3,3,3',3'- tetramethylindocarbocyanine perchlorate; Molecular Probes Inc.) was inserted and left in place for several weeks at 4 °C. Finally, the tissue was placed on a glass slide and covered with a photobleaching reagent, before viewing with the Confocal microscope.

Electrophysiology. The methods for obtaining nystatin perforated-patch recordings of membrane potential (current clamp) and ionic currents (voltage clamp) from GPN neurons were identical to those previously described for petrosal neurons (Stea and Nurse, 1992; Zhong *et al.* 1997). Some experiments were carried out using conventional whole-cell recording that resulted in intracellular dialysis (Hamill *et al.* 1981). Patch pipettes were made from Corning #7052 glass (A-M Systems Inc., Carlsborg, WA, USA) or borosilicate glass (WPI, Sarasota, FL, USA) using a Brown-Flaming horizontal puller (Model P-97, Sutter Instruments Co., San Francisco, CA, USA) and were fire-polished. When filled with intracellular recording solution, micropipettes had a resistance of 5-10

MΩ and formed gigaseals between 2 and 12 GΩ. Approximately 75 % of the series resistance (range, 10-20 MΩ) was compensated. Data were corrected for changes in junction potentials in different extracellular K^+ solutions using pClamp 8.0 software. Whole-cell currents were recorded at 22-25 °C using an Axopatch 1D Amplifier (Axon Instruments Inc., Union City, CA, USA) equipped with a 1 GΩ headstage feedback resistor. Signals were filtered at 1 kHz and stored on a Pentium II PC with the aid of a Digidata 1200A/B computer interface and pClamp 8.0 software (Axon Instruments). Hypoxia (PO_2 ~ 15 mmHg) was generated by bubbling 100 % N_2 into the perfusion reservoir and PO_2 measurements were obtained with the aid of a carbon-fiber electrode (10μm diameter, Dagan Corporation, Minneapolis, MN, USA) and a VA-10 NPI Amplifier (NPI Electronic, Hauptstrasse, Tamm, Germany). Control experiments were performed by bubbling the extracellular recording solution with compressed air instead of N_2 gas. The solution in the recording chamber (volume, 0.75-1 ml) was exchanged by perfusion under gravity and simultaneous removal by suction at a rate of 6 ml min^{-1} (Thompson and Nurse, 1998). The effects of hypoxia were examined by comparing peak currents from the average of three records at each step potential, over the range of -100 to +70 mV (10 mV increments) during 50 ms, or ramps from –100 to 25 mV during 100 ms, from a holding potential of -60 mV. In some traces high frequency noise was filtered with the help of Clampfit 8.0 software.

Solutions. For perforated-patch recording patch pipettes were filled with intracellular recording solution of the following composition (mM): K-Gluconate 110, KCl 25, Hepes

10, NaCl 5, $CaCl_2$ 2, pH adjusted to 7.2 with KOH, plus 500 $\mu g.ml^{-1}$ nystatin. For recordings during whole-cell configuration patch pipettes were filled with solution of the following composition (mM): K-Gluconate 110, KCl 25, Hepes 10, NaCl 5, $CaCl_2$ 1, 11 EGTA, pH adjusted to 7.2 with KOH. The extracellular recording solution contained (mM): NaCl 135, KCl 5, Hepes 10, glucose 10, $CaCl_2$ 2, $MgCl_2$ 2, pH adjusted to 7.4 with NaOH at room temperature. Some experiments, designed to dissect the O_2-sensitive K^+ current (IKO_2), were carried out in Ca^{2+} free extracellular recording solution containing different concentrations of K^+ (Na^+ substituted) and in mM: Hepes 10, glucose 10, $MgCl_2$ 2, $NiCl_2$ 2, pH adjusted to 7.4 with KOH or NaOH at room temperature.

Drugs. Various types of K^+ currents (as indicated in the text) were blocked using the following drugs: tetraethylammonium (TEA, 5-30 mM), 4-aminopyridine (4-AP, 2-5 mM), Ba^{2+} (BaCl, 10 mM) and quinidine (0.01-1 mM) (all obtained from Sigma). In some experiments cadmium ($CdCl_2$, 200 μM; Sigma) was used to block indirectly Ca^{2+}-dependent K^+ currents. In addition, some experiments were carried out in the presence of iberiotoxin (IbTx, 100 μM; Alomone) and apamin (100 nM, Alomone) to block large and small Ca^{2+}-dependent K^+ conductances respectively. To block voltage-dependent Na^+ currents, tetrodotoxin (TTX, 1 μM, Sigma) was added to the bathing solution. The volatile anaesthetic 2Bromo-2chloro-1,1,1trifluoroethane (halothane; 2-5 mM, Fluka), arachidonic acid (AA, 5 μM, Sigma), ruthenium red (RR, 1-10 μM, Sigma) and anandamide (AN, 1-10 μM, Sigma) were added to the extracellular solution in some experiments.

Statistics. Current densities (pA/pF) and membrane potentials (mV) were compared using paired Student's *t* tests and percentages using paired non-parametric test (Mann-Whitney), with the level of significance set at $P < 0.05$. In addition ANOVA was used for comparing difference currents, from independent groups (Fig. 2), in various experimental conditions.

RESULTS

Location and projection of GPN neurons

The neurons investigated in this study were distributed in two groups along the rat glossopharyngeal nerve (GPN) near its branch point with the carotid sinus nerve (CSN) and at a more distal location (see Fig. 1 A; rectangle). Together with a population of sensory neurons located in the rostral part of the petrosal ganglion (Wang *et al.* 1993) they give rise to a plexus of neuronal nitric oxide synthase (nNOS)-positive fibers that are thought to provide efferent inhibitory innervation to the carotid body (CB; Wang *et al.* 1993, 1994a,b, 1995a,b; Prabhakar, 1999; Fung *et al.* 2001). These neurons were revealed by retrograde labeling after placement of the lipophilic dye DiI in the carotid body (Fig. 1 B), and by NADPH-diaphorase activity (Fig. 1 C) or positive nNOS-immunoreactivity (Fig. 1 D) in whole-mounts of GPN. Interestingly, and as previously described by Wang *et al.* (1993) for neurons involved in efferent inhibition of CB chemoreceptors, GPN neurons expressed the cholinergic marker, vesicular ACh transporter (VAChT, Fig. 1 E), which was co-localised with nNOS (Fig. 1 F). Enzymatic dissociation of GPN yielded dispersed neurons that survived for several days in culture and were easily identified under phase contrast microscopy (Fig. 1 G). These cultured neurons also stained positively for NADPH-diaphorase activity (Fig. 1 H), nNOS-immunoreactivity (Fig. 1 I-J), and neurofilament immunoreactivity (NF 68kD; Fig. 1 K-L). In addition, cultured GPN neurons expressed vesicular ACh transporter (VAChT, Fig. 1 M). All VAChT immunoreactive cells in culture were found to co-express NF (e.g. Fig. 1 L-N).

Electrophysiological properties of the hypoxia-sensitive K^+ current (IKO_2) in GPN neurons

Perforated-patch recordings were made from GPN neurons usually within 1-2 days of isolation. In this study voltage- and current-clamp recordings were obtained from ~ 100 neurons and of these 85 (i.e. ~ 85%) responded to hypoxia (PO_2 ~ 15 mmHg). As shown in Fig. 2 A, hypoxia reversibly inhibited outward currents in GPN neurons at positive test potentials (n = 11); for a step to +40 mV, the mean outward current density was 42.0 ± 3.8 pA/pF before, 35.1 ± 3.5 pA/pF during ($p < 0.05$), and 41.9 ± 3.9 pA/pF after hypoxia. This effect was absent in control experiments where the extracellular solution was bubbled with compressed air instead of N_2 gas (not shown, n = 3) as well as after intracellular dialysis during recording in whole-cell configuration (not shown, n = 5). Notably, the inhibitory effect of hypoxia on the macroscopic outward currents persisted in physiological solution containing 5 mM TEA plus 2 mM 4-AP (n = 6; $p < 0.05$, Fig. 2 B), or 200 μM cadmium (n = 6; Fig. 2 C). In addition, 100 nM iberiotoxin (n = 5; Fig. 2 C), a selective blocker of large conductance Ca^{2+}-activated K^+ channels, and apamin (n = 4; not shown), a selective blocker for small conductance Ca^{2+}-activated K^+ channels, had little or no effect on the magnitude of the macroscopic outward current, and similarly a full hypoxic response remained in the presence of these blockers. In contrast, 1 mM quinidine caused a dose-dependent inhibition of the outward current (Fig. 2 E and F; n = 5 and 7 respectively), and also occluded the hypoxic response. Statistical analysis revealed that in the presence of the above K^+ channel blockers (with the exception of 1 mM quinidine) hypoxic inhibition of outward current was significant ($p < 0.05$) at

potentials > +30 mV. Moreover, the magnitude of the hypoxia-sensitive 'difference' current density (obtained by subtracting the current density during hypoxia from that during normoxia) remained unaffected in the presence of these blockers. These combined data suggest that background K^+ channels were the likely mediators of hypoxic sensitivity in these neurons rather than voltage-gated, delayed rectifier-type or Ca^{2+}-dependent K^+ channels.

To enhance the magnitude of 'leak' currents and facilitate quantification of the hypoxia-sensitive component, voltage-clamp recordings were carried out in high K^+ external solutions containing 1 μM TTX, 30 mM TEA, 5 mM 4-AP and 2 mM Ni^{2+} to block voltage-dependent currents. Representative current traces, typical of instantaneous 'leak' currents, and corresponding I-V plots are shown in Fig. 3 A for a cell exposed to this solution in symmetrical K^+ (135 mM) conditions. The hypoxia-sensitive difference current (IKO_2) was obtained by subtracting the current recorded in hypoxia from that in normoxia (Fig. 3 B). In symmetrical (135 mM) K^+ conditions IKO_2 reversed direction near 0 mV (n = 7, Fig. 3 C), the calculated Nernst K^+ equilibrium potential (E_K), and the I-V relation displayed little voltage-dependence as expected of a K^+-selective background conductance (Fig. 3 B and C). To confirm K^+ selectivity, current density versus voltage plots for IKO_2 were obtained using various extracellular K^+ concentrations. When extracellular $[K^+]$ was 75 mM (n = 4), the reversal potential of IKO_2 shifted to ~ -14 mV as predicted for E_K (Fig. 3 C). In normal extracellular K^+ (5 mM), the current density (pA/pF) versus voltage plot for IKO_2 showed moderate outward rectification and reversed near -83 mV, the calculated K^+ equilibrium potential (n = 4; Fig. 3 C).

Pharmacological properties of IKO_2

In order to test for functional similarities to other members of the background 2P domain K^+ channel family, we investigated the sensitivity of IKO_2 to various agents including barium, quinidine, the polyunsaturated fatty acid arachidonic acid (AA), and the volatile anaesthetic halothane. The effects of some of these agents on 'leak' currents and their interaction with hypoxia are illustrated in Fig. 4 A-C and summarised in Fig. 4 D. A representative example of the reversible inhibition of the background current by hypoxia under symmetrical K^+ conditions is shown in Fig. 4 A. Similarly, halothane (2-5 mM) inhibited the background K^+ current at negative potentials and interestingly, the inhibitory effect of hypoxia was occluded in the presence of halothane (Fig. 4 B). Quantitative comparison of the inhibitory effect of hypoxia and halothane, applied separately and in combination, on background K^+ current is shown in Fig. 4 D. These data suggest that IKO_2 is halothane-inhibitable in GPN neurons, in contrast to the background IKO_2 expressed in rat carotid body chemoreceptors (Buckler *et al.* 2000). In addition to halothane, both barium (10 mM) and quinidine (1 mM) occluded the effect of hypoxia in GPN neurons, indicating that IKO_2 was also barium- and quinidine-sensitive (see also Fig. 2 E and F). In contrast, AA caused potentiation of the background current as exemplified in Fig. 4 C and summarised in Fig. 4 D. In symmetrical K^+ solutions and at a membrane potential of –60 mV, whereas quinidine (1 mM), barium (10 mM) and halothane (2-5 mM) inhibited the background K^+ current by 40–100 %, AA (5 μM) caused a marked potentiation (~ 50 %) of this current (Fig. 4 D). Hypoxia had little or no effect (n = 4) when applied to preparations in which the background current was

previously potentiated by AA (Fig. 4 C). While these results may indicate that AA activated IKO_2, the data are inconclusive since in voltage-clamp studies the potentiating effects of AA were poorly reversible and therefore the interaction between AA and hypoxia could not be satisfactorily studied. Nevertheless, these effects of halothane and AA are opposite to those expected of the O_2-sensitive TASK-1-like background K^+ channels implicated in hypoxia-sensing in rat carotid body (Buckler *et al.* 2000) and of O_2-sensitive TASK-3 channels in the H-146 cell line, a model for pulmonary airway chemoreceptors (Hartness *et al.* 2001). In contrast, they more closely resemble those expected of the THIK-1 (Rajan *et al.* 2001) or TWIK-2 (Chavez *et al.* 1999) 2P domain channels.

Evidence that IKO_2 is not carried by TASK-related channels

In order to confirm that acid-sensitive TASK channels did not mediate hypoxic sensitivity in GPN neurons we determined the pH sensitivity of IKO_2. These experiments revealed that extracellular acidification (pH = 6.5 or 5.5) produced only a weak inhibition of IKO_2. A representative example is shown in Fig. 5 A, where acidic pH (6.5 or 5.5) caused only ~ 50 % inhibition of IKO_2 over a range of membrane potentials (-40 to –110 mV) under symmetrical K^+ (135 mM) conditions. This pH sensitivity is relatively weak compared to the pronounced acid sensitivity of TASK-1 channels, but is not unlike that of THIK-1 (Kcnk13), the only functional member of the THIK family described to date (Rajan *et al.* 2001). For comparison, normalised values for IKO_2 in GPN neurons and for heterologously-expressed TASK-1 in COS-7 cells (*data from* Kim *et al.* 1999) are plotted

against pH in Fig. 5 B, under symmetrical K^+ solutions and at a membrane potential of -60 mV. Furthermore in GPN neurons, alkaline pH (8.5) produced only a weak potentiation of the normalised IKO_2 relative to neutral pH (Fig. 5 B), a feature previously reported for THIK-1 channels (Rajan *et al.* 2001).

To further rule out the possible involvement of TASK-1 and TASK-3 channels in the O_2-sensitive conductance expressed in GPN neurons, we used anandamide (AN, 1-10 μM) as a blocker for TASK-1 and ruthenium red (RR, 1-10 μM) as a blocker for TASK-3, while recording membrane potential in physiological K^+ solutions. Fig. 6 shows representative examples of the effect of these blockers. Anandamide (Fig. 6 A, n = 6) had no effect on the neuronal resting potential. Furthermore, when GPN neurons were exposed to hypoxia in the presence of anandamide the response to hypoxia was unaffected. In contrast, 2 μM RR caused hyperpolarization of the neuronal resting potential (Fig. 6 B, n = 5), from –46.3 ± 4.6 mV in control solution to –53.2 ± 5.8 mV ($p < 0.05$) and –48.4 ± 5.9 mV after wash out. The cause of this hyperpolarization is unknown but it may arise secondarily from an increase in intracellular calcium. Effects of RR on Ca^{2+} signalling include inhibition of the Ca^{2+}-ATPase and mitochondrial Ca^{2+}-uptake (Rigoni and Deana, 1986; Zhou and Bers, 2002), leading to an increase in cytosolic Ca^{2+} and activation of Ca^{2+}-dependent K^+ channels. Nonetheless, GPN neurons still responded to hypoxia in the presence of RR. These data strongly suggest that the O_2-sensitive current expressed in GPN neurons is insensitive to both anandamide and ruthenium red, and therefore supports the non-involvement of TASK-1 and TASK-3 background K^+ channels in hypoxic sensitivity.

Effects of hypoxia, halothane and AA on membrane potential

Since hypoxia inhibited a background K^+ current in GPN neurons we predicted this would lead to membrane depolarization and an increase in electrical excitability. Indeed, during current clamp recordings hypoxia depolarized GPN neurons by 3–7 mV and increased membrane excitability, as illustrated in Fig. 7 A and B. In physiological K^+ solutions, the membrane potential depolarized from a mean (± s.e.m.) resting level of –49.8 ± 1.6 mV (n = 18) in normoxia to –46.8 ± 1.6 mV during hypoxia ($p < 0.001$), followed by recovery to -49.9 ± 1.6 mV after return to normoxia (Fig. 7 A right). In some neurons, depolarization due to hypoxia was accompanied by spike activity (Fig. 7 B). Similarly, 2-5 mM halothane depolarized the membrane potential from –54.8 ± 2.6 mV to –50.4 ± 3.0 mV (n = 6; $p< 0.05$), followed by recovery to –54.9 ± 2.1 mV after washout. Moreover, 2-5 mM halothane occluded the depolarizing effects of hypoxia (n = 4; see Fig. 7 C), as expected if both agents acted via inhibition of the same K^+ channels. In contrast, AA (5 μM) had the opposite effect, producing a long-lasting hyperpolarization from –47.7 ± 3.2 mV to –56.3 ± 3.3 mV (n = 3; Fig. 7 D), consistent with its enhancing effect on background K^+ currents. As observed during voltage-clamp studies the effects of AA on membrane potential recovered only slowly after washout of the drug (Fig. 7 D).

DISCUSSION

The present study revealed a novel O_2-sensing mechanism in peripheral neurons of the glossopharyngeal nerve (GPN) that innervate the rat carotid body (CB), the main arterial chemoreceptor in mammals (González *et al.* 1994; López-Barneo *et al.* 2001). These neurons were retrogradely labeled following injection of the lipophilic dye DiI in the CB, and were distributed along the GPN in two main groups, one of which was located near the branch point with the carotid sinus nerve (CSN). They also displayed positive immunoreactivity for vesicular ACh transporter (VAChT) and nNOS, and therefore correspond to neurons thought to underlie the basis for NO-mediated efferent inhibition of the CB (Wang *et al.* 1993, 1994a,b, 1995a,b; Höhler *et al.* 1994). Though we are unaware of data showing the presence of O_2-sensing mechanisms in peripheral neurons, there are several reports of the presence of such mechanisms in central neurons, particularly those located in the ventrolateral medulla (Golanov and Reis, 1999; Mazza *et al.* 2000), hippocampus (Leblond and Krnjević, 1989; Haddad and Jiang, 1997; Hammarström and Page, 2000), and cerebellum (Plant *et al.* 2002). The O_2-sensitive K^+ current expressed in GPN neurons was unaffected by the classical voltage-dependent K^+ channel blockers such as TEA and 4-AP, but it was reversibly blocked in a dose-dependent manner by quinidine. These data suggested the involvement of 'leak' or background K^+ channels and this was validated in voltage-clamp studies where the hypoxia-sensitive 'difference' current IKO_2 reversed at the calculated K^+ equilibrium potential in solutions of different extracellular K^+ concentrations. Moreover, under

symmetrical K^+ conditions this current showed little or no voltage sensitivity, as expected of background K^+ channels (Goldstein *et al.* 2001).

In general, background or resting K^+-selective channels play a key role in setting the resting membrane potential and input resistance of the cell (Lesage and Lazdunski, 2000; Goldstein *et al.* 2001; Patel and Honoré, 2001b). They are therefore important determinants of the magnitude and kinetics of synaptic inputs in neurons and help shape neuronal excitability. More recently, these channels have additionally been recognised as critical sites for neuromodulation by endogenous ligands, as well as targets for clinically important volatile anaesthetics (Goldstein *et al.* 2001; Patel and Honoré, 2001a,b; Talley and Bayliss, 2002). Moreover, they can be regulated by important biophysical and biochemical parameters including pH, temperature and O_2 tension (Buckler *et al.* 2000; Patel and Honoré, 2001b; Plant *et al.* 2002). So far, two members of the background 2P domain K^+ channel family, the acid-sensitive TASK-1 (Buckler *et al.* 2000; Plant *et al.* 2002) and TASK-3 (Hartness *et al.* 2001) channels, have been shown to possess O_2-sensitivity. These two background channels are, however, *inhibited* by arachidonic acid and *activated* by halothane, effects that are opposite to the O_2-sensitive current (IKO_2) found in GPN neurons in the present study. Moreover, the relatively weak pH sensitivity of IKO_2 contrasts with that of TASK-1 and TASK-3 channels (Duprat *et al.* 1997; Leonoudakis *et al.* 1998; Buckler *et al.* 2000; Sirois *et al.* 2000; Hartness *et al.* 2001). For example, IKO_2 displayed only ~ 50 % inhibition at pH = 5.5, compared to the almost total inhibition of TASK-1 channels expressed in either heterologous systems (Lopes *et al.*

2000, Sirois *et al.* 2000; Duprat *et al.* 1997; Leonoudakis *et al.* 1998; Kim *et al.* 1999) or native cerebellar granule neurons (Plant *et al.* 2002).

Similar to the O_2-sensitive channels in GPN neurons, two other members of the background channel family, THIK-1 (Kcnk13) and TWIK-2 (Kcnk6), are *inhibited* by halothane and *activated* by arachidonic acid. However, when rat TWIK-2 was expressed in *Xenopus* oocytes (Chavez *et al.* 1999) or COS cells (Patel *et al.* 2000), the currents were reversibly inhibited by barium and quinidine in physiological K^+ solutions, but the inhibition was not observed in a symmetrical K^+ gradient (Chavez *et al.* 1999; Patel *et al.* 2000), even with high barium concentrations (10 mM, Patel *et al.* 2000). These properties contrast with those of IKO_2 expressed in GPN neurons and in addition, TWIK-2 currents display an inward rectification and inactivation at positive test potentials (Chavez *et al.* 1999; Patel *et al.* 2000), not seen in IKO_2. Therefore, TWIK-2 is unlikely to be the O_2-sensitive conductance expressed in GPN neurons. Rather, the properties of this current, including its relatively weak pH sensitivity, more closely resembled those of the only functional member of the THIK family (THIK-1) described to date (Rajan *et al.* 2001).

The O_2-sensitive current was undetectable during voltage- and current-clamp recordings in dialysed GPN neurons studied with conventional whole-cell recording. These data suggest that the O_2-sensitive K^+ channel requires intact cytosolic components in order to be functional, as previously observed for the TASK-1-like O_2-sensitive K^+ channels expressed in carotid body chemoreceptors (Buckler *et al.* 2000). In the case of GPN neurons, in preliminary experiments we applied arachidonic acid and halothane while recording membrane potential in physiological solutions to test if the O_2-sensitive

conductance was still functional in dialysed preparations (n = 4, not shown). Interestingly, the effects of arachidonic acid and halothane did not differ from those observed during perforated-patch recordings (see Fig. 7 C, D), suggesting that the relevant background conductance was functional in dialysed cells but it lacked O_2-sensitivity. Further studies are needed in order to understand the cytosolic regulation of the background channels in GPN neurons.

While the present data point to the possible involvement of the recently identified THIK (tandem pore-domain halothane inhibited K^+ channels) subfamily of background potassium channels (Girard *et al.* 2001; Rajan *et al.* 2001) in mediating the O_2-sensitivity of GPN neurons, other candidates are not excluded. Conceivably, the O_2-sensitive current might be carried by a new member of the 2P domain family not yet described, or by a new variant of one of the already described background channels (Goldstein *et al.* 2001). Therefore, molecular identification of the O_2-sensitive K^+ conductance will be necessary to clarify which member of the 2P domain family is indeed responsible for conferring O_2-sensitivity to GPN neurons. Nevertheless, it is interesting that the pharmacological profile of IKO_2 resembles that of THIK channels. Of the two closely-related members of this family, i.e. THIK-1 and THIK-2 (58 % identity at the amino acid level; Rajan *et al.* 2001), THIK-1 was broadly expressed in several tissues and was functional when heterologously expressed in *Xenopus* oocytes (Rajan *et al.* 2001). In contrast, the expression of THIK-2 (Kcnk12) was more restricted, though it was especially abundant in brain (Rajan *et al.* 2001). Moreover, it could not be functionally expressed in *Xenopus* oocytes and therefore its physiological function awaits characterization (Girard *et al.*

2001; Rajan *et al.* 2001). Since the physiological function of THIK channels is unknown, our studies raise, for the first time, the possibility of an O_2-sensing function for this background channel family.

Physiological relevance

This study describes a novel O_2-sensitive background K^+ conductance in GPN neurons. Since background channels play a key role in setting the resting membrane potential and controlling neuronal excitability, modulation of IKO_2 may help control neuronal function during ischemic stress. In GPN neurons these O_2-sensitive channels may also play a hitherto unrecognised role in the control of respiration, since these neurons are thought to provide NO-mediated efferent inhibition of carotid body chemoreceptors (Wang *et al.* 1995b), which are excited by hypoxia. Since GPN neurons are also excited by hypoxia, via inhibition of background channels, the possibility is raised that this excitation leads to increase in intracellular calcium levels, activation of nNOS, followed by synthesis and release of NO. The resulting inhibitory effects of NO on carotid body function may provide a means of negative feedback modulation of chemoreceptor activity during hypoxia. In this way the O_2-sensitive background conductance expressed in GPN neurons may contribute to the control of respiration via regulation of carotid body function during hypoxia and conceivably, following exposure to volatile anaesthetics, e.g. halothane.

Acknowledgements

We thank Cathy Vollmer for expert technical assistance, Dr. James Mwanjewe for his generous gift of the nNOS antibody, and Dr. Juan Ianowski for his help with the DiI staining. This work was supported by a grant from the Canadian Institutes for Health Research to C.A.N. (MOP-57909). In addition, V.A.C was supported by a Dr. Sydney Segal Research Grant from The SIDS Foundation of Canada and I.M.F. by a Wellcome Trust Prize International Travelling Research Fellowship (Ref. # 16154).

Figure 1. Localisation and properties of neurons of the rat glossopharyngeal nerve (GPN) *in situ* and in culture. A, schematic drawing of the carotid bifurcation showing localisation of GPN neurons (red rectangle) embedded in the glossopharyngeal and carotid sinus (CSN) nerves (*modified* from Wang *et al.* 1993). Petrosal ganglion (PG), nodose ganglion (NG), superior cervical ganglion (SCG) and carotid body (CB) are indicated in diagram. In B, the GPN neurons (yellow arrow) are retrogradely labeled following injection of the lipophilic dye DiI into the CB; whole-mount of glossopharyngeal nerve visualised with confocal microscopy. In C, GPN neurons (black arrow) are visualised *in situ* in a whole-mount of glossopharyngeal nerve after staining for NADPH-diaphorase (NADPHd) activity. D-F, Same microscopic filed of GPN neurons *in situ* showing positive immunostaining for nNOS (D; Cy3) and the cholinergic marker VAChT (E; FITC); note co-localisation of the two markers (e.g. yellow arrow) in the same neurons (F). G and H, Corresponding phase and bright-field images of positive NADPHd activity in two adjacent neurons after two days in culture. I-J, Corresponding phase and nNOS immunofluorescence (FITC) in a cultured GPN neuron, two days after isolation. K-N, Corresponding phase and fluorescence micrographs showing a pair of cultured GPN neurons that were immunopositive for both neurofilament (NF, Fig. L; Alexa 594) and VAChT (Fig. M; FITC); overlap of the two markers is shown in N. Scale bars represent 50 μm in B and D; 150 μm in C, and 30 μm in G, I and K.

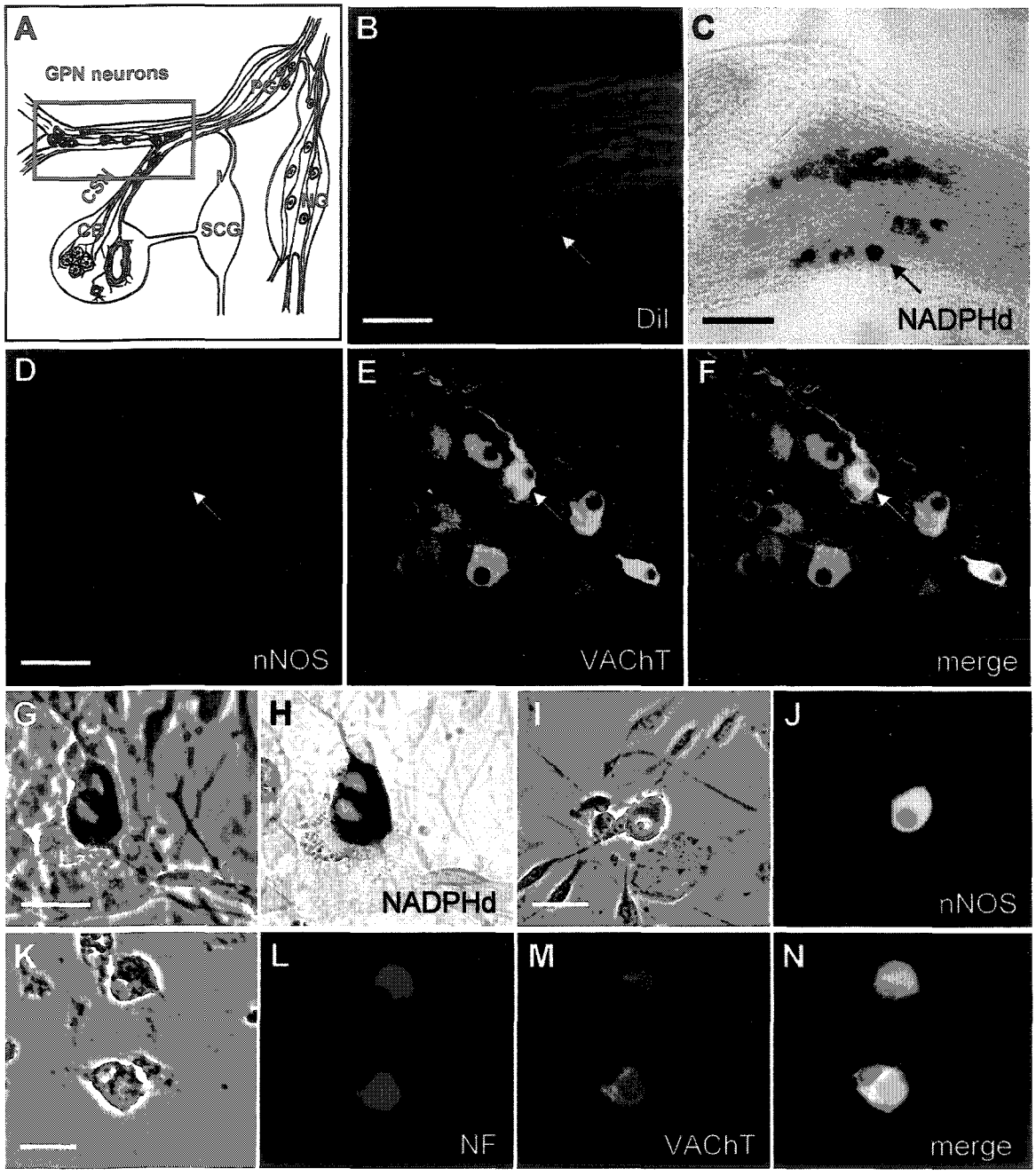
A
GPN neurons
PCG
C5L
CB
SCG
NG
B
DiI
C
NADPHd
D
nNOS
E
VAChT
F
merge
G
H
NADPHd
I
J
nNOS
K
L
NF
M
VAChT
N
merge

Figure 2. Electrophysiological responses of cultured GPN neurons to hypoxia. A, traces show a representative example of the reversible reduction of macroscopic outward current recorded in a GPN neuron after exposure to hypoxia in physiological extracellular K^+ (5 mM) solution, during various step potentials from –100 to +70 mV. I-V plots of the current density (mean ± s.e.m.; n = 11) during normoxia (Nox), hypoxia (Hox) and recovery (Rec) are shown on right; hypoxia caused a significant reduction in current density ($p < 0.05$) at potentials > 30 mV. B, traces show a representative example of the response to hypoxia in physiological solution containing 4-AP (2mM) and TEA (5 mM), during a step to +40 mV; I-V plots show mean (± s.e.m.; n = 6) current density during normoxia and hypoxia in the presence of 4-AP and TEA. Note, hypoxic inhibition of the macroscopic outward currents persisted in physiological solution containing these classical voltage-dependent K^+ channel blockers. Similar results were obtained in the presence of 200 μM Cd^{2+} (n = 6), 100 nM IbTx (n = 5) and 0.1 mM quinidine (Quid: n = 5) as shown in Figs. C, D and E respectively. However, as shown in F, higher concentrations of quinidine (1 mM) caused further suppression of the outward current and, moreover, abolished the response to hypoxia (n = 7).

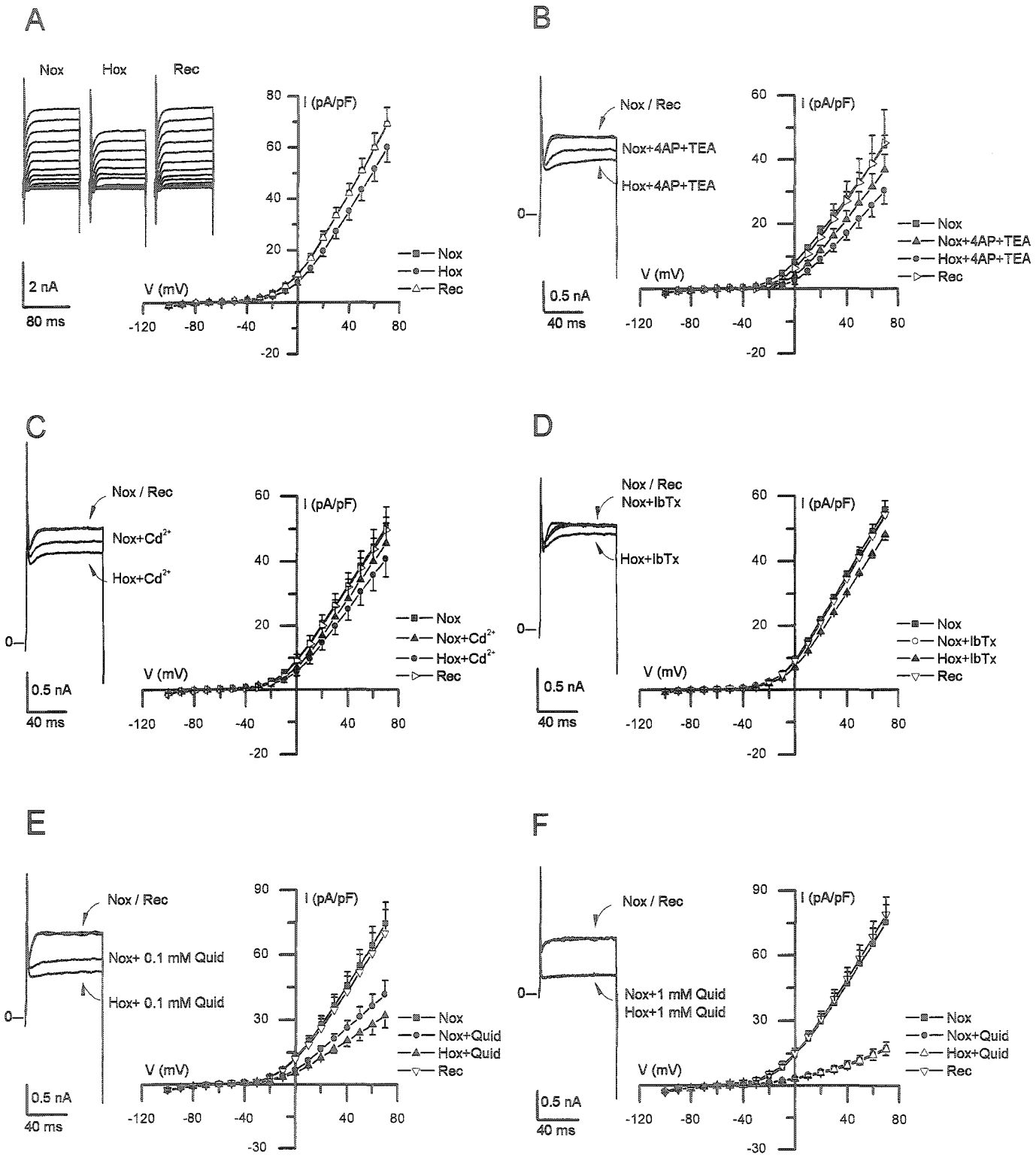
A
Nox
Hox
Rec
2 nA
80 ms
V (mV)
I (pA/pF)
Nox
Hox
Rec
B
Nox / Rec
Nox+4AP+TEA
Hox+4AP+TEA
0.5 nA
40 ms
V (mV)
I (pA/pF)
Nox
Nox+4AP+TEA
Hox+4AP+TEA
Rec
C
Nox / Rec
Nox+Cd2+
Hox+Cd2+
0.5 nA
40 ms
V (mV)
I (pA/pF)
Nox
Nox+Cd2+
Hox+Cd2+
Rec
D
Nox / Rec
Nox+IbTx
Hox+IbTx
0.5 nA
40 ms
V (mV)
I (pA/pF)
Nox
Nox+IbTx
Hox+IbTx
Rec
E
Nox / Rec
Nox+ 0.1 mM Quid
Hox+ 0.1 mM Quid
0.5 nA
40 ms
V (mV)
I (pA/pF)
Nox
Nox+Quid
Hox+Quid
Rec
F
Nox / Rec
Nox+1 mM Quid
Hox+1 mM Quid
0.5 nA
40 ms
V (mV)
I (pA/pF)
Nox
Nox+Quid
Hox+Quid
Rec

Figure 3. Electrophysiological properties of the background hypoxia-sensitive K^+ current (IKO_2) in GPN neurons. A, traces show a representative example of background or 'leak' currents before (Nox), during (Hox) and after (Rec) hypoxia, recorded in symmetrical high K^+ solution (135 mM) containing TTX (1 μM), 4-AP (5 mM), TEA (30 mM) and Ni^{2+} (2 mM; substituted for Ca^{2+}), during various voltage steps from −100 to +70 mV. Corresponding I-V plots are shown on right. B, I-V plot shows a representative example of the hypoxia-sensitive 'difference' current (IKO_2), obtained by subtracting the current density during hypoxia from that during normoxia (see A). In C, IKO_2 current density was obtained from groups of cells at three different extracellular K^+ concentrations as follows: 5 mM (n = 4), 75 mM (n = 4), and 135 mM (n = 7); note that for each case the reversal potential of IKO_2 was similar to that predicted by Nernst equation for K^+ (i.e. -80, -14 and 0 mV respectively).

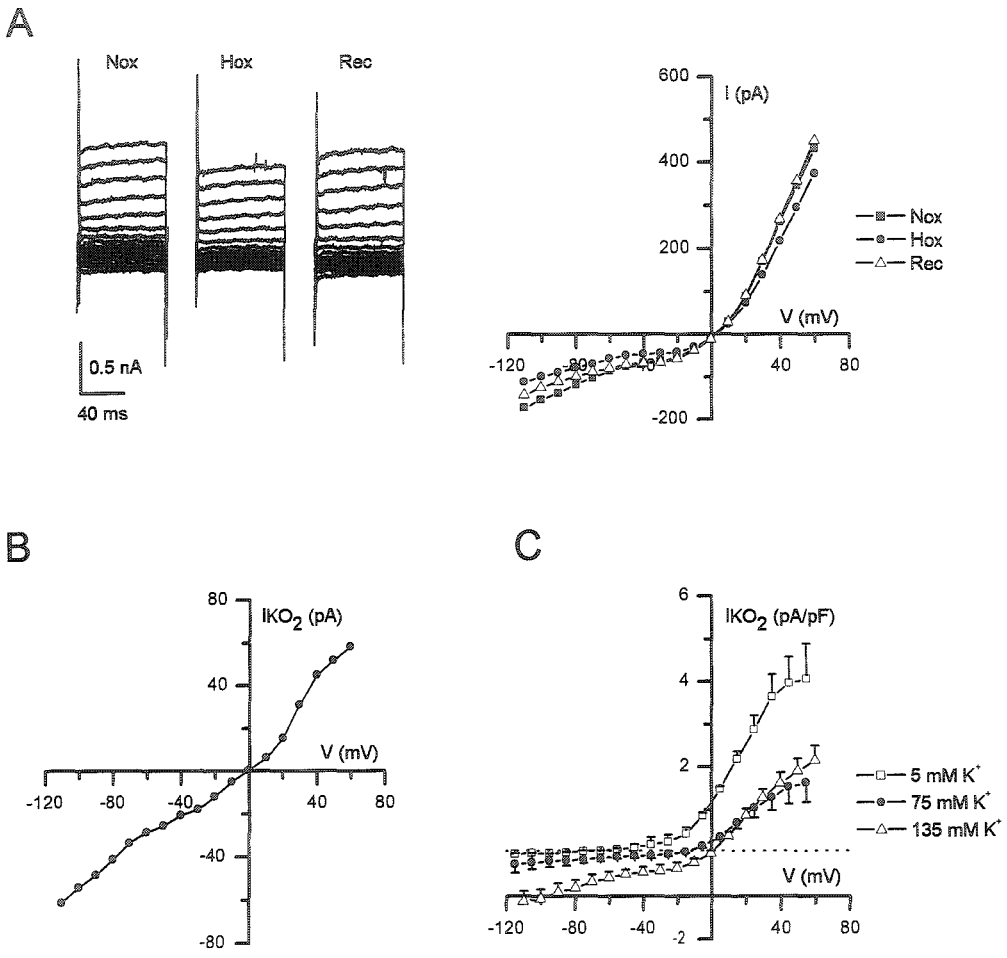
A
Nox
Hox
Rec
0.5 nA
40 ms
I (pA)
600
400
200
-200
V (mV)
-120
-80
-40
40
80
Nox
Hox
Rec
B
IKO2 (pA)
80
40
-40
-80
V (mV)
-120
-80
-40
40
80
C
IKO2 (pA/pF)
6
4
2
-2
V (mV)
-120
-80
-40
40
80
5 mM K+
75 mM K+
135 mM K+

Figure 4. Pharmacological characetrization of the background K^+ current in cultured GPN neurons. A-C, traces showing representative examples of the effect of hypoxia (A), halothane (B) and AA (C) on the background current elicited during ramp depolarization from –100 to +25 mV. Holding potential was –60 mV. Note the reversible inhibition of the current by hypoxia in A, halothane (2-5 mM) in B, as well as the occlusion of the hypoxic response in the presence of halothane (B). In contrast, 5 μM AA potentiated the background current in C, and appeared to occlude the hypoxic response. D, Effect of several agents on the background current in normoxia and hypoxia under symmetrical K^+ conditions; for each agent bars represent the difference current at –60 mV expressed as a percentage of the control current (in normoxia); the difference current was obtained by subtracting the current during the particular treatment from the control current. The effects of hypoxia (Hox), halothane (Hal, 2-5 mM), quinidine (Quid, 1 mM) and barium (Ba^{2+}, 10 mM) were all inhibitory. Note, however, that AA (5 μM) caused potentiation of the background current. In addition, when halothane and barium were applied in combination with hypoxia (Hal+Hox; Ba^{2+}+Hox) there was occlusion of the response to hypoxia ($p > 0.05$). IKO_2 was also occluded in presence of 1 mM quinidine (Quid), which completely inhibited the background current. The sample size 'n' is indicated in parentheses within bars. (*, $p < 0.05$).

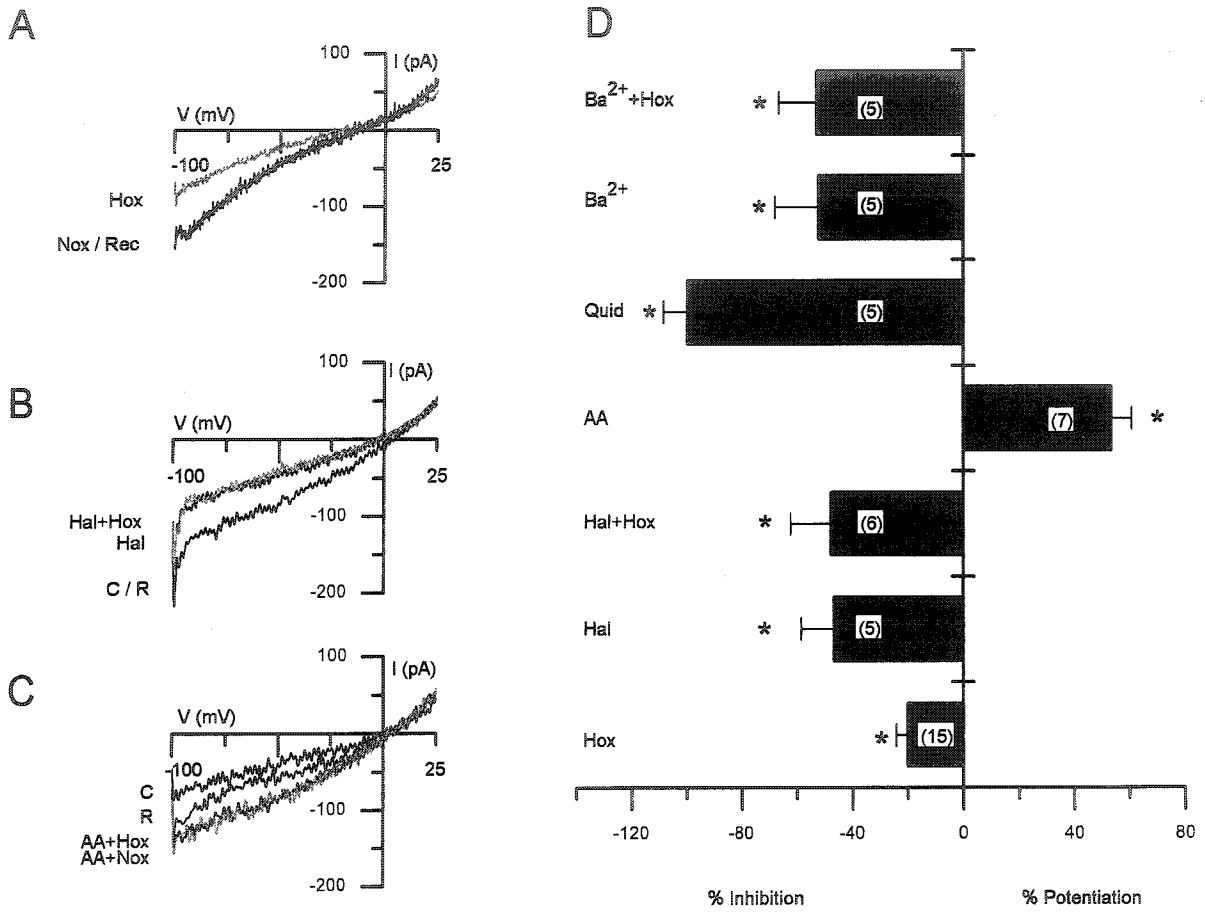
A
100
I (pA)
V (mV)
-100
25
Hox
Nox / Rec
-100
-200
B
100
I (pA)
V (mV)
-100
25
Hal+Hox
Hal
C / R
-100
-200
C
100
I (pA)
V (mV)
-100
25
C
R
AA+Hox
AA+Nox
-100
-200
D
Ba2+ +Hox
Ba2+
Quid
AA
Hal+Hox
Hal
Hox
(5)
(5)
(5)
(7)
(6)
(5)
(15)
*
-120
-80
-40
0
40
80
% Inhibition
% Potentiation

Figure 5. Regulation of the O_2-sensitive current (IKO_2) expressed in GPN neurons by extracellular pH. A, a representative example of the inhibition of IKO_2 by acidic pH in symmetrical 135 mM K^+ solutions. Acidosis (pH = 6.4 and 5.5) caused ~ 50% inhibition of IKO_2 at negative potentials. B, normalised pH sensitivity of IKO_2 in GPN neurons and TASK-1 current expressed in COS-7 cells (*data from* Kim *et al.* 1999) at –60 mV in symmetrical K^+ solutions. Note, the weak pH sensitivity of IKO_2 expressed in GPN neurons compared to TASK-1 current.

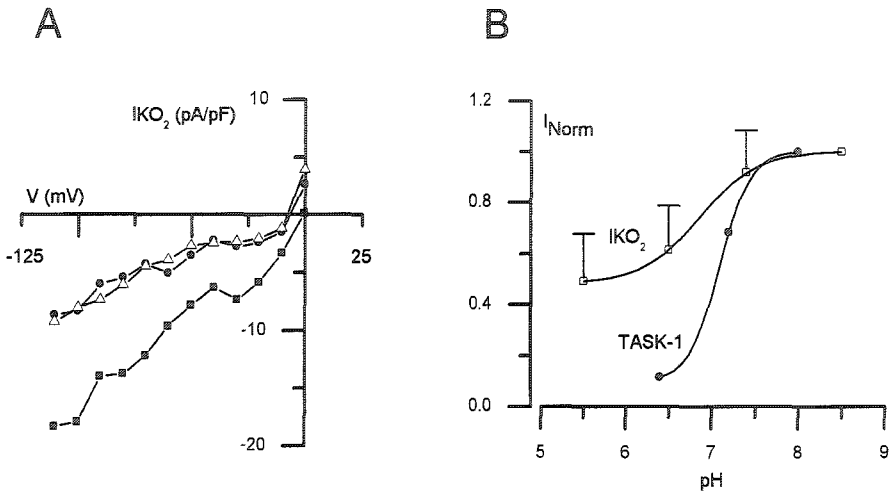
A
B
IKO2 (pA/pF)
10
V (mV)
-125
25
-10
-20
INorm
1.2
0.8
0.4
0.0
IKO2
TASK-1
5
6
7
8
9
pH

Figure 6. Effect of anandamide and ruthenium red on membrane potential and hypoxic response. A, the TASK-1 channel blocker anandamide (AN, 5 μM) was without effect on the neuronal resting potential. In addition, the response to hypoxia was unaffected in the presence of anandamide (n = 6). B, application of the TASK-3 channel blocker ruthenium red (RR, 2 μM) caused hyperpolarization of the resting potential probably due to an increase in intracellular Ca^{2+} and consequent activation of Ca^{2+}-dependent K^+ channels. However, in the presence of this agent GPN neurons still depolarised during hypoxia (n = 5).

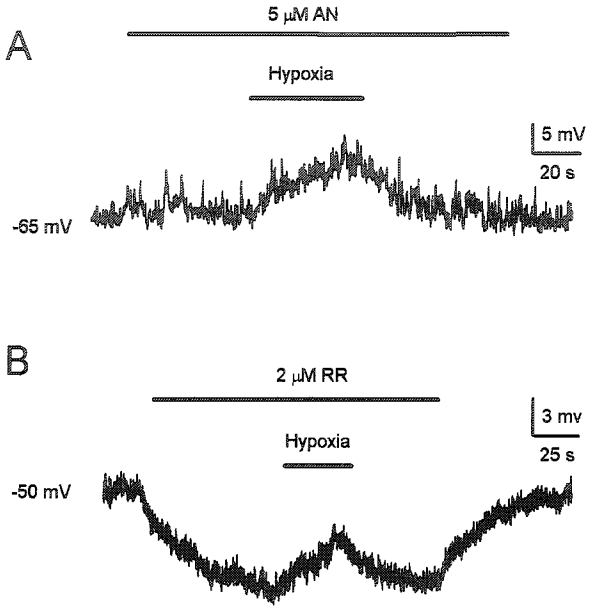
A
5 μM AN
Hypoxia
5 mV
20 s
-65 mV
B
2 μM RR
3 mv
Hypoxia
25 s
-50 mV

Figure 7. Effect of hypoxia, halothane and arachidonic acid on the membrane potential and excitability in GPN neurons. Representative examples of the hypoxia-induced membrane depolarization and action potential firing in GPN neurons during current clamp recordings are shown in A (left) and B respectively. The histogram in A (right) shows that hypoxia (Hox) caused a significant (**, $p < 0.001$) decrease of the resting potential to -46.8 ± 1.6 mV from -49.8 ± 1.6 mV ($n = 18$) during normoxia (Nox). C, representative example of the response to hypoxia before, during, and after application of halothane (Hal, 2-5 mM). Note, halothane caused membrane depolarization and occlusion of the hypoxic response. D, representative example of the effect of arachidonic acid (AA, 5 μM) on the resting potential. Note, AA caused a long-lasting hyperpolarization and its effects were poorly reversible. In the example, recovery of the resting potential was reached ~30 min after AA was removed from the extracellular solution.

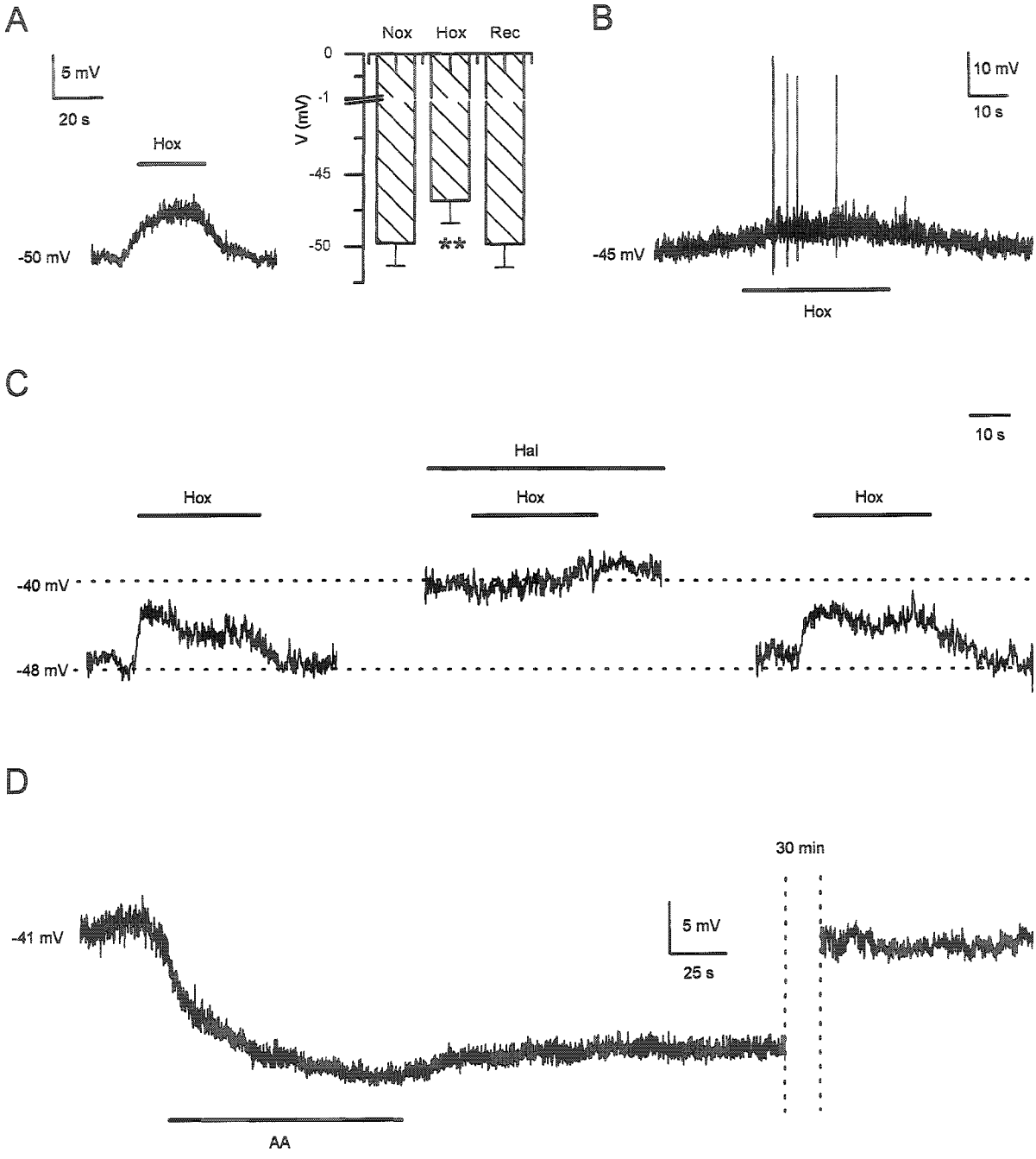
A
5 mV
20 s
Hox
-50 mV
Nox
Hox
Rec
0
-1
-45
-50
V (mV)
**
B
10 mV
10 s
-45 mV
Hox
C
10 s
Hal
Hox
Hox
Hox
-40 mV
-48 mV
D
30 min
-41 mV
5 mV
25 s
AA

CHAPTER 4

Purinergic signalling by glossopharyngeal efferent neurons to the rat carotid body via multiple P2X receptors

The work in this chapter will be submitted to the *Journal of Neuroscience*

The authors are: Verónica A. Campanucci, Min Zhang, Cathy Vollmer and Colin A. Nurse

I performed all the electrophysiological experiments with Min Zhang. In addition, I was responsible for data analysis, all immunofluorescence experiments, and preparation of the manuscript. Cathy Vollmer was involved in preparing co-cultures (Fig. 9 A-C) and paraganglia staining (Fig. 10).

ABSTRACT

The excitatory effects of ATP in the central and peripheral nervous system are mediated by a family of at least seven purinoceptor subunits (P2X1-P2X7) that form ligand-gated ion channels. In this study, we characterized the biophysical and pharmacological properties of purinergic receptors in two populations of nitric oxide synthase (NOS)-expressing neurons located in proximal and distal regions of the rat glossopharyngeal nerve (GPN). These neurons are supplied by fenestrated capillaries and innervate an O_2-chemosensory target organ, the carotid body (CB). In both populations of GPN neurons, ATP and α,β-methylene ATP (α,β-MeATP) evoked slowly desensitizing, suramin-sensitive inward currents (at –60 mV) with EC_{50} ~ 10.5 μM and ~ 3.2 μM respectively. These data suggest the involvement of purinergic P2X2-P2X3 heteromeric receptors, and the presence of both P2X2 and P2X3 subunits was confirmed by confocal immunofluorescence. Moreover, 4-benzoylbenzoyl-ATP (BzATP) evoked inward currents (EC_{50} ~ 1.9 μM) that were partially inhibited by nanomolar concentrations of brilliant blue G (BBG), a selective inhibitor of homomeric P2X7 receptors. Immunolocalization studies *in situ* confirmed that P2X7 subunits were concentrated in cell bodies of the proximal GPN neurons, in nerve endings surrounding the distal GPN neurons, and in nerve endings surrounding chemoreceptor cell clusters in the CB. Evidence for yet another P2X receptor was suggested by the occurrence of a residual ATP-evoked response that was insensitive to the combined presence of high concentrations of suramin (500 μM) and oxidized-ATP (OxATP; 300 μM), an irreversible P2X7 antagonist. A contribution from P2X4 subunits was suggested in a few

cases where the selective P2X4 modulator, ivermectin (IVM, 1-10 μM), augmented the ATP-evoked inward current at –60 mV. Double-label confocal immunofluorescence revealed that P2X4 subunits were broadly expressed in both populations of GPN neurons *in situ*, and co-localized with nNOS and P2X3 subunits. Perfusion and staining with Evan's blue dye confirmed a specialized association between blood capillaries and both populations of GPN neurons in a paraganglion-like structure, and indicated the neurons have ready access even to large blood-borne chemicals. To test whether ATP signaling via GPN neurons was involved in the efferent inhibition of the CB, we used co-cultures of GPN neurons and CB chemoreceptor (type I) cell clusters. Application of BzATP (5 μM) and ATP (5-10 μM) to GPN neurons that were juxtaposed to type I clusters in co-culture caused type I cell hyperpolarization (5-10 mV), that was prevented by application of the NO scavenger, carboxy-PTIO (500 μM). Taken together these data suggest the involvement of at least four different P2X subunits (P2X2, P2X3, P2X4 and P2X7) in purinergic signaling by GPN neurons. Moreover, activation of these receptors by ATP, which is known to be released from red blood cells and CB chemoreceptors during hypoxic stress, may contribute to the NO-dependent efferent inhibitory pathway to the rat CB.

INTRODUCTION

In addition to its well-known function as a key intracellular energy source, ATP has been recognized for its extracellular role in the regulation of various cell activities via several types of cell surface receptors (Burnstock, 1972, 1997; Evans *et al.* 1992; Edwards *et al.* 1992; North, 2002). For example, in both the peripheral and central nervous systems, ATP is known as a fast-acting neurotransmitter at excitatory purinergic synapses due to activation of P2X receptors, or as a slower-acting neuromodulator via G-protein coupled P2Y receptors (Burnstock, 1997; Ralevic and Burnstock, 1998; North and Surprenant, 2000; Khakh, 2001a,b). P2X receptors are ATP-gated ion channels that, in mammals, belong to a family of at least seven transmembrane proteins (P2X1-P2X7) as revealed by molecular cloning techniques (Dunn *et al.* 2001; Khakh, 2001a,b). Activation of P2X receptors by extracellular ATP opens cation non-selective ion channels that show significant calcium permeability (Khakh, 2001a,b). Although most of the biophysical and pharmacological properties of P2X receptors were obtained following heterologous expression of homomeric recombinant subunits, there are increasing reports of their properties in native cells (Dunn *et al.* 2001), where heteromeric combinations appear common.

In addition to the recognized roles of ATP and their receptors in synaptic function, it has also become clear that they are involved in pathological stress situations. For example, there is evidence supporting the involvement of P2X3 receptors in peripheral pain perception, triggered by ATP release from damaged or inflamed tissue (North, 2004). Additionally, ischemic conditions due to glucose/oxygen deprivation can

lead to upregulation of P2X2 and P2X4 subunits in the hippocampus of gerbils, and to neuronal loss in rat CNS explant cultures that is preventable by the inclusion of P2 receptor antagonists (Cavaliere *et al.* 2003).

Recent studies have identified an important role of ATP and P2X receptor signaling in both the peripheral (Zhang *et al.* 2000; Prasad *et al.* 2001; Rong *et al.* 2003; Zhang and Nurse, 2004) and central (Thomas and Spyer, 2000) control of breathing, in response to changes in arterial PCO_2 and PO_2. Peripheral chemoreceptors in the carotid body (CB) are stimulated by an increase in PCO_2 (and H^+ ions) as well by a decrease in PO_2 (hypoxia), resulting in a compensatory reflex increase in ventilation (González *et al.* 1994). This reflex is mediated via an increased afferent discharge in the carotid sinus nerve due, at least in part, to stimulus-induced release of ATP from CB chemoreceptor (type I) cells and subsequent activation of postsynaptic P2X2 and/or P2X2-P2X3 purinergic receptors on afferent nerve terminals (Zhang *et al.* 2000; Prasad *et al.* 2001; Rong *et al.* 2003; Zhang and Nurse, 2004). The CB also receives an efferent innervation from autonomic NOS-positive nerve fibers whose parent cell bodies reside in discrete neuronal groups situated along the glossopharyngeal (GPN) and carotid sinus nerves (Wang *et al.* 1993; Grimes *et al.* 1994; Höhler *et al.* 1994, Campanucci *et al.* 2003a). Release of nitric oxide (NO) from the terminals of these GPN neurons is thought to mediate efferent inhibition of the CB (Wang *et al.* 1994a,b, 1995a,b), thereby providing a means of negative feedback modulation of chemoreceptor function. Our recent demonstration that two discrete populations of GPN neurons are themselves excited by hypoxia, via inhibition of a halothane-sensitive background K^+ conductance (Campanucci

et al. 2003a,b), suggests this negative feedback pathway may be synchronously activated during normal CB chemoexcitation and contribute to the "push-pull" mechanism that determines the final chemoafferent discharge.

In the present study, we considered the possibility that GPN neurons might express receptors for ATP, thereby providing an alternative pathway by which these neurons could be activated during normal CB chemoexcitation and during pathological stress conditions. We also confirmed that these GPN neurons are surrounded by a specialized capillary network that is freely permeable to even large, blood-borne chemicals (McDonald and Blewett, 1981), which could include ATP, released from red blood cells during hypoxic stress (reviewed by Ellsworth, 2000). Interestingly, we found these GPN neurons expressed at least four subtypes of P2X receptors, consisting of P2X2, P2X3, P2X4 and P2X7 subunits, thereby allowing for activation over a broad range of extracellular ATP concentrations. Finally, to address whether activation of these receptors may have a physiological role leading to inhibition of CB chemoreceptor function, we tested a co-culture model of rat CB chemoreceptor clusters and juxtaposed GPN neurons. A preliminary report of some of these findings has appeared in a recent abstract (Campanucci *et al.* 2001).

METHODS

Cell culture. Wistar rat pups (9-10 days old, Harlan, Madison, WI, USA) were first stunned by a blow to the head that rendered them unconscious, and then killed by decapitation. The carotid bifurcation, surrounding ganglia and attached nerves were removed under sterile conditions. All procedures for animal handling were carried out according to the guidelines of the Canadian Council on Animal Care (CCAC). A section of the glossopharyngeal nerve (GPN), extending from its intersection with the carotid sinus nerve (CSN) to a region ~ 5 mm distal to the intersection, was dissected bilaterally from each pup. Each GPN was then cut into two segments so as to separate the two populations (proximal and distal) of GPN neurons. The two segments were separately pooled, digested with enzyme (0.1 % Collagenase, Invitrogen Canada Inc., Burlington, ON, Canada; 0.1 % trypsin, Sigma; and 0.01 % DNase, Invitrogen) and mechanically dissociated to produce dispersed GPN neurons. Each cell suspension was plated onto a thin layer of Matrigel (Collaborative Research, Bedford, MA, USA) that was previously applied to the central wells of modified 35 mm tissue culture dishes. Cultures were grown at 37 °C in a humidified atmosphere of 95 % air-5 % CO_2, and used either for patch-clamp experiments or immunofluorescence studies ~ 24-48 hr following isolation. In some experiments GPN neurons were co-cultured with rat carotid body (CB) type I cells. To produce co-cultures, an overlay of dissociated rat GPN neurons was added to a pre-existing monolayer of CB type I cells prepared as previously described (Zhong *et al.* 1997; Nurse and Zhang, 1999; Zhang *et al.* 2000). Electrophysiological recordings from co-cultures were usually carried out 3 days after the neurons were plated.

Confocal Immunofluorescence. Whole mounts of the GPN or cultured GPN neurons were fixed in 4 % para-formaldehyde overnight at 4 °C or for 15 min at room temperature, respectively. After washing in PBS (3 × 5 min) whole mounts were incubated for 72 hr at 4 °C with primary antibody; an overnight incubation was used for cultures. Primary antibodies used were: polyclonal rabbit antibodies against rat P2X2, P2X4 and P2X7 (1:200; Alomone Labs, Jerusalem, Israel), guinea pig anti-rat P2X3 (1:500; Chemicon International, Inc.; Temecula, CA, USA), polyclonal rabbit anti-rat neuronal nitric oxide synthase (nNOS; 1:200; ImmunoStar, Inc., Hudson, WI, USA), monoclonal mouse and polyclonal rabbit anti-rat tyrosine hydroxylase (TH; 1:1000; Chemicon), monoclonal mouse anti-rat neurofilament (NF 68 kDa; 1:5; Boehringer Mannheim, Montreal, QC, Canada) and monoclonal mouse anti-rat GAP 43 (1:20,000). The primary antiserum was diluted in PBS containing 1 % BSA and 0.5 % Triton X-100. After incubation, the samples were washed in PBS (3 × 5 min) and incubated in the dark for 1 hr at room temperature with the secondary antibody conjugated to Alexa 594 (1:500, Molecular Probes, OR, USA), Texas Red (1:50, Jackson Laboratories) or FITC (1:50; Cappel, Malvern, PA, USA). The secondary antiserum was diluted in PBS containing 1 % BSA and 0.5 % Triton X-100. Samples were covered with a photobleaching reagent (Vectashield; Vector Laboratories, Burlingame, CA, USA) and viewed with a confocal microscope (BIO RAD Microradiance 2000) equipped with argon (2 lines, 488 and 514 nm) and helium/neon (543 nm) lasers. Tissue was scanned in optical sections separated by 1-2 μm at a rate of 166 lines per second and scanning was controlled with the aid of Lasersharp software. Between 10 to 30 μm of tissue in each

whole-mount preparation was routinely scanned in this manner. In control experiments pre-incubation with either blocking peptide or omission of the primary antibody resulted in complete abolition of staining. Blocking peptides for P2X2, P2X4 and P2X7 (Alomone Labs.) were pre-incubated with primary antibody (3 μg peptide/ 3 μg antibody) overnight at 4 °C before application. Image processing and manipulation was performed using CorelDraw 9.

Organ culture. Whole mounts of the intact petrosal/glossopharyngeal nerve/carotid sinus nerve/CB complex were carefully dissected from rat pups (9-10 days old), taking care not to sever the carotid sinus nerve (CSN). In some cases, prior to organ culture the petrosal ganglion was removed and the remaining tissue was placed on the membrane of Transwell-COL culture plates (Costar, Cambridge, MA, USA). The preparation was semi-submerged and maintained in organ culture for 12-24 hrs at 35°C. After incubation the whole mount was processed for immunofluorescence as described above.

Paraganglia staining. Rat pups (10-14 day-old) were anesthetized by intraperitoneal administration of Somnotol (65 mg kg^{-1}), before perfusion via the aorta with phosphate-buffered saline (PBS) followed by PBS containing 4% paraformaldehyde. Fixed animals were then perfused with filtered (0.2 μm Millipore filter) Evans blue dye (100 mg dye/ml of 0.9 % NaCl; adjusted pH to 7.4), so as to stain paraganglia due to the high permeability of their blood vessels to large dye molecules (McDonald and Blewett, 1981). The carotid bifurcation was then excised and the tissue was mounted in fresh PBS.

Images were captured with a Zeiss S16 upright microscope equipped with a Retiga monochrome 12-bit digital camera (QImaging, Burnaby, BC, Canada), with the aid of Northern Eclipse software (Empix Imaging Inc., Mississauga, ON, Canada).

Nystatin perforated-patch whole-cell recording. Nystatin perforated-patch, whole-cell recording was used in this study according to procedures described in detail elsewhere (Zhong *et al.* 1997; Zhang *et al.* 2000). Patch pipettes were made from Corning #7052 glass (A-M Systems Inc., Carlsborg, WA, USA) or borosilicate glass (WPI, Sarasota, FL, USA) using a vertical puller (PP 83; Narishige Scientific Instrument Lab., Tokyo, Japan) and were fire-polished. Micropipettes had a resistance of 2-10 MΩ when filled with intracellular recording solution, and formed gigaseals between 2 and 12 GΩ. In most experiments ~ 75 % of the series resistance was compensated, and junction potentials were cancelled at the beginning of the experiment. The extracellular fluid was warmed before entering the recording chamber, where the mean temperature was 34 ± 2 °C over the time course of the experiments. Whole-cell currents or membrane potential were recorded with the aid of an Axopatch 1D amplifier (Axon Instruments Inc., Union City, CA, USA) equipped with a 1 GΩ headstage feedback resistor and a Digidata 1200 A-D converter (Axon Instruments Inc., Union City, CA, USA), and stored on a personal computer. Current and voltage clamp protocols, data acquisition and analysis were performed using pCLAMP software (version 6.0, Axon Instruments Inc.) and Axotape (version 2.02, Axon Instruments Inc.). ATP-induced currents were sampled at 0.5-1 kHz

and stored on a computer for analysis with pCLAMP (version 9.0, Axon Instruments Inc.).

Solutions and drugs. Experiments were performed using extracellular fluid of the following composition (mM): NaCl, 110; KCl, 5; $CaCl_2$, 2; $MgCl_2$, 1; glucose, 10; sucrose, 12; $NaHCO_3$ 24; at pH ~ 7.4 maintained by bubbling with 5 % CO_2. For nystatin perforated-patch recordings (Zhong *et al.* 1997; Zhang *et al.* 2000), the pipette solution contained (mM): potassium glutamate or gluconate, 115; KCl, 25; NaCl, 5; $CaCl_2$, 1; Hepes, 10 and nystatin 300 μg ml^{-1}, at pH 7.2. All solutions were filtered through a 0.2 μm Millipore filter before use. During recordings the culture was continuously perfused under gravity flow and the fluid in the recording chamber was maintained at a constant level by suction. The drugs tetrodotoxin (TTX), tetraethylammonium (TEA), ATP, α,β-methylene ATP (α,β-MeATP), 2'- & 3'-O-(4 benzoylbenzoyl)-ATP (BzATP), oxidized-ATP (Ox-ATP), ivermectin (IVM), brilliant blue G (BBG), L-NG-nitroarginine methylester (L-NAME) and 2-(4-carboxyphenyl)-4,4,5,5-tetramethyl-imidazoline-1-oxyl-3-oxide potassium or carboxy-PTIO (cPTIO) were obtained from Sigma Chemical Co. All agonists (ATP, BzATP and α,β-MeATP) were applied by a 'fast perfusion' system utilizing double-barrelled pipettes, while modulators (i.e, IVM) and antagonists (suramin, Ox-ATP and BBG) were applied to the bath by perfusion under gravity (Zhong *et al.* 1997). EC_{50} and IC_{50} values were obtained by the best fit of the data using the Hill function.

Statistics. Results are represented in the text as means ± standard error of the mean (s.e.m.). Current densities ($pA.pF^{-1}$) were compared using paired or unpaired Student's *t* test, as appropriate, and ratios were compared using a non-parametric test (Mann-Whitney); the level of significance was set at $P < 0.05$.

RESULTS

ATP-evoked responses in GPN neurons

Prior to ATP application, GPN neurons from both proximal and distal populations were tested for O_2-sensitivity by perfusing the culture with a hypoxic solution (PO_2 ~ 15 Torr) as previously described (Campanucci *et al.* 2003a). The majority (> 90 %) of neurons responded to hypoxia with membrane depolarization that sometimes triggered action potentials (Fig. 1 A). Rapid perfusion of ATP (5 μM) over such neurons also caused membrane depolarization and an increase in excitability (Fig. 1 B). Under voltage clamp at –60 mV, ATP evoked a dose-dependent inward current in GPN neurons with an apparent EC_{50} of ~ 10.5 μM (Fig. 1 B-C; n = 11). These data were not well fitted by a simple Hill equation, suggesting multiple receptors were involved. The reversal potential of the ATP-evoked current occurred near 0 mV (Fig. 1 E-F; n = 7), suggesting it was carried by non-selective cation channels. In addition, the ATP-evoked current showed typical inward rectification (Fig. 1 F), as previously described for currents carried by P2X purinergic receptors (Brake *et al.* 1994; Evans *et al.* 1996; reviewed by North, 2002).

Evidence for functional expression of P2X2-P2X3 heteromeric receptors

The kinetic profile of ATP-evoked inward currents in GPN neurons indicated a fast activation phase followed by slow inactivation (Fig. 1 C; see example traces). Such biphasic kinetics are characteristic of cells expressing P2X2 and P2X3 homomeric or P2X2-P2X3 heteromeric receptors (North, 2002). Consistent with the presence of P2X2-P2X3 heteromeric receptors (Radford *et al.* 1997), α,β-methylene ATP (α,β-MeATP)

evoked slowly desensitizing inward currents (at –60 mV) with an EC_{50} of ~ 3.2 μM (Fig. 2 A-B). These data suggest that GPN neurons express P2X2-P2X3 heteromeric receptors, however, the expression of P2X2 and P2X3 homomeric forms cannot be excluded.

Additional experiments, based on the application of the non-selective purinergic (P2) antagonist suramin (North and Surprenant, 2000), indicated that the expression pattern of P2X receptors on GPN neurons was more complex. For example, in the presence of high doses of suramin (500-1000 μM), expected to block P2X2 and P2X3 homomeric and heteromeric receptors (North and Surprenant, 2000), a residual inward current persisted during application of 50 μM ATP (Fig. 2 C-D). In Fig. 2 D, approximately 20 % of the ATP-evoked inward current remained in the presence of 500 μM suramin. These findings suggest that in addition to contributions from P2X2 and P2X3 subunits, other P2X purinergic subunits are involved.

Evidence for functional expression of P2X7 homomeric receptors

At least two types of P2X receptors, i.e. P2X7 and P2X4, display low sensitivity to suramin when heterologously expressed in their homomeric forms (Ralevic and Burnstock, 1998; North and Surprenant, 2000; Khakh 2001a,b). Using pharmacological tools we first tested for functional expression of P2X7 receptors, which show the lowest sensitivity to suramin (IC_{50} ~ 500 μM; reviewed by North and Surprenant, 2000). Low micromolar concentrations of 4-benzoylbenzoyl-ATP (BzATP), an agonist with even greater potency than ATP itself in activating P2X7 receptors (North and Surprenant, 2000; North, 2002), also elicited inward currents in ATP-sensitive GPN neurons (Fig. 3

A). The EC_{50} for a group of 4 cells exposed to BzATP was ~ 1.9 μM (Fig. 3 B). These data suggest that at least a population of purinergic receptors expressed in GPN neurons has moderate-to-high affinity for BzATP, and this is consistent with the expression of homomeric P2X7 receptors (North, 2002).

Since micromolar concentrations of BzATP also activate heterologously expressed rat P2X1, P2X2 and P2X3 homomeric, as well as rat P2X2-P2X3 heteromeric, receptors (Bianchi *et al.* 1999; North and Surprenant, 2000), it was necessary to confirm the presence of P2X7 receptors by other methods. We therefore used the antagonist brilliant blue G (BBG; 0.1-100 nM; Fig. 3 C), which is reported to be a selective blocker of heterologously expressed rat P2X7 receptors in the nanomolar concentration range (Jiang *et al.* 2000). BBG at concentrations between 10-100 nM inhibited up to ~ 40 % of the BzATP-evoked inward current (Fig. 3D; n = 5) in GPN neurons, and this component was likely due to blockade of homomeric P2X7 receptors. Further confirmation of the functional expression of P2X7 receptors was obtained following exposure to the irreversible P2X7-selective antagonist, oxidized-ATP (OxATP; Murgia *et al.* 1993). In these experiments, we first pre-incubated GPN neurons with 300 μM OxATP for 2h at 37 °C to block P2X7 receptors (Murgia *et al.* 1993), and then tested the sensitivity of the remaining ATP-evoked currents to suramin. Pre-treatment with OxATP increased the suramin sensitivity of ATP-evoked currents (Fig. 4 A-B), such that the inhibition due to 500 μM suramin significantly increased from 71 % (n = 5) in control cells to 87 % (n = 11) in cells pre-treated with OxATP ($P < 0.001$). In addition, we also studied the ATP-sensitivity of those cells pre-treated with OxATP. Interestingly, the half-maximal ATP

concentration (EC_{50}) for OxATP pre-treated cells was ~ 2.5 μM, a value significantly lower than that for control cells (EC_{50} ~ 10.5 μM; $P < 0.05$). This is illustrated by the leftward shift of the dose-response relation for cells pre-treated with OxATP (Fig. 4 C). Taken together, these data provide evidence for the functional expression of P2X7 receptors in GPN neurons, and further imply that when these receptors are chemically disabled, purinergic signalling is maintained at least in part by purinoceptors containing P2X2 and P2X3 subunits.

Functional evidence for the expression of P2X4 receptors in GPN neurons

In a few neurons (4/11) that were pre-incubated with OxATP, a substantial ATP-evoked current persisted in the presence of high doses (500-1000 μM) of suramin (not shown), suggesting the presence of another P2X receptor subtype distinct from P2X7. One candidate, homomeric P2X4 receptors, is known for its relative insensitivity to suramin (North and Surprenant, 2000). To test whether GPN neurons also expressed functional P2X4 receptors we used ivermectin (IVM), a channel modulator that has been shown to enhance specifically P2X4-mediated currents in heterologous expression systems (Khakh *et al.* 1999). IVM (2-10 μM) caused potentiation of the ATP-evoked current in 5 out of 13 (~ 38.5 %) GPN neurons tested (e.g. Fig. 5 A). For reasons that are not presently understood, this drug also had an inhibitory effect in 5/13 (~ 38.5 %) and no effect in 3/13 (~ 23 %) cases. Representative examples are shown in Fig. 5 B-C.

Immunolocalization of P2X2, P2X3, P2X7 and P2X4 subunits *in situ*

Results from the functional and pharmacological studies discussed above led us to investigate the possible expression of P2X2, P2X3, P2X7 and P2X4 subunits in GPN neurons using immunofluorescence. As previously described (Campanucci *et al.* 2003a), these neurons are concentrated in two groups, one proximal and near the carotid sinus nerve (CSN) bifurcation, and the other located more distally along the glossopharyngeal nerve. For both proximal (Fig. 6 A-C) and distal (Fig 6 D-F) populations there was co-localization of P2X2 and P2X3 subunits in the soma of GPN neurons as revealed by double-label immunofluorescence (n = 10). These data are consistent with the functional evidence for heteromeric P2X2-P2X3 receptors.

The distribution of P2X7 immunostaining was more complex at the two sites where GPN neurons were located. Whereas P2X7 subunits were immunolocalized in neurofilament (NF)-positive cell bodies of the proximal GPN neurons (n = 7; e.g. Fig. 6 G-I), they appeared targeted to nerve endings surrounding the NF-positive cell bodies of the distal population (n = 7; Fig. 6 J-L). Since both neuronal populations project to the carotid body (CB; Wang *et al.* 1994a,b; Campanucci *et al.* 2003a), we also investigated the distribution of P2X7-positive immunostaining in tissue sections of the CB. In Fig. 7 A (n = 5), nerve terminal staining in the CB was visualized by positive immunoreactivity against neurofilament (NF) and GAP-43, and there were regions of co-localization with P2X7-immunoreactivity (e.g. arrows Fig. 7B, C). Interestingly, punctate P2X7 immunostaining was seen near tyrosine hydroxylase (TH)-positive clusters of CB chemoreceptor cells as illustrated in Fig. 7 D (n = 3). To test whether this P2X7-

immunostaining in the CB was solely of GPN origin, we performed 'denervation' experiments *in vitro*, in which the petrosal ganglion (PG) was removed and the remaining tissue explant consisting of GPN, CSN, and CB was kept intact and incubated for 12 hr at 37 ^{o}C in organ culture. In these experiments P2X7 immunoreactive nerve endings were also observed near clusters of CB chemoreceptor cells (n = 5; not shown), suggesting the GPN was at least a major source of the P2X7 innervation in the CB. Control experiments in which nerve fibers in the explant were selectively stained by NF and GAP-43-immunofluorescence revealed that 12 hr *in vitro* was enough time for the disappearance of fibers originating from the PG (n = 3; not shown). In additional experiments, TH-positive CB chemoreceptor clusters were observed in close proximity to neuronal nitric oxide synthase or nNOS-positive nerve processes (Fig. 7E), consistent with the proposal that local interactions may occur between GPN processes and CB chemoreceptor cells *in situ*.

Since our electrophysiological data suggested the presence of P2X4 receptors in at least a subpopulation of GPN neurons, we used immunofluorescence to localize P2X4 subunits. Consistent with the data reported above, positive P2X4-immunofluorescence was localized in both populations of GPN neurons (Fig. 7 H-M). However, the majority of NF /GAP-43 (n = 10; Fig. 7 H-J) positive neurons observed along the GPN expressed immunoreactive P2X4 subunits. This contrasts with our electrophysiological data, which suggested that only ~ 38 % of GPN neurons expressed functional homomeric P2X4 receptors. In addition, P2X4-immunofluorescence was co-localized with that of P2X3 (n

= 5; Fig. 7 K-M), confirming the expression of multiple P2X receptors in the same neurons.

Localization of P2X7 immunofluorescence in culture

Though our electrophysiological data showed that both populations of GPN neurons expressed functional P2X7 receptors on their cell bodies, immunofluorescence studies *in situ* indicated positive P2X7 expression on surrounding nerve terminals rather than on the soma of the distal population (Fig. 6 J-L). We therefore compared immunolocalization of P2X7 subunits in GPN neurons in cultures ≤ 24 hr old, i.e. conditions used for patch clamp experiments, with cultures 48-72 hr old. Interestingly, within 24 hr after isolation, P2X7 immunofluorescence was concentrated in the cell bodies of both populations of GPN neurons (n = 10; Fig. 8 A-C). However, at 48-72 hr after isolation the P2X7 immunostaining was weaker in the cell bodies and was detected along nerve processes (n = 5; Fig. 8 D-F). These data suggest that shortly after axotomy *in vitro*, P2X7 subunits are expressed in the soma of GPN neurons, and that they are transported away from the soma as the nerve processes emerge over time in culture.

P2X receptor function in GPN neurons co-cultured with carotid body chemoreceptors

GPN neurons are positive for neuronal NOS (e.g. Figs. 7 E; 8) and are thought to mediate efferent inhibition of the CB via release of NO (Wang *et al.* 1994a,b, 1995a,b). To test whether P2X receptor activation in GPN neurons may contribute to this inhibition

we used co-cultures of GPN neurons and CB receptor (type I) cell clusters, of which the latter lack P2X receptors (Zhang *et al.* 2000; Prasad *et al.* 2001). GPN neurons, 'juxtaposed' (JGPN) to type I cell clusters in co-culture (Fig. 9 A-C), were selected for rapid application of either ATP (5-10 μM) or BzATP (5 μM), while membrane potential was simultaneously monitored in a type I cell within the adjacent cluster. As previously reported (Zhang *et al.* 2000), in most cases ATP had negligible effects on the resting potential of type I cells cultured alone (n = 10; e.g. Fig. 9 D), and this was also the case for the P2X7 receptor agonist, BzATP (n = 4; e.g. Fig. 9 E). However, in a few of these cases (n = 3; not shown), ATP caused a small hyperpolarization (< 2 mV). Therefore, ATP and BzATP seemed to be good candidates for the selective activation of P2X receptors in co-cultures of GPN neurons and type I cells (see however, Mokashi *et al.* 2003; Xu *et al.* 2003). Interestingly, application of BzATP (5 μM) to JGPN neurons caused a strong hyperpolarization (~ 8 mV) of type I cells within the adjacent cluster (Fig. 9 G); the membrane potential hyperpolarized from a mean resting level of –44.7 ± 3.1 mV to –52.2 ± 3.3 mV (n = 8) during BzATP application. In 2 cases (e.g. Fig. 9 F) BzATP also caused inhibition of the spontaneous activity that is sometimes seen in type I cells within large clusters (Zhang and Nurse, 2000). Since BzATP tended to produce long-term changes in type I cell membrane potential, we tested the effects of the naturally occurring nucleotide, ATP, which is itself released from type I cells during CB chemoexcitation (Zhang *et al.* 2000; Zhang and Nurse, 2004). As exemplified in Fig. 9 H, ATP also caused a strong hyperpolarization (~ 8 mV) in type I cells without producing

any long-term changes in membrane potential; the latter increased from a mean resting level of –44.6 ± 3.0 mV to –54.5 ± 3.3 mV (n = 7) in the presence of ATP.

We next investigated whether or not NO was responsible for the hyperpolarization observed in type I cells, by exposing co-cultures to the NO scavenger, carboxy-PTIO (cPTIO; Summers *et al.* 1999). As illustrated in Fig. 9 I, pre-incubation (> 2 min) with 500-1000 μM cPTIO abolished the ATP-induced hyperpolarization in co-cultures (n = 3).

Paraganglia staining

During hypoxia, potential sources of ATP that could stimulate P2X receptors on GPN neurons or their processes include ATP released from CB type I cells (Zhang *et al.* 2000) and from red blood cells in the circulation (Bergfeld and Forrester 1992; Ellsworth *et al.* 1995). To confirm that the microenvironment around GPN neurons *in situ* has ready access even to large molecules in the circulation, we fixed and perfused rat pups with solution containing Evans blue dye (McDonald and Blewett, 1981). This procedure revealed the anatomical structure of blood vessels surrounding the area where both populations of GPN neurons were concentrated (n = 4; Fig. 10 A-B). As previously described (McDonald and Blewett, 1981), these groups of neurons or 'paraganglia' are closely related to tortuous blood vessels that seem to spiral around the area surrounding the GPN neurons (Fig. 10 C). Deposits of Evans blue dye were observed at these locations (Fig. 10 C) confirming the high permeability of these blood vessels to the dye. These data suggest that GPN paraganglia may have direct access to substances released

into the blood stream, for example ATP, released from red blood cells during hypoxia (Bergfeld and Forrester 1992; Ellsworth *et al.* 1995; reviewed by Ellsworth, 2000).

DISCUSSION

In this study we characterized the responses to ATP of O_2-sensitive paraganglion neurons that are embedded in the rat glossopharyngeal nerve (GPN), and are thought to provide efferent inhibition of carotid body (CB) chemoreceptors (Prabhakar *et al.* 1993; Wang *et al.* 1993, 1994a,b, 1995a,b; Grimes *et al.* 1994; Höhler *et al.* 1994; Prabhakar 1999). These GPN neurons are distributed in two distinct populations, a proximal one near the branch point of the GPN and carotid sinus nerve (CSN), and a more distal one located further along the GPN (Campanucci *et al.* 2003a). Both populations express neuronal nitric oxide synthase (nNOS)-immunoreactivity and innervate the CB (Wang *et al.* 1993, 1994a,b, 1995a,b; Campanucci *et al.* 2003a), where local release of NO is proposed to inhibit the CB response to hypoxia. In addition to its well-known function as a physiologically important CB chemoexcitant, hypoxia also directly excites GPN neurons, presumably leading to an increase in intracellular Ca^{2+}, NOS activation, and NO release (this study; Campanucci *et al.* 2003a).

Expression of multiple P2X receptors in GPN neurons

Our present findings indicate that both populations of GPN neurons are also sensitive to ATP, thereby providing an alternative pathway by which these neurons could be activated, leading to NO release. In particular, ATP induced membrane depolarization under current clamp and activated rapid inward currents during voltage clamp recordings. The ATP-evoked responses were complex and the involvement of multiple P2X receptors was suggested, since a single Hill equation did not produce an adequate fit to the dose-

response data. We obtained evidence for the involvement of P2X2, P2X3, P2X4 and P2X7 subunits in the ATP response of GPN neurons. Electrophysiological and pharmacological data were consistent with the immunolocalization studies showing the presence of these four purinergic subunits in GPN neurons *in situ*. The combined data suggested that the functional expression of at least heteromeric P2X2-P2X3, homomeric P2X4 and homomeric P2X7 receptors. The occurrence of heteromeric P2X2-P2X3 receptors was inferred from the observation that application of the ATP agonist, α,β-methylene ATP (α,β-MeATP), also activated inward currents but with slow desensitization kinetics characteristic of heteromeric P2X2-P2X3 receptors (Lewis *et al.* 1995; Radford *et al.* 1997; reviewed by Ralevic and Burnstock, 1998; North and Surprenant, 2000; North, 2002). These data, however, do not rule out the possibility that homomeric P2X2 and homomeric P2X3 receptors are also present.

Several pharmacological approaches were used to obtain evidence for functional expression of P2X7 receptors in GPN neurons. First, the synthetic P2X7 agonist, 4-benzoylbenzoyl ATP (BzATP), evoked inward currents that were blocked by nanomolar concentrations of brilliant blue G (BBG), a selective P2X7 antagonist (Jiang *et al.* 2000). Second, pre-incubation with the irreversible and selective P2X7 antagonist, oxidized ATP (OxATP), resulted in blockade of a suramin-insensitive component of the ATP-evoked current as expected of P2X7 homomeric receptors (Murgia *et al.* 1993). Third, in cells pre-treated with OxATP there was a significant reduction in the half-maximal dose for the ATP response (i.e. EC_{50} reduced from ~ 10.5 μM to ~ 2.5 μM), suggesting that ATP was more effective at the remaining purinoceptors when P2X7 receptors were chemically

disabled. In heterologous expression systems, P2X7 homomeric receptors are weakly activated by ATP, but are highly sensitive to the synthetic ATP analog, BzATP (Chessell *et al.* 1998; reviewed by North and Surprenant, 2000; North, 2002). Consistent with our electrophysiological data, P2X7 purinergic subunits were immunolocalized in both populations of GPN neurons in culture. Though P2X7 subunits were localized in the cell bodies of proximal GPN neurons *in situ*, the distal population appeared to be contacted by P2X7-immunopositive nerve endings. This raises the possibility that local networks or circuits involving purinergic transmission may provide a means of cell-to-cell communication among GPN neurons. The fact that P2X7-immunoreactive nerve endings persisted in explant cultures of intact GPN-carotid sinus nerve-carotid body preparations, after 24 hr *in vitro*, precludes a significant contribution from the petrosal ganglion. Though P2X7 nerve endings appeared to terminate on the soma of distal GPN neurons *in situ*, surprisingly the soma failed to express P2X7-immunoreactivity. This contrasted with our electrophysiological findings *in vitro*, where isolated distal GPN neurons showed functional evidence for P2X7 receptors. The reasons for this discrepancy are not completely understood, though it is noteworthly that in cultures > 24 hr old, P2X7 immunostaining was more prominent in growing neuronal processes. Thus, the possibility of a selective targeting of P2X7 subunits to the terminals of distal GPN neurons *in situ* cannot be excluded. Indeed, it has been reported that P2X7 receptors are targeted to presynaptic terminals in nervous tissue such as hippocampus, medulla oblongata, spinal cord, and nodose ganglion (Deuchars *et al.* 2001; Armstrong *et al.*

2002; Sperlágh *et al.* 2002), suggesting that the receptor may be involved in the normal regulation of synaptic transmission at many presynaptic sites.

Our electrophysiological and immunofluorescence studies also uncovered a role for P2X4 receptors in GPN neurons. Initially, the presence of these receptors was suggested by the observation that a sub-population of neurons possessed a suramin-insensitive component of ATP-evoked current that was unaffected by the P2X7 antagonist, OxATP. Confirmation was obtained in additional experiments where ivermectin (IVM), which selectively potentiates homomeric P2X4 currents in heterologous expression systems (Khakh *et al.* 1999), enhanced ATP-evoked currents in ~ 38.5 % (5/13) of the neurons. Surprisingly, our immunofluorescence data indicated almost all GPN neurons were positive for P2X4 immunoreactivity. The reasons for this discrepancy are unknown, though it is possible that the P2X4 subunit was not targeted to the cell membrane in the majority of cases. Alternatively, P2X4 subunits in GPN neurons may form a new heteromultimer variant with a different pharmacological profile than the homomeric form of the receptor. Though P2X4 subunits are known to form heteromultimers with P2X6 subunits (North and Surprenant, 2000), the possible presence of such P2X4-P2X6 heteromeric receptors does not resolve the issue since they are also potentiated by IVM (Khakh *et al.* 1999). Interestingly, IVM caused inhibition of the ATP-evoked response in ~ 38 % of the cells tested, while the remaining ~ 23 % were unaffected. An inhibitory effect of IVM has been reported in other native neuronal tissues, e.g. rat dorsal root ganglion neurons (De Roo *et al.* 2003), though the mechanisms are not understood.

A comparison of fitted curves for the ATP dose-response for P2X receptors expressed in GPN neurons, and for heterologously expressed P2X2-P2X3 heteromultimers (Lewis *et al.* 1995), homomeric P2X4 (Bo *et al.* 1995) and homomeric P2X7 (Chessell *et al.* 1998) receptors is shown in Fig. 11. The EC_{50} for ATP on P2X receptors in GPN neurons was close to that for P2X4 receptors, but the dose-response curve deviated from that of P2X4 receptors at lower and higher ATP concentrations (Fig. 11). The deviation is consistent with the additional presence of P2X2-P2X3 and P2X7 receptors, which should allow GPN neurons to be activated over a broad range of ATP concentrations, given that P2X2-P2X3 heteromultimers possess an EC_{50} of ~ 1 μM, whereas P2X4 and P2X7 homomeric possess EC_{50} values of 10 and ≥ 100 μM, respectively.

Role of GPN neurons in carotid body chemoreceptor inhibition

There is a large body of evidence supporting the involvement of NO in the efferent inhibition of rat (Grimes *et al.* 1994; Höhler *et al.* 1994) and cat (Prabhakar *et al.* 1993; Wang *et al.* 1993, 1994a,b, 1995a,b) carotid bodies (CB). The major source of NO is a plexus of nNOS-positive nerve fibers including sensory C-fibers, associated with clusters of CB chemoreceptor (type I) cells, and autonomic fibers from microganglion neurons, associated with the CB vasculature (Wang *et al.* 1995b). In our immunofluorescence studies on cryosections of the rat CB, nNOS-positive fibers were indeed found in close proximity to type I cells. However, the fact that they were also P2X7-immunoreactive (our unpublished observations; see also Fig. 7 B), and persisted

after petrosal denervation *in vitro,* suggested that they originated from the paraganglion neurons (see Campanucci *et al.* 2003a). Although we did observe P2X7-positive immunoreactivity associated with blood vessels in the rat CB (Fig. 7 B), this labeling did not co-localize with neuronal markers (Fig. 7 A-C), and was likely due to the known expression of P2X7 subunits in smooth muscle and endothelium of blood vessels (Ramirez and Kunze, 2002; Liu *et al.* 2004; reviewed by Burnstock, 2002).

In this study we also made an interesting and novel observation concerning the physiological role of GPN neurons in the efferent inhibition of CB chemoreceptor function. In co-cultures of CB chemoreceptor clusters and 'juxtaposed' GPN neurons, selective activation of P2X receptors on the neurons by ATP or its analog, BzATP, caused hyperpolarization of the chemoreceptor cell. This inhibitory effect was prevented by pre-incubation with the NO scavenger, carboxy-PTIO (cPTIO), suggesting that NO was the 'inhibitory signal' released upon purinergic activation of co-cultured GPN neurons.

A physiological model for the activation of GPN neurons

In the present work we characterized ATP-evoked responses in GPN neurons mediated by purinoceptors containing at least four types of P2X subunits i.e. heteromeric P2X2-P2X3, homomeric P2X4 and homomeric P2X7 receptors. We hypothesize that activation of GPN neurons by ATP leads to Ca^{2+} influx via these P2X receptors, and/or voltage-dependent Ca^{2+} channels, activated by ATP-induced membrane depolarization. This in turn leads to nNOS activation, increased NO production and release, and

ultimately inhibition of CB chemoreceptors. The fact that GPN neurons were excited by ATP (this study) and by hypoxia (Campanucci *et al.* 2003a) raises the question as to the physiological significance (see also, Shibuya *et al.* 1999; Luo *et al.* 2000). Staining of whole-mounts of the GPN during perfusion with the large molecular weight Evans blue dye confirmed that GPN neurons were associated with an intricate network of fenestrated blood vessels (McDonald and Blewett, 1981), thereby providing easy access to blood borne substances, such as ATP. Interestingly, it has been known for some time that red blood cells contain millimolar quantities of ATP (Miseta *et al.* 1993), which is released in response to hypoxia (Bergfeld and Forrester, 1992; Ellsworth *et al.* 1995; reviewed by Ellsworth, 2000). Therefore, this source of ATP, available in the blood stream during hypoxic stress, is a potential way of activating GPN neurons via the circulation. This, together with the direct excitatory effects of hypoxia on the membrane potential of GPN neurons (Fig. 1 A; see also Campanucci *et al.* 2003a), allows for robust stimulation of these neurons during hypoxia, leading to NO production and release.

Figure 1. ATP-evoked responses in O_2-sensitive GPN neurons. A-B, Representative traces showing the effects of hypoxia (Hox) and ATP respectively, on membrane potential of the same distal GPN neuron, 24 hr after isolation. Traces obtained during current clamp recording. C, voltage-clamp current recordings of ATP-evoked inward currents at –60 mV, due to increasing concentrations of ATP applied to a distal GPN neuron. D, Dose- response curve for ATP is shown on the right for a group of 11 GPN neurons (apparent EC_{50} = 10.5 μM). E, Traces of ATP-evoked current in a GPN neuron at different membrane potentials. F, I-V plot of ATP-evoked current for a group of 7 neurons; note inward rectification and reversal potential ~ 0 mV.

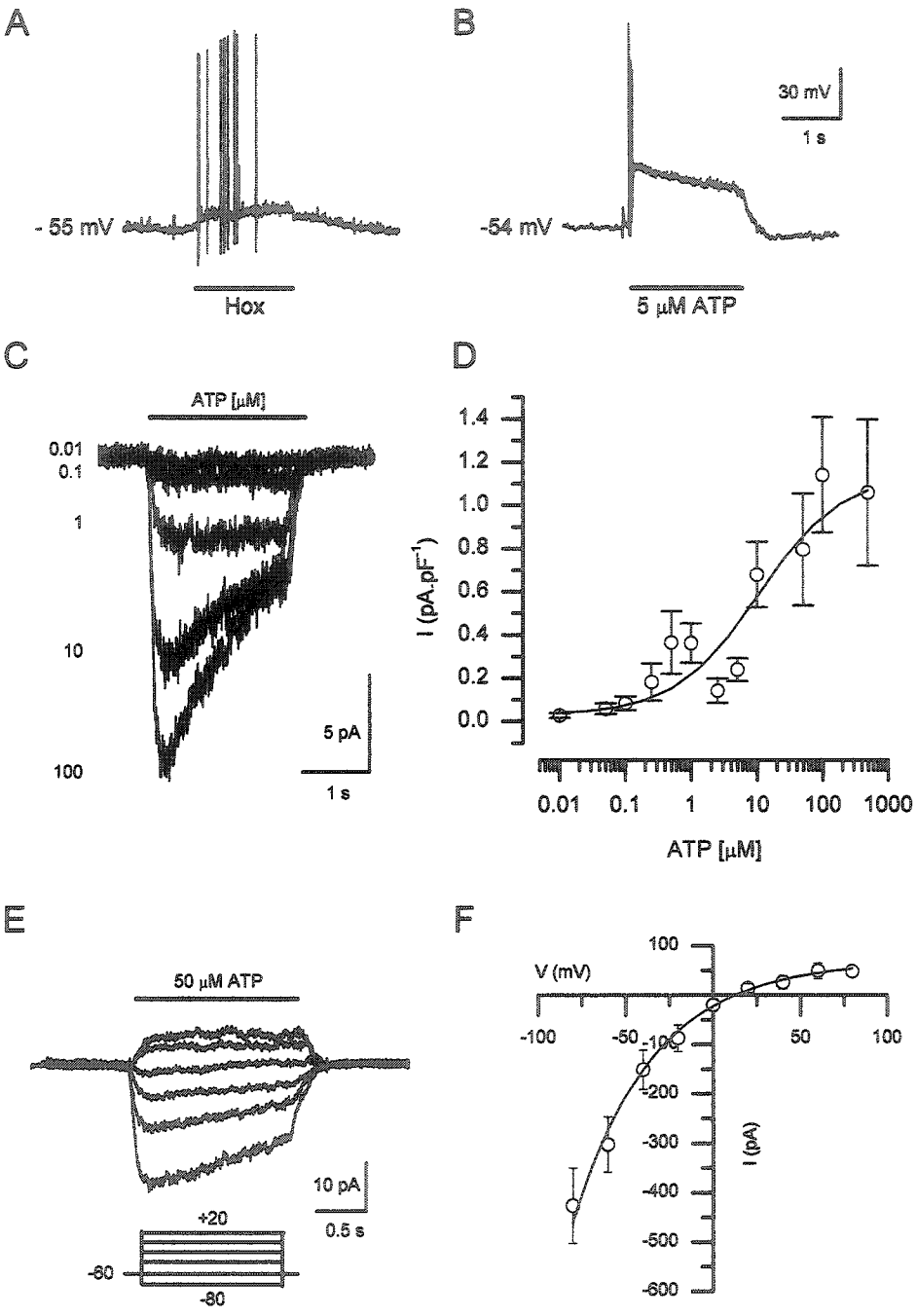
A
- 55 mV
Hox
B
30 mV
1 s
-54 mV
5 μM ATP
C
ATP [μM]
0.01
0.1
1
10
100
5 pA
1 s
D
I (pA.pF^{-1})
1.4
1.2
1.0
0.8
0.6
0.4
0.2
0.0
0.01
0.1
1
10
100
1000
ATP [μM]
E
50 μM ATP
10 pA
0.5 s
+20
-60
-80
F
100
V (mV)
-100
-50
50
100
-100
-200
-300
-400
-500
-600
I (pA)

Figure 2. Effects of ATP agonists and antagonists on GPN neurons. A, Current traces show a representative example of α,β-MeATP-evoked currents at –60 mV, due to increasing concentrations of the agonist on a distal GPN neuron. B, Dose-response curve for α,β-MeATP is shown for a group of 5 distal neurons (EC_{50} = 3.2 μM). C, current traces evoked by application of 50 μM ATP in the presence of increasing doses (values on left; μM) of the non-selective P2 receptor antagonist, suramin. D, Dose-response curve of the inhibitory effect of suramin on the ATP-evoked response in a group of 5 distal GPN neurons. Note that even high doses of suramin were insufficient to block completely the currents evoked by 50 μM ATP.

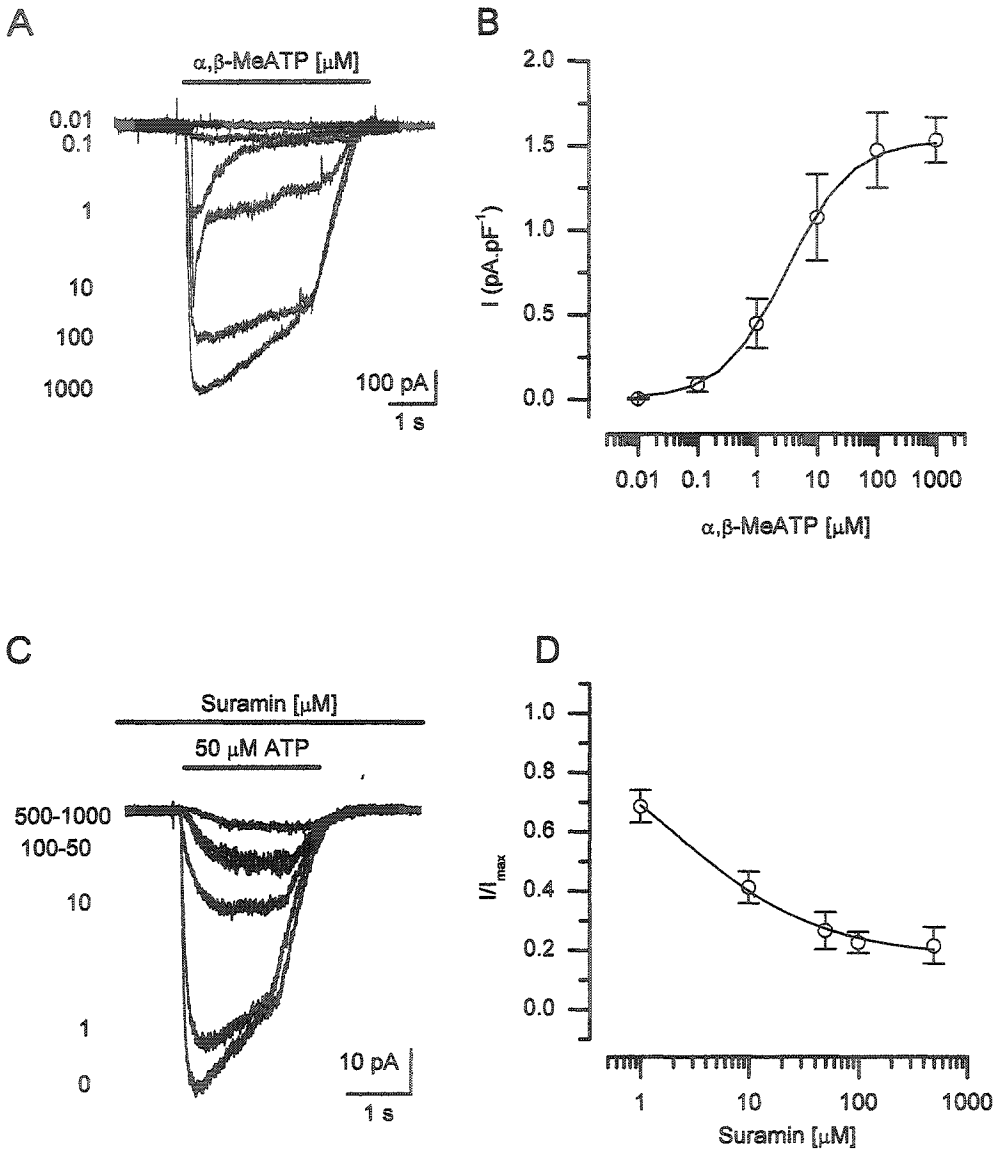
A
α,β-MeATP [μM]
0.01
0.1
1
10
100
1000
100 pA
1 s
B
I (pA.pF⁻¹)
2.0
1.5
1.0
0.5
0.0
0.01 0.1 1 10 100 1000
α,β-MeATP [μM]
C
Suramin [μM]
50 μM ATP
500-1000
100-50
10
1
0
10 pA
1 s
D
I/I_max
1.0
0.8
0.6
0.4
0.2
0.0
1 10 100 1000
Suramin [μM]

Figure 3. Effects of P2X7 agonists and antagonists on GPN neurons. A, Representative current traces elicited by application of ATP (10 μM) and the high-potency P2X7 agonist BzATP (10 μM) at –60 mV on a distal GPN neuron. B, Dose-response curve for BzATP is shown for a group of 4 distal GPN neurons (EC_{50} = 1.9 μM). C, Example current traces showing the effects of the P2X7 receptor blocker BBG on BzATP-evoked currents; concentrations of BBG are shown on right of traces. D, Dose-response curve for BBG inhibition of BzATP-evoked currents (n = 5). Note that BBG at nanomolar concentrations blocked a component of the BzATP-evoked current, suggesting the functional expression of P2X7 homomeric receptors in GPN neurons.

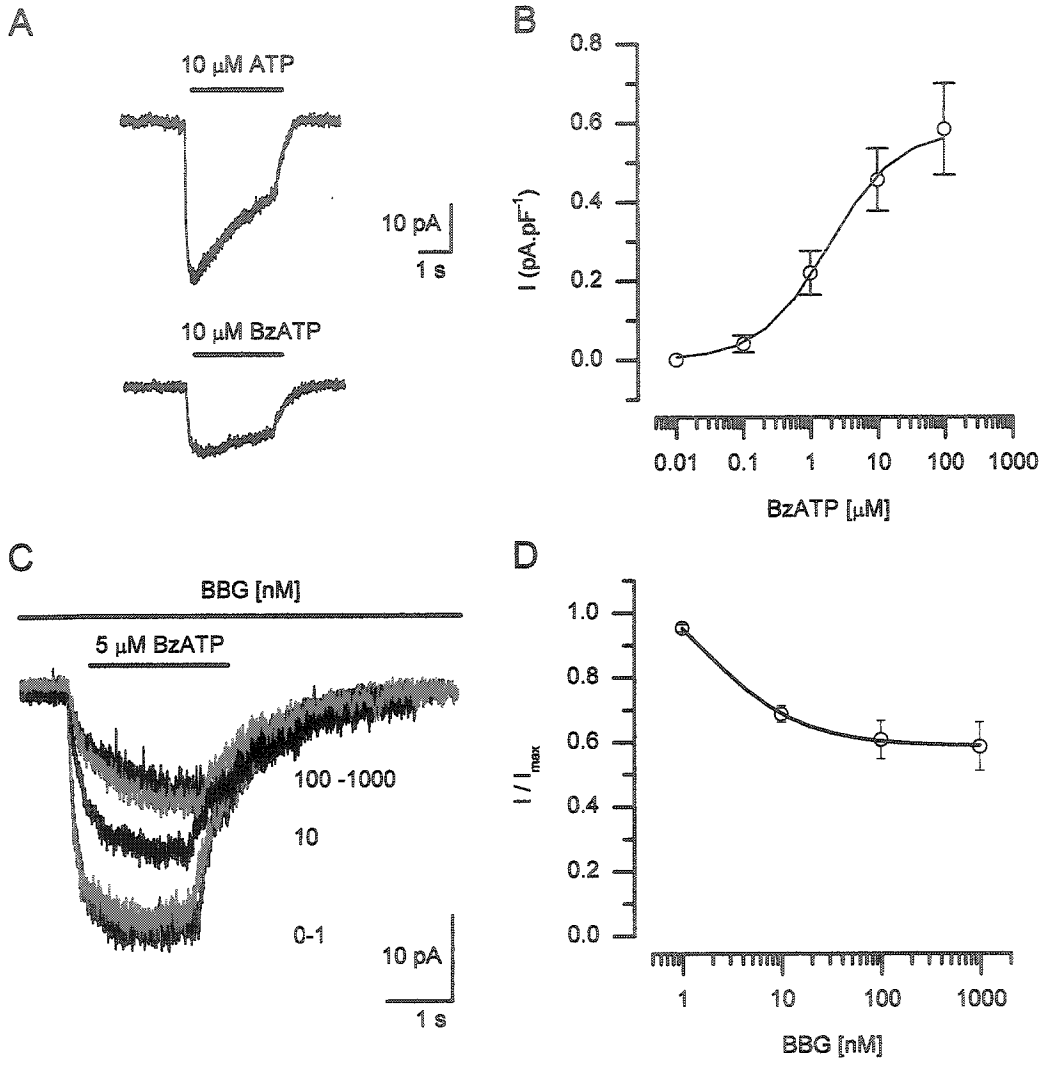
A
10 μM ATP
10 pA
1 s
10 μM BzATP
B
0.8
0.6
0.4
0.2
0.0
I (pA.pF⁻¹)
0.01
0.1
1
10
100
1000
BzATP [μM]
C
BBG [nM]
5 μM BzATP
100 -1000
10
0-1
10 pA
1 s
D
1.0
0.8
0.6
0.4
0.2
0.0
I / I max
1
10
100
1000
BBG [nM]

Figure 4. Effect of pre-treatment with OxATP on the suramin-sensitivity of the ATP-evoked response in GPN neurons. A, Example traces showing the effects of 0 and 500 μM suramin on the ATP-evoked (50 μM) currents from cells under two different conditions, control (left traces) and after pre-incubation with the irreversible P2X7-selective blocker, 500 μM OxATP (2hr at 37 ^{o}C; right traces). Note that after pre-incubation with OxATP, suramin (500 μM) abolished the ATP-evoked response in this cell. B, Histogram comparing the ATP-evoked current density ($pA.pF^{-1}$) with and without 500 μM suramin. Data are presented as mean ± s.e.m.; black bars represent control (without OxATP; n = 11) and white bars represent cells pre-treated with OxATP (n = 11); *a*: $p < 0.05$; *b*: $p < 0.001$. C, Dose-response curve for ATP is shown for cells pre-incubated with OxATP. Data obtained from OxATP pre-treated cells (solid line) are compared with those from control untreated cells (dotted line); note the significant reduction in EC_{50} for OxATP-treated group (EC_{50} ~ 2.5 μM) relative to control (EC_{50} ~ 10.5 μM; $P < 0.05$; n = 5).

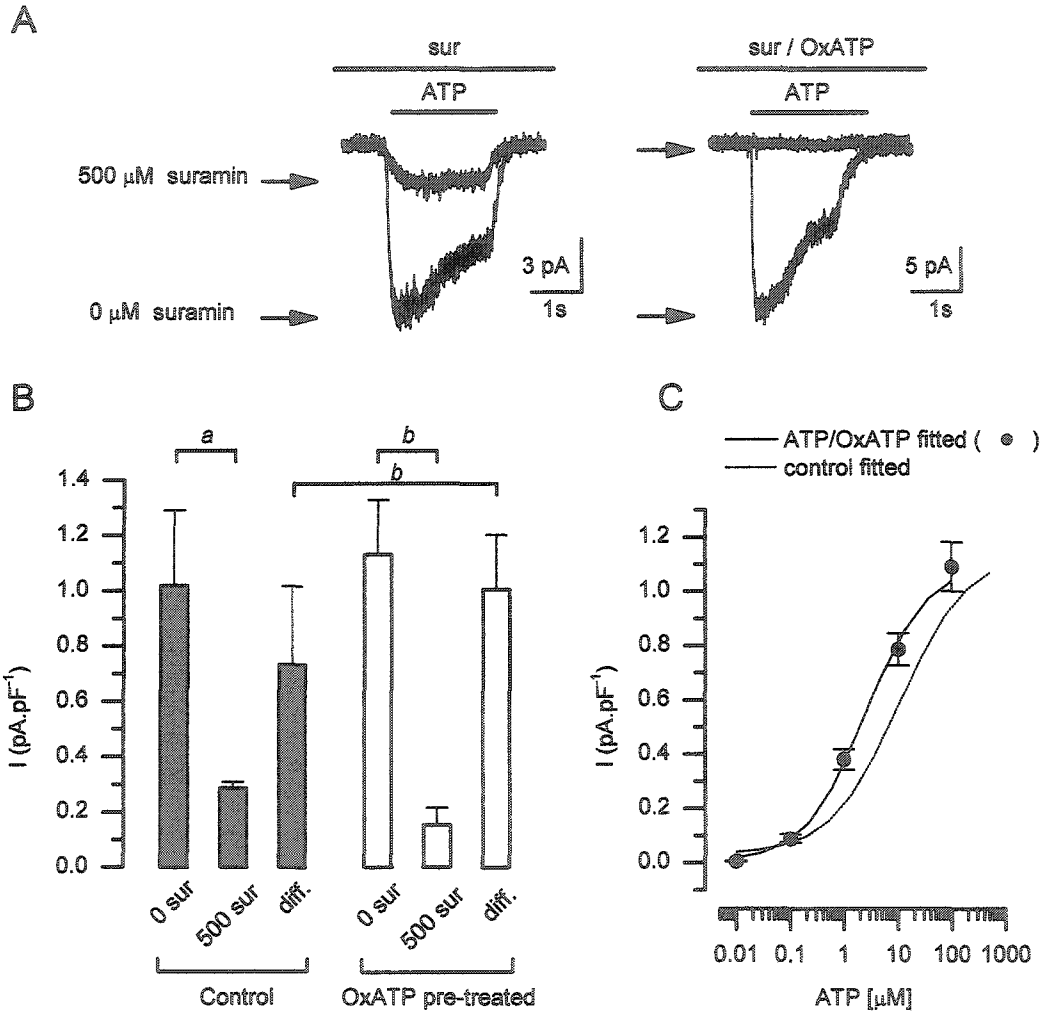
A
sur
ATP
sur / OxATP
ATP
500 µM suramin
0 µM suramin
3 pA
1s
5 pA
1s
B
a
b
b
I (pA.pF⁻¹)
1.4
1.2
1.0
0.8
0.6
0.4
0.2
0.0
0 sur
500 sur
diff.
0 sur
500 sur
diff.
Control
OxATP pre-treated
C
ATP/OxATP fitted (●)
control fitted
I (pA.pF⁻¹)
1.2
1.0
0.8
0.6
0.4
0.2
0.0
0.01 0.1 1 10 100 1000
ATP [µM]

Figure 5. Effects of ivermectin (IVM) on the ATP-evoked current in GPN neurons. A, IVM (10 μM) caused potentiation of the currents evoked by 2 μM ATP; this occurred in 5/13 cells tested. These data provide functional evidence for the expression of P2X4 purinergic receptors in GPN neurons. In addition, IVM caused inhibition of the ATP-evoked response in 5/13 cells (as exemplified in B) and had no effect in the remaining 3/13 cases (C).

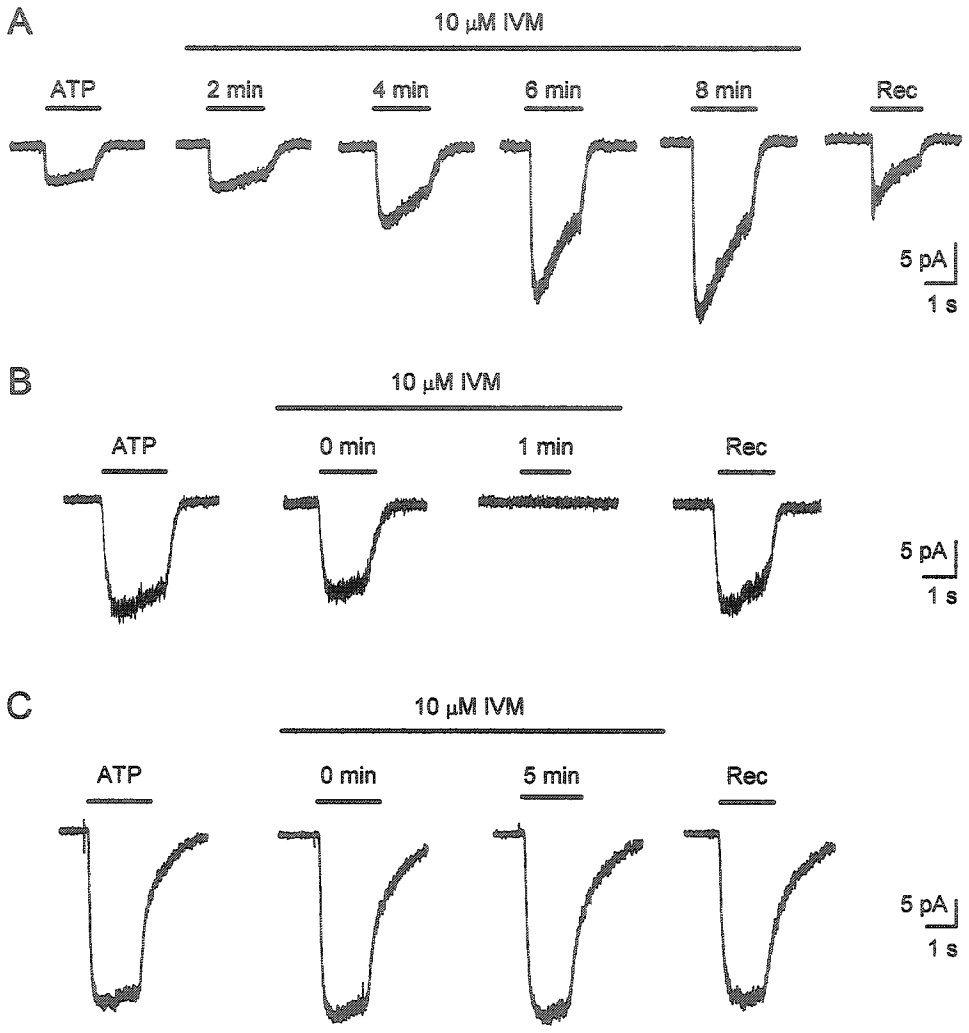
A
10 μM IVM
ATP
2 min
4 min
6 min
8 min
Rec
5 pA
1 s
B
10 μM IVM
ATP
0 min
1 min
Rec
5 pA
1 s
C
10 μM IVM
ATP
0 min
5 min
Rec
5 pA
1 s

Figure 6. Localization of purinergic subunits in GPN neurons *in situ* by confocal immunofluorescence. Proximal neurons located at the bifurcation of the GPN and CSN expressed both P2X2 (A; Texas Red) and P2X3 (B; FITC) immunofluorescence; note co-localization in merged images, C. Similarly, many neurons at the distal bifurcation co-expressed P2X2 and P2X3 subunits (D-F). Figure G-I shows co-localization of P2X7 purinergic subunit with the neuronal marker, neurofilament (NF), in proximal GPN neurons. In contrast, in Figs. J-L, the distal GPN neurons failed to express P2X7 subunits in their NF-positive soma (K), but were surrounded by P2X7-positive nerve endings (J-L). Scale bars represents 50 μm in A-L.

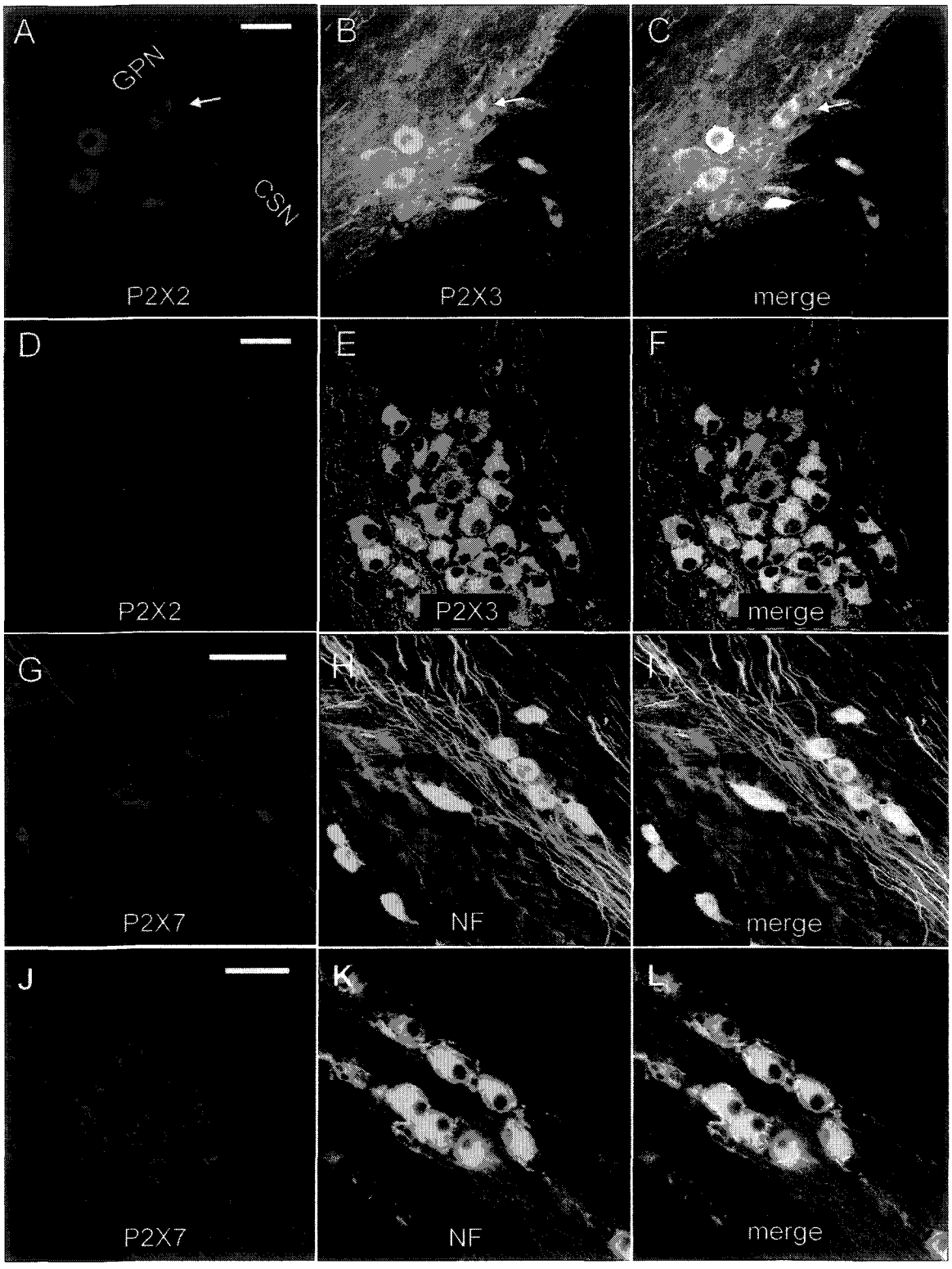
A
GPN
CSN
P2X2
B
P2X3
C
merge
D
P2X2
E
P2X3
F
merge
G
P2X7
H
NF
I
merge
J
P2X7
K
NF
L
merge

Figure 7. Immunolocalization of P2X subunits in GPN neurons and in nerve processes adjacent to CB chemoreceptors *in situ*. A-C, Co-localization of P2X7 (green) and neuronal markers (NF+GAP-43; red) on nerve endings in tissue sections of rat CB. Nerve processes surround CB type I cell clusters (not labeled in this section); arrows in B, C show regions of co-localization. Note P2X7 labeling at lower right in B and C was not associated with nerve endings. D, Localization of TH and P2X7 immunoreactivity in CB tissue sections; note punctuate P2X7 immunostaining (green) is closely associated with a TH-positive (red) type I cell cluster. E, localization of nNOS and P2X7-immunostaining in CB tissue section. Note close association of punctate nNOS immunoreactive processes (green) with TH-positive (red) type I cells. H-J, Confocal images showing co-localization of P2X4 subunits in proximal, NF+GAP-43 -positive GPN neurons. In Figs. K-M, there is co-localization of P2X4 and P2X3 subunits in the distal population of GPN neurons. In control experiments, pre-incubation with blocking peptides for P2X7 and P2X4 antibodies, abolished all immunostaining in Figs. F and G respectively. Scale bars represent 50 μm (A-C), 10 μm (D-E), and 100 μm (H-M).

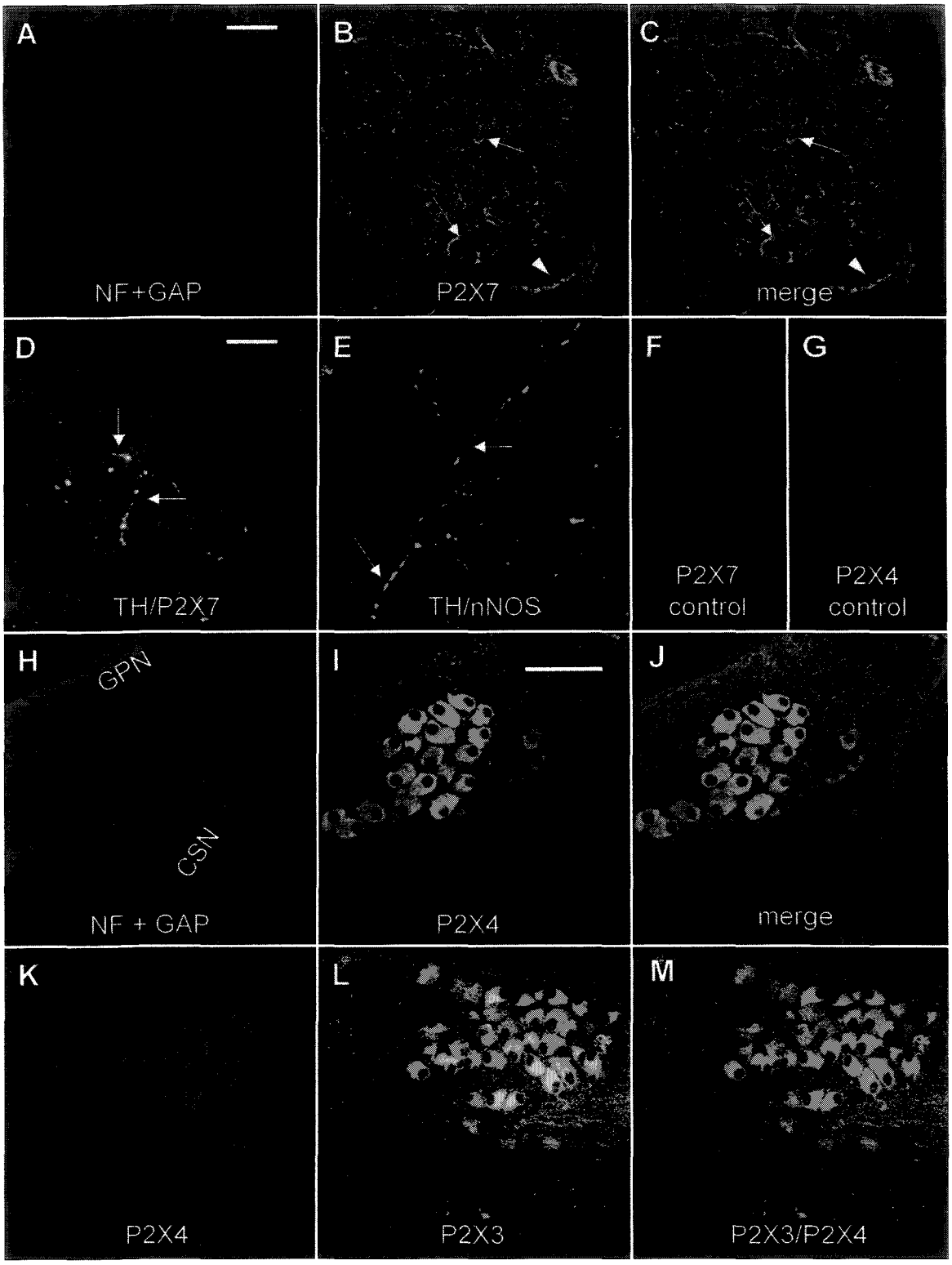
A
B
C
NF+GAP
P2X7
merge
D
E
F
G
TH/P2X7
TH/nNOS
P2X7
control
P2X4
control
H
GPN
CSN
I
J
NF + GAP
P2X4
merge
K
L
M
P2X4
P2X3
P2X3/P2X4

Figure 8. Confocal immunolocalization of nNOS and P2X7 subunits in cultured GPN neurons from the distal population. A-C, co-localization of nNOS and P2X7 immunoreactivity in same neuronal cell body ~ 24 hr after isolation, i.e. approximate culture duration for patch clamp experiments. D-F, Similar experiment as in A-C, except that immunostaining was done 48-72 hr after cell isolation. Note that at this time, P2X7 subunits were less concentrated in cell bodies and were detected along neuronal processes and their endings. Scale bars represent 30 μm.

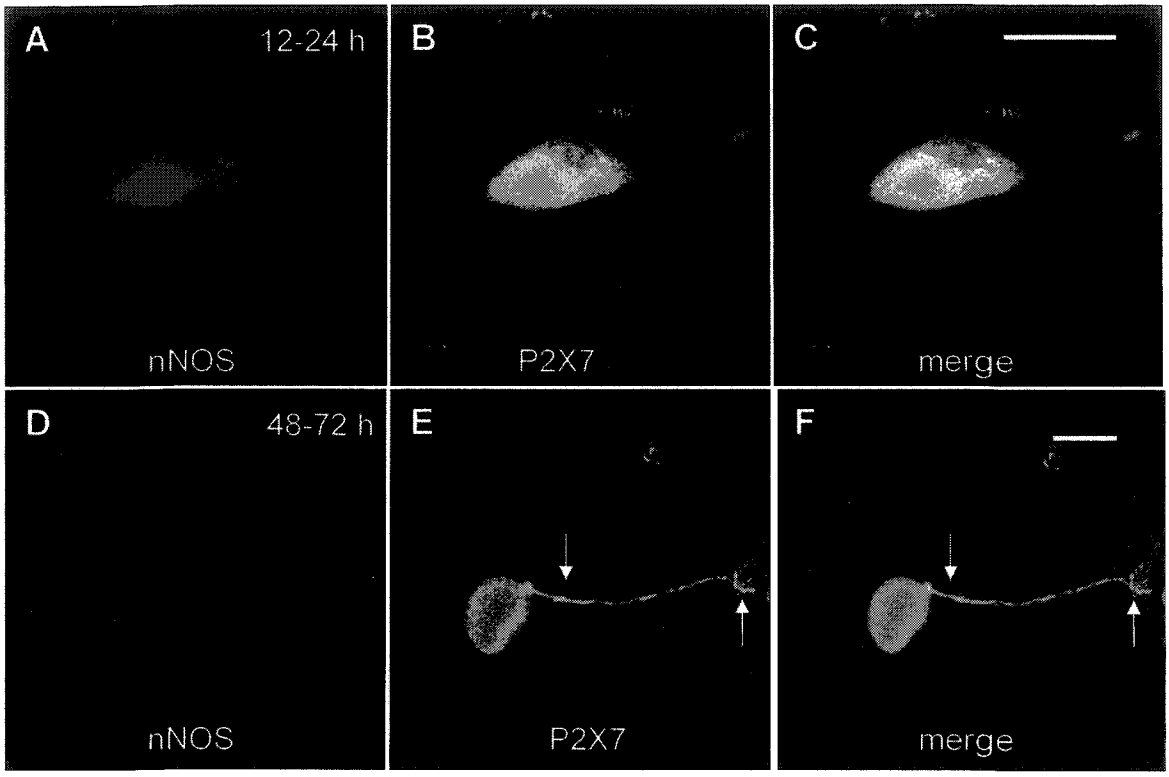
A
12-24 h
nNOS
B
P2X7
C
merge
D
48-72 h
nNOS
E
P2X7
F
merge

Figure 9. Effects of ATP and BzATP on the membrane potential of type I cells cultured with and without 'juxtaposed' GPN (JGPN) neurons. A-C, Confocal immunofluorescence of co-culture showing a cluster of TH-positive type I cells (green) in intimate association with several JGPN neurons and their processes, that were positive for NF and GAP-43 (red). D-E, Lack of effect of ATP (10 μM) and BzATP (5 μM), applied by rapid perfusion during period indicated by upper horizontal bars, on the membrane potential of type I cells cultured alone. In F-I, recordings were obtained from type I cells in close proximity to JGPN neurons (as in Fig. A-C), which therefore could be directly stimulated during application of the P2X agonist. In F, application of BzATP caused inhibition of spontaneous activity in a type I cell, whereas in G and H there was a marked type I cell hyperpolarization during application of BzATP and ATP, respectively. In I, a 2 min preincubation of the co-culture with the NO scavenger carboxy-PTIO (cPTIO, 500 μM) abolished the ATP-induced hyperpolarization in a type I cell, presumably mediated indirectly via activation of adjacent JGPN neurons.

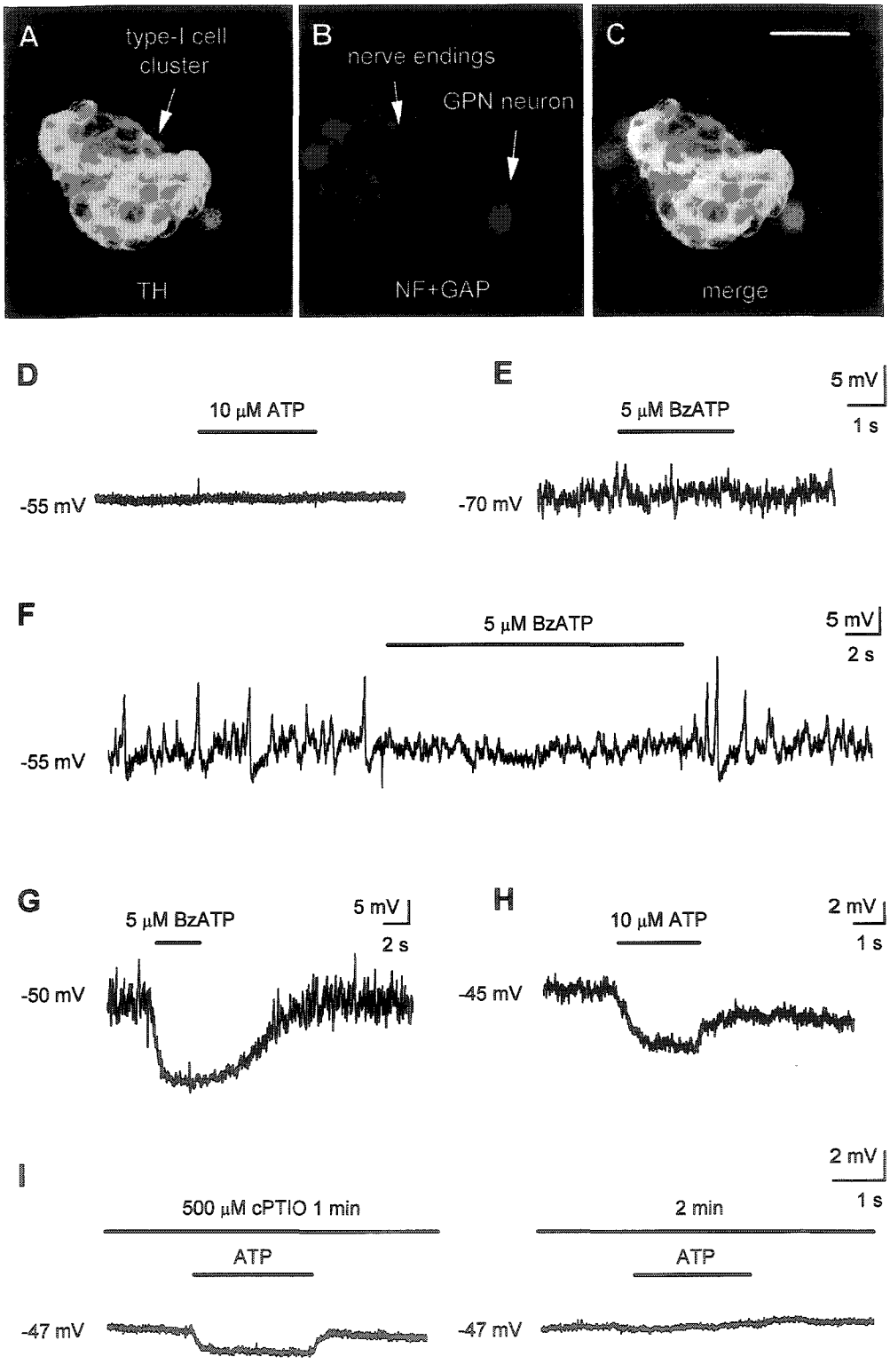
A
type-I cell cluster
TH
B
nerve endings
GPN neuron
NF+GAP
C
merge
D
10 μM ATP
-55 mV
E
5 μM BzATP
5 mV
1 s
-70 mV
F
5 μM BzATP
5 mV
2 s
-55 mV
G
5 μM BzATP
5 mV
2 s
-50 mV
H
10 μM ATP
2 mV
1 s
-45 mV
I
500 μM cPTIO 1 min
ATP
-47 mV
2 min
ATP
2 mV
1 s
-47 mV

Figure 10. GPN paraganglia staining after perfusion with Evans blue dye. In A, localized dye staining (arrow) occurred in the area where proximal GPN neurons are concentrated. Also note strong dye staining in CB tissue. B, Localized dye staining in the area (boxed) where the distal population of GPN neurons are concentrated. C, Higher magnification of the boxed area marked in B, showing blood vessel staining and dye deposit in the surrounding tissue. Scale bars represent 100 μm (A-B) and 10 μm (C).

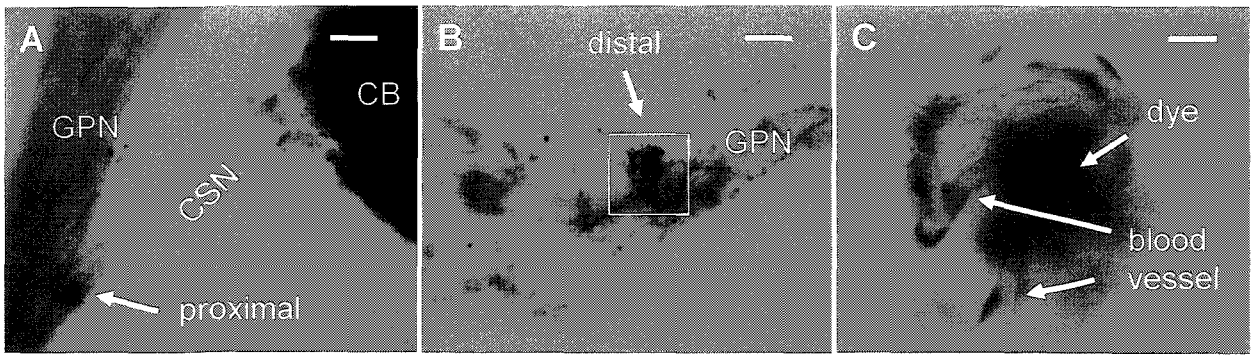
A
CB
GPN
CSN
proximal
B
distal
GPN
C
dye
blood
vessel

Figure 11. Fitted curves for the dose-response relation for ATP at P2X receptors expressed in GPN neurons, compared with heterologously expressed P2X2-P2X3 heteromultimeric receptors (Lewis *et al.* 1995), and P2X4 (Bo *et al.* 1995) and P2X7 (Chessell *et al.* 1998) homomultimeric receptors. The curve for native receptors in GPN neurons reflects a combination of the properties of the other receptors.

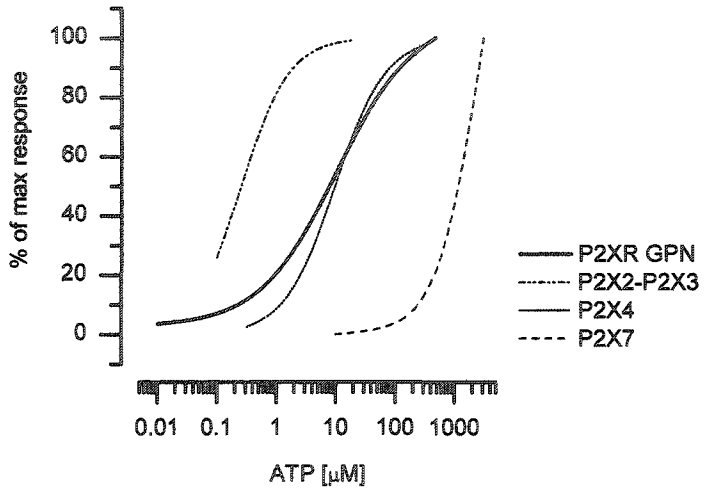
% of max response
100
80
60
40
20
0
0.01
0.1
1
10
100
1000
ATP [μM]
P2XR GPN
P2X2-P2X3
P2X4
P2X7

CHAPTER 5

General Discussion

Over the past 10-15 years, paraganglion neurons from the rat glossopharyngeal nerve (GPN) have been reported to play an important role in the efferent inhibition of carotid body (CB) chemoreceptors, thereby contributing to the regulation of breathing in mammals (Wang *et al.* 1993, 1994a, 1995a; Prabhakar, 2000). This physiological role was based in part on *in situ* anatomical experiments demonstrating that these neurons expressed neuronal nitric oxide synthase (nNOS) and innervated the CB. In addition, *in vitro* experiments showed that this inhibition was NO dependent and denervation of the carotid sinus nerve (CSN), which carries these nNOS-positive fibers, was reported to abolish the CB efferent inhibition (Wang *et al.* 1993, 1994a,b, 1995a,b). However, many issues remained unclear. Importantly, there was no electrophysiological charaterization of these GPN neurons, and the mechanisms by which they become activated during CB chemoreception were largely unknown. This thesis has contributed novel insights to these two areas.

As a first step I carried out anatomical experiments (i.e. vital dye D289 and DiI retrograde labeling) confirming both the known location and the efferent target, i.e. the CB, of these neurons. A new contribution from my studies was the revelation that, in addition to the previously described population of GPN neurons located at the CSN bifurcation, there was also another group concentrated at a more distal location along the nerve, which possessed similar characteristics, i.e. nNOS-expression and innervation of the CB. These two groups of neurons had similar passive membrane properties and expressed a variety of voltage-dependent Na^+, Ca^{2+} and K^+ channels. In addition, they also possessed voltage-independent background or 'leak' K^+ channels, among which was a unique population of O_2-sensitive K^+ channels. Furthermore, the neurons were sensitive to a variety of neurotransmitters, of which the responses to ATP were characterized in some detail. ATP was found to act on multiple ionotropic P2X receptors on GPN neurons, including heteromeric P2X2-P2X3, homomeric P2X4 and homomeric P2X7. As discussed in the Appendix 2, these neurons also expressed receptors for acetylcholine, dopamine and serotonin. The combined data taken together revealed that GPN neurons are strategically located and adapted to contribute to the regulation of breathing during stress conditions, e.g. hypoxia. As a consequence, this thesis provides a novel interpretation and a broader view of the role played by GPN neurons in carotid body chemoreceptor function during hypoxia.

O_2-sensitivity of GPN neurons

Physiological role for THIK-1 channels

While O_2-sensing mechanisms have been extensively studied in central neurons (Golanov and Reis, 1999; Mazza *et al.* 2000, Leblond and Krnjević, 1989; Haddad and Jiang, 1997; Hammarström and Page, 2000, Plant *et al.* 2002), Chapter 3 of this thesis contributes the first study on the mechanisms of O_2-sensing by a peripheral neuron. GPN neurons were found to express a unique population of O_2-sensitive background K^+ channels that belong to the two-pore (2P) domain family of K^+ channels. In general, background K^+-selective channels play a key role in setting the resting membrane potential and input resistance of the cell (Lesage and Lazdunski, 2000; Goldstein *et al.* 2001; Patel and Honoré, 2001b). They are therefore important determinants of the magnitude and kinetics of synaptic inputs in neurones and help shape neuronal excitability. Indeed, in Chapter 2 of this thesis, action potential properties in GPN neurons were modulated by hypoxia, which caused membrane depolarization and an increase in action potential frequency and duration. Other members of the background 2P domain K^+ channel family that are O_2-sensitive include the acid-sensitive TASK-1 - (Buckler *et al.* 2000; Plant *et al.* 2002), and TASK-3 (Hartness *et al.* 2001), as well as the stretch-sensitive TREK-1 (Miller *et al.* 2003). Neither of these three, however, appeared to be involved in the O_2-sensitivity of GPN neurons.

In GPN neurons, the pharmacological properties of the O_2-sensitive background conductance resembled those reported for the recently cloned tandem pore domain, halothane-inhibited K^+ (THIK)-subfamily of background K^+ channels (Rajan *et al.* 2001).

This family comprises THIK-1 (Kcnk13) and THIK-2 (Kcnk12) channels, which are highly expressed in various areas of the brain (Rajan *et al.* 2001). In addition, THIK-1 was recently localized in cerebellar Purkinje neurons (Bushell *et al.* 2002), and both mesenteric and pulmonary arteries (Gardener *et al.* 2004). However, except for the role suggested in this thesis, no other physiological function has been linked to these channels. My initial attempts to test for expression of THIK-1 and/or THIK-2 in isolated GPN neurons by RT-PCR techniques were unsuccessful, probably due to the high GC content of the mRNA. Toward the end of this thesis I used another approach (in collaboration with the laboratory of Dr. Ian Fearon), where I tested whether or not heterologous expression of THIK channels resulted in their modulation by low PO_2 (see Appendix 1). Interestingly, and consistent with the data presented in Chapter 3, THIK-1, the only member of the pair that was functionally expressed in HEK 293 cells, was reversibly inhibited by hypoxia. These novel exciting data suggest that THIK-1 channels may indeed play a role during hypoxia, which is an important deleterious factor contributing to neuronal death in pathological situations such as brain ischemia.

In addition, data presented in Chapters 2, 3 showed that PO_2 modulation of the background K^+ current was undetectable during voltage- and current-clamp recordings in dialysed GPN neurons, studied with conventional whole-cell recording. Since the halothane-sensitivity remained intact, these data suggested that the O_2-sensitivity of the K^+ channel required intact cytosolic components in order to be functional, as previously observed for the TASK-1-like O_2-sensitive K^+ channels expressed in carotid body chemoreceptors (Buckler *et al.* 2000). In contrast, when we expressed THIK-1 channels

in HEK 293 cells (Appendix 1), the O_2-sensitivity of these channels persisted in the 'dialysed' whole-cell configuration. The reasons for this discrepancy are presently unclear, but may simply reflect differences between native cells and cell lines.

GPN neurons and PO_2 sensitivity

Studies on the PO_2-dose response relation in GPN neurons revealed that the hypoxic inhibition of K^+ channel activity was roughly linear over a PO_2 range of 5-80 Torr (see Chapter 3). These data resembled the dose-response curve for PO_2 vs K^+ channel activity in rabbit CB (Montoro *et al.* 1996), however, it contrasted with the PO_2 vs cytosolic $[Ca^{2+}]$ and dopamine secretion in the same preparation (Montoro *et al.* 1996). In the latter study, even though K^+ currents in rabbit type I cells were modulated at PO_2 just below normoxia (~ 150 Torr), their secretory responses to hypoxia occurred only below a threshold PO_2 level of ~ 70 Torr. In the case of GPN neurons, neither cytosolic $[Ca^{2+}]$ nor NO production was measured during hypoxia. Since nNOS is Ca^{2+}-calmodulin dependent (see General Introduction), the possible existence in GPN neurons of a threshold PO_2 for synthesis and release of NO cannot be excluded. Preliminary evidence that hypoxia may increase Ca^{2+} currents in GPN neurons (see later, Appendix 4), adds to the intricate mechanisms these cells possess for regulation of intracellular Ca^{2+}, and therefore NOS activation.

ATP sensitivity of GPN neurons

GPN neurons were sensitive to ATP, thereby providing an alternative pathway by which these neurons could be activated, leading to Ca^{2+} influx, NOS activation and NO synthesis and release. The ATP-evoked responses were complex involving multiple P2X receptors (Chapter 4). The electrophysiological, pharmacological and immunocytochemical studies reported in this thesis suggested the functional expression of at least heteromeric P2X2-P2X3, homomeric P2X4 and homomeric P2X7 receptors. This variety of P2X receptors expressed in a single cell type would allow GPN neurons to be activated over a broad range of ATP concentrations, given that P2X2-P2X3 heteromultimers possess an EC_{50} of ~ 1 μM ATP (Lewis *et al.* 1995), whereas P2X4 (Bo *et al.* 1995) and P2X7 homomeric (Chessell *et al.* 1998) possess EC_{50} values of 10 and ≥ 100 μM, respectively. This purinergic pathway appears particularly effective for increasing intracellular Ca^{2+} and NOS activation, since P2X are not only Ca^{2+} permeable (North and Surprenant, 2000), but their activation causes membrane depolarization and an increase in Ca^{2+} influx via voltage-gated Ca^{2+} channels.

The fact that GPN neurons were sensitive to ATP raises the question about its physiological significance. In this thesis (Chapter 4), I obtained confirmation that GPN neurons were associated with an intricate network of fenestrated blood vessels (McDonald and Blewett, 1981), that were freely permeable to large dye molecules, e.g. Evans blue dye. These findings suggest that any circulating ATP in the blood stream would have direct access to the soma and/or terminals of GPN neurons at the two sites identified in this study. Interestingly, it has been known for some time that red blood cells

release ATP in response to hypoxia (Bergfeld and Forrester, 1992; Ellsworth *et al.* 1995; reviewed by Ellsworth, 2000), thereby providing a source of ATP for activating GPN neurons via the circulation. Additionally, my immunofluorescence studies demonstrate that P2X7 subunits were expressed on nerve endings in the vicinity of CB chemoreceptor cells *in situ*. Thus ATP, which is released from CB chemoreceptors cells during hypoxia (Zhang *et al.* 2000), represents another potential source of ATP for activation of GPN efferent terminals in the CB. Therefore, during hypoxic conditions GPN neurons and/or their processes may be activated not only by the direct action of hypoxia itself, via inhibition of THIK-like background K^+ channels, but also secondarily by ATP, released from circulating red blood cells and CB chemoreceptors. This dual activation of GPN neurons would produce a robust increase in Ca^{2+} influx and nNOS activation, followed by NO synthesis and release, and ultimately inhibition of CB chemoreception.

What is the O_2-sensor in GPN neurons?

My electrophysiological data indicated that the hypoxic inhibition of background K^+ channels in GPN neurons required an intact cytoplasm since it was seen with perforated-patch, but not conventional whole-cell recording. This result was similar to that reported for the O_2-sensitive TASK1-like background K^+ channels in CB type I cells (Buckler *et al.* 2000). This thesis, however, did not resolve the molecular identity of the O_2-sensor in GPN neurons. Indeed, despite the large body of evidence describing the various cellular effects of hypoxia, the signalling mechanisms by which O_2 sensing is mediated remain largely elusive. As recently reviewed (López-Barneo, 2003), the

different sensing mechanisms could be simplified in two main models: (1) a reversible heme-based ligand, producing allosteric shifts of the sensor, and (2) a substrate, capable of direct oxidation of the sensor or enzymatically converted to reactive oxygen species (ROS) which, in turn, mediate the action on the effector molecules. In the first model, i.e. the 'ligand model', the O_2 sensor can be viewed as a hemoprotein that in the deoxy-conformation modulates, directly or indirectly, the effector (i.e. background K^+ channels). In the second model, the ROS-producing systems include NADPH oxidase (Cross *et al.* 1990; Acker *et al.* 1994; Fu *et al.* 2000) and the mitochondrion (Chandel *et al.* 1998; Archer *et al.* 1993; Waypa *et al.* 2001; Waypa and Schumaker, 2002). In CB chemoreceptors, there is controversy as to whether or not the O_2 sensor is located in the mitochondria (Duchen and Biscoe, 1992; Wilson *et al.* 1994; Ortega-Saénz *et al.* 2003; Wyatt and Buckler, 2004).

In preliminary experiments (see Appendix 3), I tested that hypothesis that ROS of mitochondrial origin were the cytoplasmic signal regulating the hypoxic inhibition of THIK-like K^+ channels in GPN neurons. Application of rotenone (1-5 μM), which blocks the electron transport chain (ETC) at complex I, caused a dose-dependent inhibition of outward current in GPN neurons. However, the hypoxic inhibition of outward current still persisted in the presence of the rotenone (Appendix 3). These data contrast with those in rat CB chemoreceptors where rotenone, acting at the mitochondrial ETC (Wyatt and Buckler, 2004) or at some other extra-mitochondrial site (Ortega-Sáenz *et al.* 2003), occluded the effect of hypoxia. These data suggest that GPN neurons possess a different O_2 sensor from CB chemoreceptors, in addition to differences in the K^+ channel subtype

that is regulated by PO_2. Since background THIK-like channels were inhibited by hypoxia in GPN neurons, and THIK-1 channels were O_2-sensitive when heterologously expressed in HEK 293 cells (Appendix 1), I also tested whether rotenone had any effect on these THIK-1 channels. In concert with results on GPN neurons, rotenone (1-5 μM) had no effect on THIK-1 currents expressed in HEK cells (Appendix 1). These data, together with the fact that THIK-1 channels did not require an intact cytoplasm for modulation by hypoxia, suggest that cytosolic ROS of mitochondrion origin (specifically at complex I) are unlikely to be involved in the O_2-sensitivity of GPN neurons. However, inhibitors of other mitochondrial complexes need to be tested in future experiments to rule out the involvement of mitocondrial ROS in this O_2-sensitive system. Similarly, inhibitors of NADPH oxidase, or use of the NADPH oxidase-knock out mouse model, should be tested to address whether or not ROS from other sources are involved.

GPN neurons and their role in CB efferent inhibition – A working model

The term 'efferent inhibition' refers to the effects of centrifugal neural activity that can be recorded from the central stump of the CSN, resulting in inhibition of the CB chemoreceptor activity (Biscoe and Sampson, 1968; Fidone and Sato, 1970; Neil and O'Regan, 1971). This efferent inhibition could be prevented by application of NOS inhibitors which, together with the localization of NOS in CSN fibers (Prabhakar *et al.* 1993; Wang *et al.* 1993), suggested that it was mediated by NO. However, the neurophysiological mechanisms underlying the genesis of CB efferent inhibition are poorly understood. While NO was thought to be the inhibitory neurotransmitter

modulating CB basal discharge, there were contradictory reports demonstrating that hypoxia inhibited NOS activity in bovine cerebellum (Rengasamy and Johns, 1991). However, in the *in vitro* cat CB preparation NO donors inhibited, and NOS inhibitors augmented, the chemoreceptor response to hypoxia (Wang *et al.* 1994a). Moreover, nNOS mutant mice exhibited significantly greater respiratory responses during hypoxia than wild type control mice, suggesting that NO derived from nNOS modulates respiration during hypoxia (Kline *et al.* 1998). Lack of or insufficient O_2 availability during hypoxia is one potential mechanism for regulating NO production since O_2 is a cofactor in the NOS-dependent conversion of arginine to NO and citrulline (see General Introduction). Indeed, it has been suggested that since NO seems to be constantly generated, perhaps the inhibition of NO production may contribute to the increase in sensory discharge in the CSN during hypoxia (Prabhakar, 1999).

In Chapter 4 of this thesis, I used a novel co-culture approach to elucidate the role of GPN neurons in CB efferent inhibition. When GPN neurons were co-cultured with CB type I cell clusters, selective activation of the neurons via P2X receptors, by rapid application of ATP or its analog BzATP, caused hyperpolarization of adjacent type I cell. Moreover, this hyperpolarization could be prevented by addition of the NO scavenger, carboxy PTIO, suggesting that NO was the 'inhibitory signal' released upon purinergic activation of the GPN neurons. Further experimentation is required to determine if NO is released from GPN neurons during hypoxia, as proposed in Chapters 2, 3 of this thesis.

The experiments conducted during this thesis have led to a 'working model' for the role of GPN neurons in the efferent inhibition of the rat CB via their activation by

hypoxia and ATP. As summarized in Fig. 1, a reduction in blood PO_2 (hypoxemia) causes at least four effects: (1) Inhibition of background (TASK-1-like) K^+ and large-conductance Ca^{2+} activated (BK) K^+ channels in carotid body type I cells (reviewed by López-Barneo, 2001), leading to or enhancing membrane depolarization, activation of L-type Ca^{2+} channels, and neurotransmitter (ATP and ACh) release (Zhang *et al.* 2000). These neurotransmitters act on petrosal sensory nerve endings via P2X2-P2X3 receptors (Prasad *et al.* 2001) and nicotinic ACh receptors (nAChR) leading to a compensatory reflex increase in ventilation and restoration of blood PO_2. (2) ATP, released from type I cells, may act on nearby GPN nerve terminals which may express multiple P2X receptors (P2XR), including heteromeric P2X2-P2X3, homomeric P2X4 and homomeric P2X7 receptors. Activation of these P2XRs causes Ca^{2+} influx and nNOS activation, leading to NO synthesis and release. NO actions on type I cells lead to inhibition of neurotransmitter release via membrane hyperpolarization (this study; see also Silva and Lewis, 2002), and/or direct inhibition of L-type Ca^{2+} channels (Summers *et al.* 1999). (3) Hypoxia causes red blood cells to release ATP (reviewed by Ellsworth, 2000), which may directly stimulate GPN neurons via P2XRs (see 4) and endothelial cells via P2Y receptors (reviewed by Ellsworth, 2000). These pathways lead to NO production and release via nNOS in GPN neurons and eNOS in endothelial cells (McCullough *et al.* 1997; Collins *et al.* 1998), ultimately causing inhibition of CB type I cell function. (4) Hypoxia also causes direct activation of GPN neurons by inhibiting background K^+ channels (Chapter 3; Campanucci *et al.* 2003a), leading to depolarization and/or increased firing, voltage-gated Ca^{2+} entry followed by nNOS activation and NO release.

Thus, activation of GPN neurons by low PO_2 and/or ATP release during hypoxic stress would lead to efferent inhibition of CB chemoreceptors, thereby providing a dual mechanism for negative feedback control of respiration via the same neuronal pathway.

Are Ca^{2+} channels O_2-sensitive in GPN neurons?

As reported in Appendix 4, during perforated-patch recording in physiological solutions I observed a hypoxia-induced potentiation of a transient inward current in several GPN neurons at potentials ~ -30 mV. This transient current was insensitive to TTX and fully inhibited by cadmium. These preliminary data suggested that hypoxia potentiated a Ca^{2+} current, which in these neurons is carried by at least L, N, T, R and P/Q Ca^{2+} channels (see Chapter 2). However, I was unable to detect any effect of hypoxia on isolated Ca^{2+} currents during conventional whole-cell recording. Unfortunately, these currents could not be accurately studied with nystatin-perforated patch recording, and hence the proposed hypoxia-induced augmentation of Ca^{2+} currents in GPN neurons could not be investigated in detail.

Although my data were inconclusive, the possible modulation of Ca^{2+} channels by hypoxia is interesting in the case of GPN neurons. As discussed above, nNOS activation is Ca^{2+}-dependent, and therefore, augmentation of a Ca^{2+} conductance would contribute to NO release and CB efferent inhibition during hypoxia. In addition, it has been recently reported that ATP potentiates neuronal T-type Ca^{2+} currents in thalamocortical neurons by a phosphorylation mechanism (Leresche *et al.* 2004). Since there seems to be an available source of ATP surrounding GPN neurons during hypoxia (see above),

potentiation of Ca^{2+} currents under these conditions could contribute to the physiological responses of these neurons. However, further experimentation is required to clarify this point.

Future directions

The work presented in this thesis has raised several questions that remain to be addressed in future research:

1) Molecular identification of background K^+ channels expressed in GPN neurons

Since GPN neurons express an O_2-sensitive background K^+, proper molecular characterization of the different types of background K^+ channels expressed in these cells should be performed by RT-PCR techniques. I did attempt to detect the expression of THIK-1 and THIK-2 by this molecular method, however, I was unsuccessful due to the high GC content of the THIK-1 and THIK-2 mRNA. Further experimentation with this approach, and with immunocytochemical localization of THIK-1 and THIK-2 proteins in GPN neurons *in situ*, is required.

2) Identification of the O_2-sensitive Ca^{2+} conductance

I was unable to detect any effect of hypoxia on Ca^{2+} currents in GPN neurons during conventional whole-cell recording. However, I did observe potentiation of a cadmium-sensitive Ca^{2+} current activated at ~ -30 mV in physiological solutions, during nystatin-perforated patch recording. In this thesis I also observed that GPN neurons

expressed a variety of voltage-dependent Ca^{2+} channels that were dissected pharmacologically. Therefore, in order to study the putative augmentation of Ca^{2+} currents it would be interesting to repeat the experiments in the presence of selective blockers for the different types of Ca^{2+} channels present (see Chapter 2). This method should allow at least a pharmacological characterization of this O_2-sensitive Ca^{2+} conductance in GPN neurons.

3) Are THIK-2 channels also O_2-sensitive?

Electrophysiological and pharmacological data presented in Chapter 3 implied that the expression of background, two-pore (2P) domain, K^+ channels in GPN neurons was responsible for conferring O_2-sensitivity in these neurons. The properties of these channels were closely related to those of the THIK channel family members, i.e. THIK-1 and THIK-2 (Rajan *et al.* 2001). This prediction was recently confirmed following expression of THIK-1 in HEK 293 cells and the demonstration that THIK-1 currents were reversibly inhibited by low PO_2 (see Appendix 1). However, as reported by Rajan *et al.* (2001) for a different expression system, i.e. *Xenopus* oocytes, the expression of THIK-2 in HEK 293 cells did not result in functional channels in our study, and therefore their sensitivity to hypoxia could not be tested. Since these channels are widely expressed in the central nervous system at the mRNA level (Rajan *et al.* 2001), it would be useful to define conditions for the functional heterologous expression of THIK-2 channels. Additionally, it would be of interest to test the effect of hypoxia on central neurons that express THIK-2, but not THIK-1 nor other O_2-sensitive background K^+ channels.

4) Which neurotransmitter receptors mediate the responses to dopamine, serotonin and acetylcholine in GPN neurons?

In this thesis, I initially studied the effects of various neurotransmitters on GPN neurons (Appendix 2). However, only the receptors involved in ATP sensitivity of GPN neurons were characterized in detail (Chapter 4). Characterization of the neurotransmitter receptors for dopamine, serotonin and acetylcholine will contribute to a broader understanding of alternative ways of activating these neurons, the synaptic circuitry involved in cell-to-cell communication between these neurons, and the efferent inhibitory pathway to CB chemoreceptors. Interestingly, we did observe in preliminary experiments that 5-HT receptor blockers inhibited activity in spontaneously active neurons (Appendix 2).

Figure 1. Working model for the role of GPN neurons in efferent inhibition of the rat CB via their activation by hypoxia and ATP. A reduction in arterial PO_2 causes: (1) Inhibition of background (TASK1-like) and high-conductance Ca^{2+} activated (BK) K^+ channels in type I cells, leading to depolarization, Ca^{2+} influx and neurotransmitter (ACh and ATP) release. These neurotransmitters act on petrosal sensory nerve endings via P2X receptors (P2XR) and nicotinic ACh receptors (nAChR) and initiate compensatory reflexes leading to restoration of blood PO_2. (2) ATP may act on P2XR on nearby GPN nerve terminals, leading to Ca^{2+} influx via P2XR and/or depolarization-induced opening of voltage-gated Ca^{2+} channels. The rise in intracellular Ca^{2+} activates neuronal NOS (nNOS) leading to NO synthesis and release. NO action results in hyperpolarization of type I cells probably via activation of BK channels (Silva and Lewis, 2002), leading to reduction in neurotransmitter release. The latter may also result from NO-induced inhibition of L-type Ca^{2+} channels (Summers *et al.* 1999). (3) Hypoxia may also cause release of ATP from red blood cells (RCB), which in turn may act on purinergic P2Y receptors on the endothelial cells, leading to activation of eNOS and release of NO. This new available source of ATP may diffuse through fenestrated capillaries (permeable to Evan's blue dye) and excite paraganglion (GPN) neurons, thereby activating the efferent pathway (see 2). (4) Finally, hypoxia may also cause direct activation of GPN neurons by inhibiting background K^+ channels (Campanucci *et al.* 2003), leading to depolarization and/or an increase in firing frequency. The resulting entry of extracellular Ca^{2+} via various voltage-dependent Ca^{2+} channels leads to NOS activation, followed by NO synthesis and release.

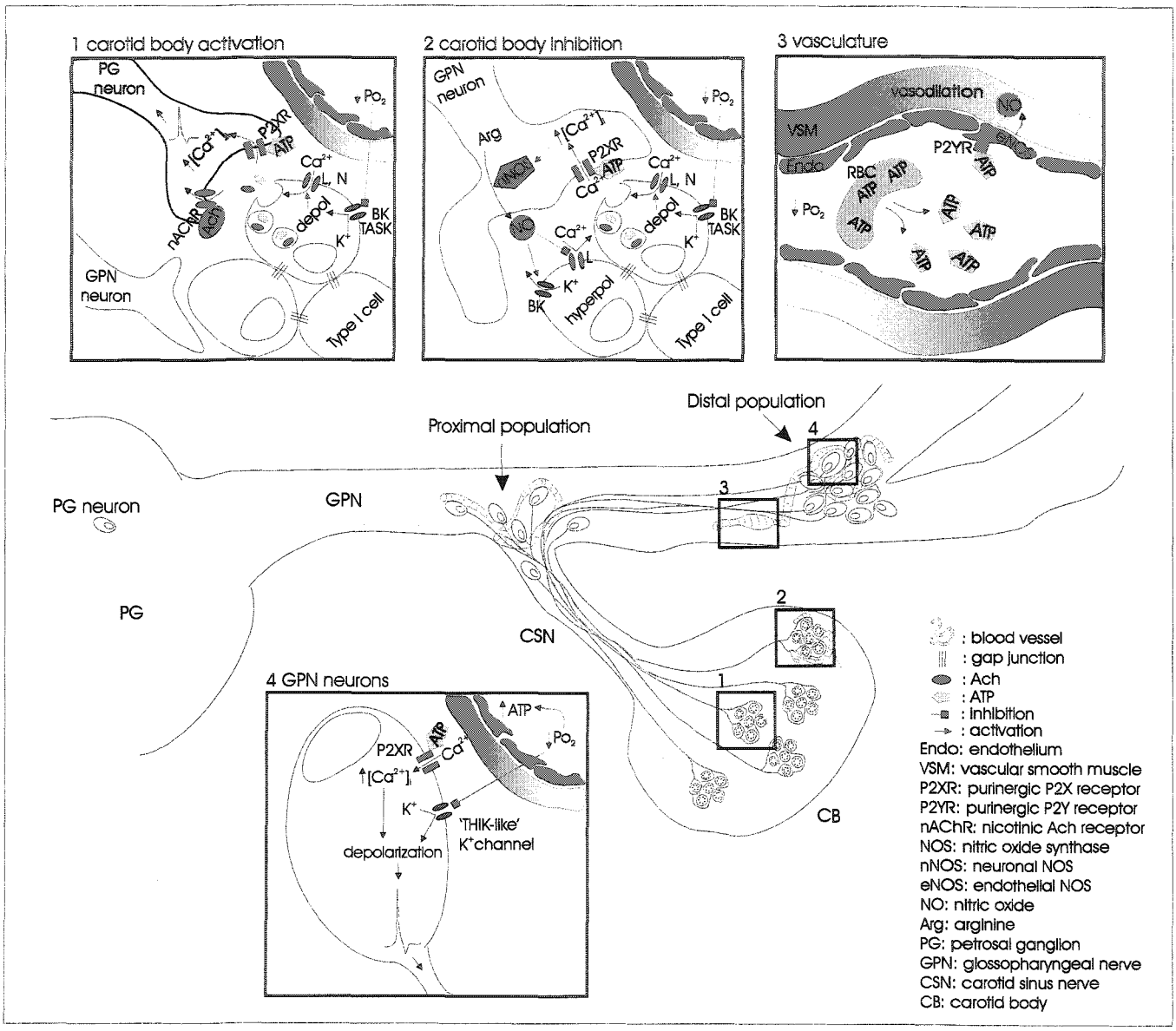
1 carotid body activation
PG neuron
Po_2
$[Ca^{2+}]_i$
P2XR
ATP
Ca^{2+}
L, N
depol
BK
TASK
K^+
nAChR
ACh
GPN neuron
Type I cell
2 carotid body inhibition
GPN neuron
Arg
NOS
NO
hyperpol
BK
3 vasculature
vasodilation
VSM
Endo
RBC
P2YR
eNOS
Distal population
Proximal population
4
3
2
1
PG neuron
GPN
PG
CSN
CB
4 GPN neurons
'THIK-like' K^+channel
depolarization
: blood vessel
: gap junction
: Ach
: ATP
: inhibition
: activation
Endo: endothelium
VSM: vascular smooth muscle
P2XR: purinergic P2X receptor
P2YR: purinergic P2Y receptor
nAChR: nicotinic Ach receptor
NOS: nitric oxide synthase
nNOS: neuronal NOS
eNOS: endothelial NOS
NO: nitric oxide
Arg: arginine
PG: petrosal ganglion
GPN: glossopharyngeal nerve
CSN: carotid sinus nerve
CB: carotid body

REFERENCES

Acker H 1994. Mechanisms and meaning of cellular oxygen sensing in the organism. Respir. Physiol. 95:1–10.

Alcayaga J, Barrios M, Bustos F, Miranda G, Molina MJ, Iturriaga R (1999) Modulatory effect of nitric oxide on acetylcholine-induced activation of cat petrosal ganglion neurons in vitro. Brain Res 825:194-8.

Alcayaga J, Iturriaga R, Ramirez J, Readi R, Quezada C, Salinas P (1997) Cat carotid body chemosensory responses to non-hypoxic stimuli are inhibited by sodium nitroprusside in situ and in vitro. Brain Res 767:384-7.

Archer SL, Huang J, Henry T, Peterson D, Weir EK (1993) A redox-based O_2 sensor in rat pulmonary vasculature. Circ. Res. 73:1100-12.

Archer SL, Souil E, Dinh-Xuan AT, Schremmer B, Mercier JC, El Yaagoubi A, Nguyen-Huu L, Reeve HL, Hampl V (1998) Molecular identification of the role of voltage-gated K^+ channels, Kv1.5 and Kv2.1, in hypoxic pulmonary vasoconstriction and control of resting membrane potential in rat pulmonary artery myocytes. J. Clin Invest 101, 2319-30.

Armstrong JN, Brust TB, Lewis RG, MacVicar BA (2002) Activation of presynaptic P2X7-like receptors depresses mossy fiber-CA3 synaptic transmission through p38 mitogen-activated protein kinase. J Neurosci 22:5938-45.

Ashmole I, Goodwin PA, Stanfield, PR (2001) TASK-5, a novel member of the tandem pore K^+ channel family. Pflügers Arch - Eur J Physiol 442, 828-33.

Astrup J, Sorensen PM, Sorensen HR (1981) Oxygen and glucose consumption related to Na^+-K^+ transport in canine brain. Stroke 12:726-30.

Balice-Gordon RJ, Lichtman JW (1993) In vivo observations of pre- and postsynaptic changes during the transition from multiple to single innervation at developing neuromuscular junctions. J Neurosci 13:834-55.

Banasiak KJ, Burenkova O, Haddad GG (2004) Activation of voltage-sensitive sodium channels during oxygen deprivation leads to apoptotic neuronal death. Neuroscience 126:31-44.

Banasiak KJ, Xia Y, Haddad GG (2000) Mechanisms underlying hypoxia-induced neuronal apoptosis. Prog Neurobiol 62:215-49.

Benot AR, López-Barneo J (1990) Feedback inhibition of Ca^{2+} currents by dopamine in glomus cells of the carotid body. Eur J Neurosci 2:809-12.

Bergfeld GR, Forrester T (1992) Release of ATP from human erythrocytes in response to a brief period of hypoxia and hypercapnia. Cardiovasc Res 26:40-7.

Bianchi BR, Lynch KJ, Touma E, Niforatos W, Burgard EC, Alexander KM, Park HS, Yu H, Metzger R, Kowaluk E, Jarvis MF, van Biesen T (1999) Pharmacological characterization of recombinant human and rat P2X receptor subtypes. Eur J Pharmacol 376:127-38.

Bin-Jaliah I, Maskell PD, Kumar P (2004) Indirect sensing of insulin-induced hypoglycaemia by the carotid body in the rat. J Physiol 556:255-66.

Biscoe TJ, Sampson SR (1968) Rhythmical and non-rhythmical spontaneous activity recorded from the central cut end of the sinus nerve. J Physiol 196:327-38.

Black JA, Liu S, Tanaka M, Cummins TR, Waxman SG (2004) Changes in the expression of tetrodotoxin-sensitive sodium channels within dorsal root ganglia neurons in inflammatory pain. Pain 108:237-47.

Bo X, Zhang Y, Nassar M, Burnstock G, Schoepfer R (1995) A P2X purinoceptor cDNA conferring a novel pharmacological profile. FEBS Lett 375:129-33.

Bradley JE, Anderson UA, Woolsey SM, Thornbury KD, McHale NG, Hollywood MA (2004) Characterization of T-type calcium current and its contribution to electrical activity in rabbit urethra. Am J Physiol Cell Physiol 286:C1078-88.

Brake AJ, Wagenbach MJ, Julius D (1994) New structural motif for ligand-gated ion channels defined by an ionotropic ATP receptor. Nature 371:519-23.

Brickley SG, Revilla V, Cull-Candy SG, Wisden W, Farrant M (2001) Adaptive regulation of neuronal excitability by a voltage-independent potassium conductance. Nature 409:88-92.

Brosenitsch TA, Katz DM (2001) Physiological patterns of electrical stimulation can induce neuronal gene expression by activating N-type calcium channels. J Neurosci 21:2571-9.

Brosenitsch TA, Salgado-Commissariat D, Kunze DL, Katz DM (1998) A role for L-type calcium channels in developmental regulation of transmitter phenotype in primary sensory neurons. J Neurosci 18:1047-55.

Buckler KJ (1997) A novel oxygen-sensitive potassium current in rat carotid body type I cells. J Physiol 498:649-62.

Buckler KJ (1999) Background leak K^+-currents and oxygen sensing in carotid body type 1 cells. Respir Physiol 115:179-87.

Buckler KJ, Williams BA, Honoré E (2000) An oxygen-, acid- and anaesthetic-sensitive TASK-like background potassium channel in rat arterial chemoreceptor cells. J Physiol 525:135-42.

Burnstock G (1972) Purinergic nerves. Pharmacol Rev 24:509-81.

Burnstock G (1997) The past, present and future of purine nucleotides as signalling molecules. Neuropharmacology 36:1127-39.

Burnstock G (2002) Purinergic signaling and vascular cell proliferation and death. Arterioscler Thromb Vasc Biol 22:364-73.

Bushell T, Clarke C, Mathie A, Robertson B (2002) Pharmacological characterization of a non-inactivating outward current observed in mouse cerebellar Purkinje neurones. British J Pharmacol 135:705-12.

Campanucci VA, Fearon IM, Nurse CA (2003a) A novel O_2-sensing mechanism in rat glossopharyngeal neurons mediated by a halothane-inhibitable background K+ conductance. J Physiol 548:731-43.

Campanucci VA, Fearon IM, Nurse CA (2003b) O_2-sensing mechanisms in efferent neurons to the rat carotid body. Adv Exp Med Biol 536:179-85.

Campanucci VA, Zhang M, Vollmer C, Nurse CA (2001) O_2-sensing and ATP sensitivity in neurons from the rat glossopharyngeal nerve. Soc Neurosci Abstr # 632.3.

Cavaliere F, Florenzano F, Amadio S, Fusco FR, Viscomi MT, D'Ambrosi N, Vacca F, Sancesario G, Bernardi G, Molinari M, Volonte C (2003) Up-regulation of P2X2, P2X4 receptor and ischemic cell death: prevention by P2 antagonists. Neuroscience 120:85-98.

Chandel NS, Maltepe E, Goldwasser E, Mathieu CE, Simon MC, Schumacker PT (1998) Mitochondrial reactive oxygen species trigger hypoxia-induced transcription. Proc Natl Acad Sci USA 95:11715-20.

Chandel NS, Schumacker PT (2000) Cellular oxygen sensing by mitochondria: old questions, new insight. J Appl Physiol 88:1880-9.

Chavez RA, Gray AT, Zhao BB, Kindler CH, Mazurek MJ, Mehta Y, Forsayeth JR, Yost CS (1999) TWIK-2, a new weak inward rectifying member of the tandem pore domain potassium channel family. J Biol Chem 274, 7887-92.

Chessell IP, Simon J, Hibell AD, Michel AD, Barnard EA, Humphrey PP (1998) Cloning and functional characetrization of the mouse P2X7 receptor. FEBS Lett 439:26-30.

Clark RB, Tse A, Giles WR (1990) Electrophysiology of parasympathetic neurones isolated from the interatrial septum of bull-frog heart. J Physiol 427:89-125.

Collins DM, McCullough WT, Ellsworth ML (1998) Conducted vascular responses: communication across the capillary bed. Microvasc Res 56:43-53.

Cross AR, Henderson L, Jones OT, Delpiano MA, Hentschel J, Acker H (1990) Involvement of an NAD(P)H oxidase as a PO_2 sensor protein in the rat carotid body. Biochem J 272:743-7.

Cummins TR, Dib-Hajj SD, Waxman SG, Donnelly DF (2002) Characterization and developmental changes of Na^+ currents of petrosal neurons with projections to the carotid body. J Neurophysiol 88:2993-3002.

Cummins TR, Donnelly DF, Haddad GG (1991) Effect of metabolic inhibition on the excitability of isolated hippocampal CA1 neurons: developmental aspects. J Neurophysiol 66:1471-82.

Cummins TR, Jiang C, Haddad GG (1993) Human neocortical excitability is decreased during anoxia via sodium channel modulation. J Clin Invest 91:608-15.

Dawes GS, Gardner WN, Johnston BM, Walker DW (1983) Breathing in fetal lambs: the effect of brain stem section. J Physiol 335:535-53.

De Roo M, Rodeau JL, Schlichter R (2003) Dehydroepiandrosterone potentiates native ionotropic ATP receptors containing the P2X2 subunit in rat sensory neurones. J Physiol 552:59-71.

Decher N, Maier M, Dittrich W, Gassenhuber J, Bruggemann A, Busch AE, Steinmeyer K (2001). Characetrization of TASK-4, a novel member of the pH-sensitive, two-pore domain potassium channel family. FEBS Lett 492, 84-89.

Deuchars SA, Atkinson L, Brooke RE, Musa H, Milligan CJ, Batten TF, Buckley NJ, Parson SH, Deuchars J (2001) Neuronal P2X7 receptors are targeted to presynaptic terminals in the central and peripheral nervous systems. J Neurosci 21:7143-52.

Donnelly DF (1996) Chemoreceptor nerve excitation may not be proportional to catecholamine secretion. J Appl Physiol 81:657-64.

Donnelly DF (1999) K^+ currents of glomus cells and chemosensory functions of carotid body. Respir Physiol 115:151-60.

Duchen MR, Biscoe TJ (1992) Mitochondrial function in type I cells isolated from rabbit arterial chemoreceptors. J Physiol 450:13-31.

Dunn PM, Zhong Y, Burnstock G (2001) P2X receptors in peripheral neurons. Progress in Neurobiology 65(2):107-34.

Duprat F, Lesage F, Fink M, Reyes R, Heurteaux C, Lazdunski M (1997). TASK, a human background K^+ channel to sense external pH variations near physiological pH. EMBO J 16, 5464-71.

Duranteau J, Chandel NS, Kulisz A, Shao Z, Schumacker PT (1998) Intracellular signaling by reactive oxygen species during hypoxia in cardiomyocytes. J Biol Chem 273:11619-24.

Edwards FA, Gibb AJ, Colquhoun D (1992) ATP receptor-mediated synaptic currents in the central nervous system. Nature 359:144-7.

Ellsworth ML (2000) The red blood cell as an oxygen sensor: what is the evidence? Acta Physiol Scand 168:551-9.

Ellsworth ML, Forrester T, Ellis CG, Dietrich HH (1995) The erythrocyte as a regulator of vascular tone. Am J Physiol 269:H2155-61.

Elmslie KS (2004) Calcium channel blockers in the treatment of disease. J Neurosci Res 75:733-41.

Evans RJ, Derkach V, Surprenant A (1992) ATP mediates fast synaptic transmission in mammalian neurons. Nature 357:503-5.

Evans RJ, Lewis C, Virginio C, Lundstrom K, Buell G, Surprenant A, North RA (1996) Ionic permeability of, and divalent cation effects on, two ATP-gated cation channels (P2X receptors) expressed in mammalian cells. J Physiol 497:413-22.

Eyzaguirre C, Zapata P (1984) Perspectives in carotid body research. J Appl Physiol 57:931-57.

Fearon IM, Ball SG, Peers C (2000a) Clotrimazole inhibits the recombinant human cardiac L-type Ca^{2+} channel alpha 1C subunit. Br J Pharmacol 129:547-54.

Fearon IM, Palmer AC, Balmforth AJ, Ball SG, Varadi G, Peers C (2000b) Hypoxic and redox inhibition of the human cardiac L-type Ca^{2+} channel. Adv Exp Med Biol 475:209-18.

Fearon IM, Palmer AC, Balmforth AJ, Ball SG, Varadi G, Peers C (1999) Modulation of recombinant human cardiac L-type Ca^{2+} channel alpha1C subunits by redox agents and hypoxia. J Physiol 514:629-37.

Fearon IM, Randall AD, Perez-Reyes E, Peers C (2000c) Modulation of recombinant T-type Ca^{2+} channels by hypoxia and glutathione. Pflügers Arch 441:181-8.

Fearon IM, Zhang M, Vollmer C, Nurse CA (2003) GABA mediates autoreceptor feedback inhibition in the rat carotid body via presynaptic GABAB receptors and TASK-1. J Physiol 553:83-94.

Fidone SJ, Sato A (1970) Efferent inhibition and antidromic depression of chemoreceptors A-fibers from the cat carotid body. Brain Res 22: 181-93.

Fitzgerald RS (2000) Oxygen and carotid body chemotransduction: the cholinergic hypothesis - a brief history and new evaluation. Respir Physiol 120:89-104.

Förstermann U, Boissel JP, Kleinert H (1998) Expressional control of the 'constitutive' isoforms of nitric oxide synthase (NOS I and NOS III). FASEB J 12:773-90.

Franco-Obregon A, López-Barneo J (1996a) Differential oxygen sensitivity of calcium channels in rabbit smooth muscle cells of conduit and resistance pulmonary arteries. J Physiol 491:511-8.

Franco-Obregon A, López-Barneo J (1996b) Low PO_2 inhibits calcium channel activity in arterial smooth muscle cells. Am J Physiol 271:H2290-9.

Franco-Obregon A, Ureña J, López-Barneo J (1995) Oxygen-sensitive calcium channels in vascular smooth muscle and their possible role in hypoxic arterial relaxation. Proc Natl Acad Sci USA 92:4715-9.

Friedman JE, Haddad GG (1994) Removal of extracellular sodium prevents anoxia-induced injury in freshly dissociated rat CA1 hippocampal neurons. Brain Res 641:57-64.

Fu XW, Wang D, Nurse CA, Dinauer MC, Cutz E (2000). NADPH oxidase is an O_2 sensor in airway chemoreceptors: Evidence from K^+ current modulation in wild-type and oxidase-deficient mice. Proc Nat Acad Sci USA 97:4374-4379.

Fung ML, Ye JS, Fung PC (2001). Acute hypoxia elevates nitric oxide generation in rat carotid body in vitro. Pflügers Arch 442, 903-909.

Gardener MJ, Johnson IT, Burnham MP, Edwards G, Heagerty AM (2004) Functional evidence of a role of two-pore domain potassium channels in rat mesenteric and pulmonary arteries. British J Pharmacol 142:192-202.

Girard C, Duprat F, Terrenoire C, Tinel N, Fosset M, Romey G, Lazdunski M, Lesage F (2001) Genomic and functional characteristics of novel human pancreatic 2P domain K^+ channels. Biochem Biophys Res Commun 282:249-56.

Golanov EV, Reis DJ (1999) A role for KATP-channels in mediating the elevations of cerebral blood flow and arterial pressure by hypoxic stimulation of oxygen-sensitive neurons of rostral ventrolateral medulla. Brain Res 827:10-14.

Goldstein SA, Bockenhauer D, O'Kelly I, Zilberberg N (2001) Potassium leak channels and the KCNK family of two-P-domain subunits. Nat Rev Neurosci 2, 175-184.

González C, Almaraz L, Obeso A, Rigual R (1994) Carotid body chemoreceptors: from natural stimuli to sensory discharges. Physiol Rev 74:829-98.

Grimes PA, Lahiri S, Stone R, Mokashi A, Chug D (1994) Nitric oxide synthase occurs in neurons and nerve fibers of the carotid body. Adv Exp Med Biol 360:221-4.

Haddad GG, Jiang C (1993) Mechanisms of anoxia-induced depolarization in brainstem neurons: in vitro current and voltage clamp studies in the adult rat. Brain Res 625:261-8.

Haddad GG, Jiang C (1997) O_2-sensing mechanisms in excitable cells: role of plasma membrane K^+ channels. Annu Rev Physiol 59:23-42.

Hamill OP, Marty A, Neher E, Sakmann B, Sigworth FJ (1981) Improved patch-clamp techniques for high-resolution current recording from cells and cell-free membrane patches. Pflügers Arch 391:85-100.

Hammarström AK, Gage PW (2000) Oxygen-sensing persistent sodium channels in rat hippocampus. J Physiol 529:107-18.

Hartness ME, Lewis A, Searle GJ, O'Kelly I, Peers C, Kemp PJ (2001) Combined antisense and pharmacological approaches implicate hTASK as an airway O_2-sensing K^+ channel. J Biol Chem 276:26499-508.

Henrich M, Hoffmann K, Konig P, Gruss M, Fischbach T, Godecke A, Hempelmann G, Kummer W (2002) Sensory neurons respond to hypoxia with NO production associated with mitochondria. Mol Cell Neurosci 20:307-322.

Herzog RI, Cummins TR, Ghassemi F, Dib-Hajj SD, Waxman SG (2003a) Distinct repriming and closed-state inactivation kinetics of Nav1.6 and Nav1.7 sodium channels in mouse spinal sensory neurons. J Physiol 551:741-50.

Herzog RI, Liu C, Waxman SG, Cummins TR (2003b) Calmodulin binds to the C terminus of sodium channels Nav1.4 and Nav1.6 and differentially modulates their functional properties. J Neurosci 23:8261-70.

Hodgkin AL, Huxley AF (1952) A quantitative description of membrane current and its application to conduction and excitation in nerve. J Physiol 117:500-44.

Höhler B, Mayer B, Kummer W (1994) Nitric oxide synthase in the rat carotid body and carotid sinus. Cell Tissue Res 276:559-64.

Holscher C (1997) Nitric oxide, the enigmatic neuronal messenger: its role in synaptic plasticity. Trends Neurosci 20:298-303.

Horn EM, Waldrop TG (1997) Oxygen-sensing neurons in the caudal hypothalamus and their role in cardiorespiratory control. Respir Physiol 110:219-28.

Horn R, Marty A (1988) Muscarinic activation of ionic currents measured by a new whole-cell recording method. J Gen Physiol 92:145-59.

Jackson A, Nurse CA (1998) Role of acetylcholine receptors and dopamine transporter in regulation of extracellular dopamine in rat carotid body cultures grown in chronic hypoxia or nicotine. J Neurochem 70:653-62.

Jaffrey SR, Snyder SH (1995) Nitric oxide: a neural messenger. Annu Rev Cell Dev Biol 11:417-40.

Jiang C, Haddad GG (1994) A direct mechanism for sensing low oxygen levels by central neurons. Proc Natl Acad Sci USA 91:7198–201.

Jiang C, Haddad GG (1994) Oxygen deprivation inhibits a K^+ channel independently of cytosolic factors in rat central neurons. J Physiol 481:15-26.

Jiang LH, Mackenzie AB, North RA, Surprenant A (2000) Brilliant blue G selectively blocks ATP-gated rat P2X7 receptors. Mol Pharmacol 58:82-8.

Jones SW (1990) Whole-cell and microelectrode voltage clamp. Neuromethods. In: Neurophysiological techniques: Basic methods and concepts (Vol. 14). Eds. AA Boulton, GB Baker and CH Vanderwolf. The Humana Press, Clifton, NJ, pp 143-192.

Jordan D (1994) Central integration of chemoreceptor afferent activity. Adv Exp Med Biol 360:87-98.

Khakh BS (2001a) Molecular physiology of P2X receptors and ATP signalling at synapses. Nat Rev Neurosci 2:165-74.

Khakh BS, Burnstock G, Kennedy C, King BF, North RA, Seguela P, Voigt M, Humphrey PP (2001b) International union of pharmacology. XXIV. Current

status of the nomenclature and properties of P2X receptors and their subunits. Pharmacol Rev 53:107-18.

Khakh BS, Proctor WR, Dunwiddie TV, Labarca C, Lester HA (1999) Allosteric control of gating and kinetics at P2X4 receptor channels. J Neurosci 19:7289-99.

Kim Y, Bang H, Kim D (1999). TBAK-1 and TASK-1, two-pore K^+ channel subunits: kinetic properties and expression in rat heart. Am J Physiol 277:H1669-H1678.

Kim Y, Bang H, Kim D (2000). TASK-3, a new member of the tandem pore K^+ channel family. J Biol Chem 275:9340 –9347.

Kimura M, Sawada K, Miyagawa T, Kuwada M, Katayama K, Nishizawa Y (1998) Role of glutamate receptors and voltage-dependent calcium and sodium channels in the extracellular glutamate/aspartate accumulation and subsequent neuronal injury induced by oxygen/glucose deprivation in cultured hippocampal neurons. J Pharmacol Exp Ther 285:178-85.

Kleinberg ME, Finkelstein A (1984) Single-length and double-length channels formed by nystatin in lipid bilayer membranes. J Membr Biol 80:257-69.

Kline DD, Prabhakar NR (2000) Peripheral chemosensitivity in mutant mice deficient in nitric oxide synthase. Adv Exp Med Biol 475:571-9.

Kline DD, Yang T, Huang PL, Prabhakar NR (1998) Altered respiratory responses to hypoxia in mutant mice deficient in neuronal nitric oxide synthase. J Physiol 511:273-87.

Kline DD, Yang T, Premkumar DR, Thomas AJ, Prabhakar NR (2000) Blunted respiratory responses to hypoxia in mutant mice deficient in nitric oxide synthase-3. J Appl Physiol 88:1496-508.

Koos BJ, Chau A, Matsuura M, Punla O, Kruger L (1998) Thalamic locus mediates hypoxic inhibition of breathing in fetal sheep. J Neurophysiol 79:2383-93.

Koyama Y, Coker RH, Stone EE, Lacy DB, Jabbour K, Williams PE, Wasserman DH (2000) Evidence that carotid bodies play an important role in glucoregulation in vivo. Diabetes 49:1434-42.

Krnjević K, Cherubini E, Ben-Ari Y (1989) Anoxia on slow inward currents of immature hippocampal neurons. J Neurophysiol 62:896-906.

Lancaster JRJr, Stuehr DJ (1996) The intracellular reactions of nitric oxide. In Nitric Oxide: Principles and Actions (Lancaster, Jr, J. R., ed.), pp. 139-175, Academic Press, San Diego.

Leblond J, Krnjević K (1989) Hypoxic changes in hippocampal neurons. J Neurophysiol 62:1-14.

Leonoudakis D, Gray AT, Winegar BD, Kindler CH, Harada M, Taylor DM, Chavez RA, Forsayeth JR, Yost CS (1998). An open rectifier potassium channel with two pore domains in tandem cloned from rat cerebellum. J Neurosci 18:868-77.

Leresche N, Hering J, Lambert RC (2004) Paradoxical potentiation of neuronal T-type Ca^{2+} current by ATP at resting membrane potential. J Neurosci 24:5592-602.

Lesage F, Lazdunski M (2000). Molecular and functional properties of two-pore-domain potassium channels. Am J Physiol Renal Physiol 279:F793-801.

Lewis C, Neidhart S, Holy C, North RA, Buell G, Surprenant A (1995) Coexpression of P2X2 and P2X3 receptor subunits can account for ATP-gated currents in sensory neurons. Nature 377:432-5.

Lichtman JW, Magrassi L, Purves D (1987) Visualization of neuromuscular junctions over periods of several months in living mice. J Neurosci 7:1215-22.

Lipton SA, Singel DJ, Stamler JS (1994) Nitric oxide in the central nervous system. Prog Brain Res 103:359-64.

Liu C, Mather S, Huang Y, Garland CJ, Yao X (2004) Extracellular ATP facilitates flow-induced vasodilatation in rat small mesenteric arteries. Am J Physiol Heart Circ Physiol 286:H1688-95.

Lopes CM, Gallagher PG, Buck ME, Butler MH, Goldstein SA (2000). Proton block and voltage gating are potassium-dependent in the cardiac leak channel Kcnk3. J Biol Chem 275:16969-78.

López- López JR, González C, Pérez-García MT (1997) Properties of ionic currents from isolated adult rat carotid body chemoreceptor cells: effect of hypoxia. J Physiol 499:429-41.

López-Barneo J (2003) Oxygen and glucose sensing by carotid body glomus cells. Curr Opin Neurobiol 13:493-9.

López-Barneo J, López- López JR, Ureña J, González C (1988) Chemotransduction in the carotid body: K^+ current modulated by PO_2 in type I chemoreceptor cells. Science 241:580-2.

López-Barneo J, Pardal R, Ortega-Sáenz P (2001) Cellular mechanism of oxygen sensing. Annu Rev Physiol 63:259-87.

Lukyanetz EA, Shkryl VM, Kravchuk OV, Kostyuk PG (2003) Action of hypoxia on different types of calcium channels in hippocampal neurons. Biochim Biophys Acta 1618:33-8.

Luo Y, Kaur C, Ling EA (2000) Hypobaric hypoxia induces fos and neuronal nitric oxide synthase expression in the paraventricular and supraoptic nucleus in rats. Neurosci Lett 296:145-8.

Macmicking JD, Xie QW, Nathan C (1997) Nitric oxide and macrophage. Annu Rev Immunol 1997;15:323-50.

Magrassi L, Purves D, Lichtman JW (1987) Fluorescent probes that stain living nerve terminals. J Neurosci 7:1207-14.

Mantegazza M, Yu FH, Catterall WA, Scheuer T (2001) Role of the C-terminal domain in inactivation of brain and cardiac sodium channels. Proc Natl Acad Sci USA 98:15348-53.

Martin-Body RL, Johnston BM (1988) Central origin of the hypoxic depression of breathing in the newborn. Respir Physiol 71:25-32.

Marty A, Neher E (1995) Tight-seal whole-cell recording. In: Single-channel recording, 2nd Edition. Eds. B Sackman and E Neher. Plenum Press, NY, pp. 31-52.

Mayer B, Hemmens B (1997) Biosynthesis and action of nitric oxide in mammalian cells. Trends Biochem Sci 22:477-81.

Mazza E Jr, Edelman NH, Neubauer JA (2000) Hypoxic excitation in neurons cultured from the rostral ventrolateral medulla of the neonatal rat. J Appl Physiol 88, 2319-29.

McCullough WT, Collins DM, Ellsworth ML (1997) Arteriolar responses to extracellular ATP in striated muscle. Am J Physiol 272:H1886-91.

McDonald DM (1981) Peripheral chemoreceptors. In: Regulation of Breathing. Part 1. Edited by T.F. Hornbein. Marcel Dekker, Inc. New York, pp 105-319.

McDonald DM, Blewett RW (1981) Location and size of carotid body-like organs (paraganglia) revealed in rats by the permeability of blood vessels to Evans blue dye. J Neurocytol 10:607-43.

McDonald DM, Mitchell RA (1975) The innervation of glomus cells, ganglion cells and blood cells in the rat carotid body: a quantitative ultrastructural analysis. J Neurocytol, 4: 177-230.

Meyers JR, MacDonald RB, Duggan A, Lenzi D, Standaert DG, Corwin JT, Corey DP (2003) Lighting up the senses: FM1-43 loading of sensory cells through nonselective ion channels. J Neurosci 23:4054-65.

Millar JA, Barratt L, Southan AP, Page KM, Fyffe RE, Robertson B, Mathie A (2000) A functional role for the two-pore domain potassium channel TASK-1 in cerebellar granule neurons. Proc Natl Acad Sci USA 97:3614-8.

Mironov SL, Richter DW (2001) Oscillations and hypoxic changes of mitochondrial variables in neurons of the brainstem respiratory centre of mice. J Physiol 533:227-36.

Miseta A, Bogner P, Berenyi E, Kellermayer M, Galambos C, Wheatley DN, Cameron IL (1993) Relationship between cellular ATP, potassium, sodium and magnesium concentrations in mammalian and avian erythrocytes. Biochim Biophys Acta 1175:133-9.

Mokashi A, Li J, Roy A, Baby SM, Lahiri S (2003) ATP causes glomus cell [Ca2+]c increase without corresponding increases in CSN activity. Respir Physiol Neurobiol 138:1-18.

Montoro RJ, Ureña J, Fernandez-Chacon R, Alvarez de Toledo G, López-Barneo J (1996) Oxygen sensing by ion channels and chemotransduction in single glomus cells. J Gen Physiol 107:133-143.

Murgia M, Hanau S, Pizzo P, Rippa M, Di Virgilio F (1993) Oxidized ATP. An irreversible inhibitor of the macrophage purinergic P2Z receptor. J Biol Chem 268:8199-203.

Neil E and O'Regan RG (1969) Effects of sinus and aortic nerve efferents on arterial chemoreceptor function. J Physiol:200:69-71.

Neil E, O'Regan RG (1971) The effect of electrical stimulation of the distal end of the carotid sinus and aortic nerve on peripheral chemoreceptor activity in the cat. J Physiol 215:15-32.

Newcomb R, Szoke B, Palma A, Wang G, Chen X, Hopkins W, Cong R, Miller J, Urge L, Tarczy-Hornoch K, Loo JA, Dooley DJ, Nadasdi L, Tsien RW, Lemos J, Miljanich G (1998) Selective peptide antagonist of the class E calcium channel from the venom of the tarantula Hysterocrates gigas. Biochemistry 37:15353-62.

North RA (2002) Molecular physiology of P2X receptors. Physiol Rev 82:1013-67.

North RA (2004) P2X3 receptors and peripheral pain mechanisms. J Physiol 554:301-8.

North RA, Surprenant A (2000) Pharmacology of cloned P2X receptors. Annu Rev Pharmacol Toxicol 40:563-80.

Nurse CA, Farraway L (1989) Characterization of Merkel cells and mechanosensory axons of the rat by styryl pyridinium dyes. Cell Tissue Res 255:125-8.

Nurse CA, Zhang M (1999) Acetylcholine contributes to hypoxic chemotransmission in co-cultures of rat type 1 cells and petrosal neurons. Respir Physiol 115:189-99.

Ortega-Sáenz P, Pardal R, García-Fernandez M, López-Barneo J (2003) Rotenone selectively occludes sensitivity to hypoxia in rat carotid body glomus cells. J Physiol 548:789-800.

Pardal R, López-Barneo J (2002) Low glucose--sensing cells in the carotid body. Nat Neurosci 5:197-8.

Pardal R, Ludewig U, García-Hirschfeld J, López-Barneo J (2000) Secretory responses of intact glomus cells in thin slices of rat carotid body to hypoxia and tetraethylammonium. Proc Natl Acad Sci USA 97:2361-6.

Parsons DF, Williams GR, Chance B (1966) Characteristics of isolated and purified preparations of the outer and inner membranes of mitochondria. Ann N Y Acad Sci 137:643-66.

Patel AJ, Honoré E (2001a). Anesthetic-sensitive 2P domain K^+ channels. Anesthesiology 95:1013-1021.

Patel AJ, Honoré E (2001b). Properties and modulation of mammalian 2P domain K^+ channels. Trends Neurosci 24:339-46.

Patel AJ, Maingret F, Magnone V, Fosset M, Lazdunski M, Honoré E (2000). TWIK-2, an inactivating 2P domain K^+ channel. J Biol Chem 275:28722-30.

Peers C (1990) Hypoxic suppression of K^+ currents in type I carotid body cells: selective effect on the Ca^{2+}-activated K^+ current. Neurosci Lett 119:253-6.

Peers C (1997). Oxygen-sensitive ion channels. Trends Pharmacol Sci 18, 405-408.

Peers C, Buckler KJ (1995) Transduction of chemostimuli by the type I carotid body cell. J Membr Biol 144:1-9.

Penner R (1995) A practical guide to patch clamping. In: Single-channel recording, 2nd Edition. Eds. B Sackman and E Neher. Plenum Press, NY, pp. 3-30.

Plant LD, Kemp PJ, Peers C, Henderson Z, Pearson HA (2002) Hypoxic depolarization of cerebellar granule neurons by specific inhibition of TASK-1. Stroke 33:2324-8.

Prabhakar NR (1994) Neurotransmitters in the carotid body. Adv Exp Med Biol 360:57-69.

Prabhakar NR (1999). NO and CO as second messengers in oxygen sensing in the carotid body. Respir Physiol 115:161-8.

Prabhakar NR (2000) Oxygen sensing by the carotid body chemoreceptors. J Appl Physiol 88:2287-95.

Prabhakar NR, Kumar GK, Chang CH, Agani FH, Haxhiu MA (1993) Nitric oxide in sensory function of the carotid body. Brain Res 625:16-22.

Prasad M, Fearon IM, Zhang M, Laing M, Vollmer C, Nurse CA (2001) Expression of P2X2 and P2X3 receptor subunits in rat carotid body afferent neurones: role in chemosensory signalling. J Physiol 537:667-77.

Prenen GH, Go KG, Postema F, Zuiderveen F, Korf J (1988) Cerebral cation shifts in hypoxic-ischemic brain damage are prevented by the sodium channel blocker tetrodotoxin. Exp Neurol 99:118-32.

Qu Y, Curtis R, Lawson D, Gilbride K, Ge P, DiStefano PS, Silos-Santiago I, Catterall WA, Scheuer T (2001) Differential modulation of sodium channel gating and persistent sodium currents by the beta1, beta2, and beta3 subunits. Mol Cell Neurosci 18:570-80.

Radford KM, Virginio C, Surprenant A, North RA, Kawashima E (1997) Baculovirus expression provides direct evidence for heteromeric assembly of P2X2 and P2X3 receptors. J Neurosci 17:6529-33.

Rajan S, Wischmeyer E, Karschin C, Preisig-Muller R, Grzeschik KH, Daut J, Karschin A, Derst C (2001). THIK-1 and THIK-2, a novel subfamily of tandem pore domain K^+ channels. J Biol Chem 276, 7302-7311.

Ralevic V, Burnstock G (1998) Receptors for purines and pyrimidines. Pharmacol Rev 50:413-92.

Ramirez AN, Kunze DL (2002) P2X purinergic receptor channel expression and function in bovine aortic endothelium. Am J Physiol Heart Circ Physiol 282:H2106-16.

Rengasamy A, Johns RA (1991) Characterization of endothelium-derived relaxing factor/nitric oxide synthase from bovine cerebellum and mechanism of modulation by high and low oxygen tensions. J Pharmacol Exp Ther 259:310-6.

Reyes R, Duprat F, Lesage F, Fink M, Salinas M, Farman N, Lazdunski M (1998) Cloning and expression of a novel pH-sensitive two pore domain K^+ channel from human kidney. J Biol Chem 273:30863-69.

Rigoni F, Deana R (1986) Ruthenium red inhibits the mitochondrial Ca^{2+} uptake in intact bovine spermatozoa and increases the cytosolic Ca^{2+} concentration. Febs Letters 198:103-8.

Rong W, Gourine AV, Cockayne DA, Xiang Z, Ford AP, Spyer KM, Burnstock G (2003) Pivotal role of nucleotide P2X2 receptor subunit of the ATP-gated ion channel mediating ventilatory responses to hypoxia. J Neurosci 23:11315-21.

Schuman EM, Madison DV (1994) Nitric oxide and synaptic function. Annu Rev Neurosci 17:153-83.

Shibuya I, Tanaka K, Hattori Y, Uezono Y, Harayama N, Noguchi J, Ueta Y, Izumi F, Yamashita H (1999) Evidence that multiple P2X purinoceptors are functionally expressed in rat supraoptic neurones. J Physiol 514:351-67.

Silva JM, Lewis DL (2002) Nitric oxide enhances Ca^{2+}-dependent K^+ channel activity in rat carotid body cells. Pflügers Arch 443:671-5.

Sirois JE, Lei Q, Talley EM, Lynch C 3rd, Bayliss DA (2000) The TASK-1 two-pore domain K^+ channel is a molecular substrate for neuronal effects of inhalation anesthetics. J Neurosci 20:6347-54.

Solomon IC, Edelman NH, Neubauer JA (2000) Pre-Botzinger complex functions as a central hypoxia chemosensor for respiration in vivo. J Neurophysiol 83:2854-68.

Sperlágh B, Kofalvi A, Deuchars J, Atkinson L, Milligan CJ, Buckley NJ, Vizi ES (2002) Involvement of P2X7 receptors in the regulation of neurotransmitter release in the rat hippocampus. J Neurochem 81:1196-211.

Stea A, Nurse CA (1992) Whole-cell currents in two subpopulations of cultured rat petrosal neurons with different tetrodotoxin sensitivities. Neuroscience 47:727-36.

Stuehr DJ (1997) Structure-function aspects in the nitric oxide synthases. Annu Rev Pharmacol Toxicol 37:339-59.

Stuehr DJ (1999) Mammalian nitric oxide synthases. Biochim Biophys Acta 1411:217-30.

Summers BA, Overholt JL, Prabhakar NR (1999) Nitric oxide inhibits L-type Ca^{2+} current in glomus cells of the rabbit carotid body via a cGMP-independent mechanism. J Neurophysiol 81:1449-57.

Summers BA, Overholt JL, Prabhakar NR (2002) CO_2 and pH independently modulate L-type Ca^{2+} current in rabbit carotid body glomus cells. J Neurophysiol 88:604-12.

Summers BA, Overholt JL, Prabhakar NR. (2000) Augmentation of L-type calcium current by hypoxia in rabbit carotid body glomus cells: evidence for a PKC-sensitive pathway. J Neurophysiol. 84(3):1636-44.

Sun MK, Reis DJ (1994) Hypoxia-activated Ca^{2+} currents in pacemaker neurones of rat rostral ventrolateral medulla in vitro. J Physiol 476:101-16.

Talley EM, Bayliss DA (2002) Modulation of TASK-1 (Kcnk3) and TASK-3 (Kcnk9) potassium channels. Volatile anesthetics and neurotransmitters share a molecular site of action. J Biol Chem 277:17733-42.

Talley EM, Solorzano G, Lei Q, Kim D, Bayliss DA (2001) CNS distribution of members of the two-pore-domain (KCNK) potassium channel family. J Neurosci 21:7491-505.

Thomas T, Spyer KM (2000) ATP as a mediator of mammalian central CO_2 chemoreception. J Physiol 523:441-7.

Thompson RJ, Nurse CA (1998) Anoxia differentially modulates multiple K^+ currents and depolarizes neonatal rat adrenal chromaffin cells. J Physiol 512:421-34.

Urenjak J, Obrenovitch TP (1996) Pharmacological modulation of voltage-gated Na^+ channels: a rational and effective strategy against ischemic brain damage. Pharmacol Rev 48:21-67.

Vallance P, Leiper J (2002) Blocking NO synthesis: how, where and why? Nat Rev Drug Discov 1:939-50.

Vega-Sáenz De Miera E, Lau DH, Zhadina M, Pountney D, Coetzee WA, Rudy B (2001) Kt3.2 and kt3.3, two novel human two-pore K^+ channels closely related to task-1. J Neurophysiol 86:130-42.

Wang G, Zhou P, Repucci MA, Golanov EV, Reis DJ (2001) Specific actions of cyanide on membrane potential and voltage-gated ion currents in rostral ventrolateral medulla neurons in rat brainstem slices. Neurosci Lett 309:125-9.

Wang ZZ, Bredt DS, Fidone SJ, Stensaas LJ (1993) Neurons synthesizing nitric oxide innervate the mammalian carotid body. J Comp Neurol 336:419-32.

Wang ZZ, Dinger BG, Stensaas LJ, Fidone SJ (1995a) The role of nitric oxide in carotid chemoreception. Biol Signals 4:109-16.

Wang ZZ, Stensaas LJ, Bredt DS, Dinger B, Fidone SJ (1994a) Localization and actions of nitric oxide in the cat carotid body. Neuroscience 60:275-86.

Wang ZZ, Stensaas LJ, Bredt DS, Dinger BG, Fidone SJ (1994b) Mechanisms of carotid body inhibition. Adv Exp Med Biol 360:229-35.

Wang ZZ, Stensaas LJ, Dinger BG, Fidone SJ (1995b) Nitric oxide mediates chemoreceptor inhibition in the cat carotid body. Neuroscience 65:217-29.

Waypa GB, Chandel NS, Schumacker PT (2001) Model for hypoxic pulmonary vasoconstriction involving mitochondrial oxygen sensing. Circ Res 88:1259-66.

Waypa GB, Schumacker PT (2002) O_2 sensing in hypoxic pulmonary vasoconstriction: the mitochondrial door re-opens. Respir Physiol Neurobiol 132:81-91.

Weber ML, Taylor CP (1994) Damage from oxygen and glucose deprivation in hippocampal slices is prevented by tetrodotoxin, lidocaine and phenytoin without blockade of action potentials. Brain Res 664:167-77.

Weir EK, Archer SL (1995) The mechanism of acute hypoxic pulmonary vasoconstriction: the tale of two channels. FASEB J 9:183-9.

Wilson DF, Mokashi A, Chugh D, Vinogradov S, Osanai S, Lahiri S (1994) The primary oxygen sensor of the cat carotid body is cytochrome a3 of the mitochondrial respiratory chain. FEBS Lett 351:370-4

Wu LG, Borst JG, Sakmann B (1998) R-type Ca^{2+} currents evoke transmitter release at a rat central synapse. Proc Natl Acad Sci USA 95:4720-5.

Wu LG, Saggau P (1994) Pharmacological identification of two types of presynaptic voltage-dependent calcium channels at CA3-CA1 synapses of the hippocampus. J Neurosci 14:5613-22.

Wyatt CN, Buckler KJ (2004) The effect of mitochondrial inhibitors on membrane currents in isolated neonatal rat carotid body type I cells. J Physiol. 556:175-91.

Wyatt CN, Peers C (1995) Ca^{2+}-activated K^+ channels in isolated type I cells of the neonatal rat carotid body. J Physiol 483:559-65.

Xu J, Tse FW, Tse A (2003) ATP triggers intracellular Ca^{2+} release in type II cells of the rat carotid body. J Physiol 549:739-47.

Youngson C, Nurse C, Yeger H, Cutz E (1993) Oxygen sensing by airway chemoreceptors. Nature 365:153-5.

Zhang M, Fearon IM, Zhong H, Nurse CA (2003) Presynaptic modulation of rat arterial chemoreceptor function by 5-HT: role of K^+ channel inhibition via protein kinase C. J Physiol 551:825-42.

Zhang M, Nurse CA (2000) Does endogenous 5-HT mediate spontaneous rhythmic activity in chemoreceptor clusters of rat carotid body? Brain Res 872:199-203.

Zhang M, Nurse CA (2004) CO_2/pH chemosensory signalling in co-cultures of rat carotid body receptors and petrosal neurons: role of ATP and ACh. J Neurophysiol (in press).

Zhang M, Zhong H, Vollmer C, Nurse CA (2000) Co-release of ATP and ACh mediates hypoxic signalling at rat carotid body chemoreceptors. J Physiol 525:143-58.

Zhong H, Zhang M, Nurse CA (1997) Synapse formation and hypoxic signalling in co-cultures of rat petrosal neurones and carotid body type 1 cells. J Physiol 503:599-612.

Zhou Z, Bers DM (2002) Time course of action of antagonists of mitochondrial Ca^{2+} uptake in intact ventricular myocytes. Pflügers Archiv 445:132-8.

APPENDIX 1

O_2-sensitivity of heterologously expressed THIK-1 background K^+ channels

This work was performed in collaboration with Dr. Fearon's laboratory. I was responsible for performing electrophysiological experiments and data analysis involving the O_2-sensitivity of THIK-1 channels. Steve Brown was responsible for transfecting and culturing HEK 293 cells, Dr. I O'Kelly was responsible for obtaining the cDNA construct containing THIK-1 and THIK-2 genes, and Dr. I. Fearon was responsible for screening of clones expressing THIK-1 and THIK-2 channels. A manuscript, including the work presented in this appendix, is currently under preparation.

INTRODUCTION

Background or 'leak' potassium channels, called two-pore (2P) domain K^+ channels, are voltage-independent K^+-selective channels that play a key role in setting the resting membrane potential and input resistance of the cell. So far three members of the 2P K^+ channel family, TASK-1 (Kcnk3), TASK-3 (Kcnk9), and TREK-1 (Kcnk2) have been found to be O_2-sensitive in different tissues. A TASK-1-like conductance has been shown to be O_2-sensitive in rat carotid body chemoreceptors (Buckler *et al.* 2000) and rat cerebellar granule neurones (Plant *et al.* 2002), whereas human TASK-3 appears to be O_2-sensitive in the lung carcinoma cell line H146, which is a model for pulmonary neuroepithelial bodies (Hartness *et al.* 2001), and human TREK-1 was reported to be O_2-sensitive when expressed in HEK 293 cells (Miller *et al.* 2003).

Recently, we characterized an O_2-sensitive background K^+ conductance in paraganglion neurons from the rat glossopharyngeal nerve (GPN; Campanucci *et al.* 2003a), which are thought to play an important role in the efferent inhibition of carotid body (CB) chemoreceptors (Prabhakar *et al.* 1993; Wang *et al.* 1993, 1994a, 1995a, Prabhakar, 2000). This conductance possessed pharmacological characteristics similar to THIK-1 (Kcnk13) background K^+ channels. In this study, we addressed directly whether or not members of the THIK family are O_2-sensitive by first expressing THIK-1 (Kcnk13) and THIK-2 (Kcnk12) channels in the HEK 293 cell line, and then testing the effects of hypoxia. This appendix summarizes preliminary data obtained from THIK-1-expressing HEK 293 cells.

METHODS

Culture of HEK 293 cells. Cells were grown in minimum essential medium with Earle's salts and L-glutamine (Gibco), containing 9 % (v/v) fetal calf serum (Globepharm), 1 % (v/v) non-essential amino acids, gentamicin (50 mg/L 10000 U/L penicillin G, 10 mg/L streptomycin, and 0.25 mg/L amphotericin (all Gibco) at 37 °C in a humidified atmosphere of air/CO2 (19:1). Stably transfected cell lines were maintained continuously under the appropriate selection. Cells were cultured in 35 mm dishes and split twice per week at a ratio of 1:5.

Transient transfection of HEK 293 cells. After splitting the previous day and seeding at ~ 60 % confluency in a 35 mm dish, wild-type HEK 293 cells were transfected with 5 mg of either pCDNA3.1-THIK-1 or pCDNA3.1-THIK-2 using ExGen 500 (Fermentas, Burlington, ON, Canada), according to the manufacturer's instructions. In some of these transient expression studies, to allow visual selection of transfected cells they were co-transfected with 0.5 mg of pEGFP-C1 (Clontech). Cells were used in electrophysiological studies 48 hr post-transfection.

Stable transfection of pCDNA3.1-THIK-1. Cells were transfected as described above with 3 mg of pCDNA3.1-THIK-1. Three days post-transfection, the medium was replaced with one containing 400 mg/ml G418 (Invitrogen). Selection was applied for 2 weeks, after which individual colonies could be visualised using an inverted microscope equipped with Hoffman modulation contrast optics (Nikon, Mississauga, ON, Canada).

Colonies were picked and seeded in wells of a 96-well plate and allowed to reach confluency, after which they were transferred to 35 mm dishes for further culture and for examination of K^+ currents. Of the ~ 20 clones screened, > 75 % were positive for K^+ channel activity, and a single clone was identified for further study based on the number of cells within the clone expressing current, the size of these currents, and the membrane potential of the cells within the clone. This clone was sub-cloned to ensure a pure population of stably-transfected cells. G418 selection was continued throughout the cloning process and in all subsequent sub-culturing.

Electrophysiology. Methods used for conventional whole-cell recordings in HEK 293 cells were identical to those described in Chapter 2 and 3 of this thesis.

RESULTS AND DISCUSSION

In physiological solutions, THIK-1 currents from stably expressing HEK 293 cells, possessed outward or 'open rectification', and a reversal potential approximately equal to E_K (~ -80 mV). These data are consistent with high expression of voltage-independent K^+ channels (Fig. 1 C, n = 8). THIK-1 currents, measured at +30 mV, were reversibly inhibited when exposed to a hypoxic solution (PO_2 ~ 15 Torr; Fig. 1 D; n = 5). These data contrast with recordings from wild type, untransfected cells, which possess an almost undetectable background current and in which hypoxia was ineffective (Fig. 1 A, B). Furthermore, application of the volatile anesthetic, halothane (5 mM), a reversible inhibitor of THIK-1 channels (Rajan *et al.* 2001), caused inhibition of the outward THIK-

1 currents and occlusion of the hypoxic response (Fig. 2 A; n = 10). In contrast, arachidonic acid (AA), a reversible potentiator of THIK-1 channels (Rajan *et al.* 2001), enhanced outward THIK-1 currents (Fig. 2 B; n = 5). Preliminary data show that hypoxia was still effective in the presence of AA (Fig. 2 C), causing inhibition of the THIK-1 current.

Exposure to hypoxic solutions during current clamp recording caused membrane depolarization of ~ 2 mV (Fig. 3 A; n = 3). Consistently, application of halothane caused a similar depolarization and occluded the hypoxia-induced depolarization (Fig. 3 B, n = 2). These data confirm that hypoxia and halothane act via a common pathway. In contrast, application of AA caused membrane hyperpolarization but the hypoxia-induced depolarization was still detectable in the presence of AA (Fig. 3 C; n = 2).

As previously described by Rajan *et al.* (2001) for the expression of THIK-2 channels in *Xenopus* oocytes, our attempts at expressing THIK-2 channels in HEK 293 cells were unsuccessful. Therefore, the question remains open whether or not THIK-2 (Kcnk12) is also an O_2-sensitive K^+ channel.

These novel data are strikingly consistent with our previous report on the THIK-like currents from GPN neurons (Chapter 3). However, we only observed hypoxic-modulation of the background currents in GPN neurons when recording with the nystatin-perforated patch configuration. These data led to the conclusion that hypoxic modulation required an intact cytoplasm, as previously reported for other O_2-sensitive background K^+ channels (i.e. TASK1-like in the CB chemoreceptors; Buckler *et al.* 2000). However, when THIK-1 channels were expressed in HEK 293 cells, responses to hypoxia were

observed with conventional whole-cell recordings. The reasons for this discrepancy are presently unclear, but may simply reflect differences between native cells and cell lines.

As presented in Appendix 3 of this thesis, inhibitors of mitochondrial complex I (e.g. rotenone) did not mimic hypoxia in causing inhibition of background K^+ currents in GPN neurons. Similarly, exposure of HEK 293-expressing THIK-1 cells to rotenone (1-5 μM) had no effect on the magnitude of the THIK-1 current recorded at +30 mV (Fig. 2 D; n = 3). These data, together with the persistence of O_2-sensitivity in dialysed whole-cell preparations suggest that cytoplasmic factors are not involved in the hypoxic modulation of THIK-1 channels, at least in heterologous expression systems. Thus, the broad expression of THIK-1 channels in the central nervous system (Rajan *et al.* 2001), may be related to a signalling role in pathological stress conditions such as brain ischemia, which is associated with local tissue hypoxia.

Figure 1. Voltage-clamp recordings from HEK 293 cells. A, Example traces and I-V plot of currents recorded from a wild type HEK 293 cell. Note that these cells possess a very little background current compared to cells expressing THIK-1 channels (see C). B, Lack of effect of hypoxia on currents in wild type cells (at +30 mV). C, I-V plot of current recorded from THIK-1-expressing cells (n = 8); note increased magnitude of the currents, which show outward rectification and reversal potential near E_K (~ -83 mV). D, Hypoxia reversibly inhibited THIK-1 currents in HEK 293 cells (n = 5; at +30 mV). Scale in all traces represents 500 pA (vertical) and 20 ms (horizontal). N: normoxia, H: hypoxia and R: recovery.

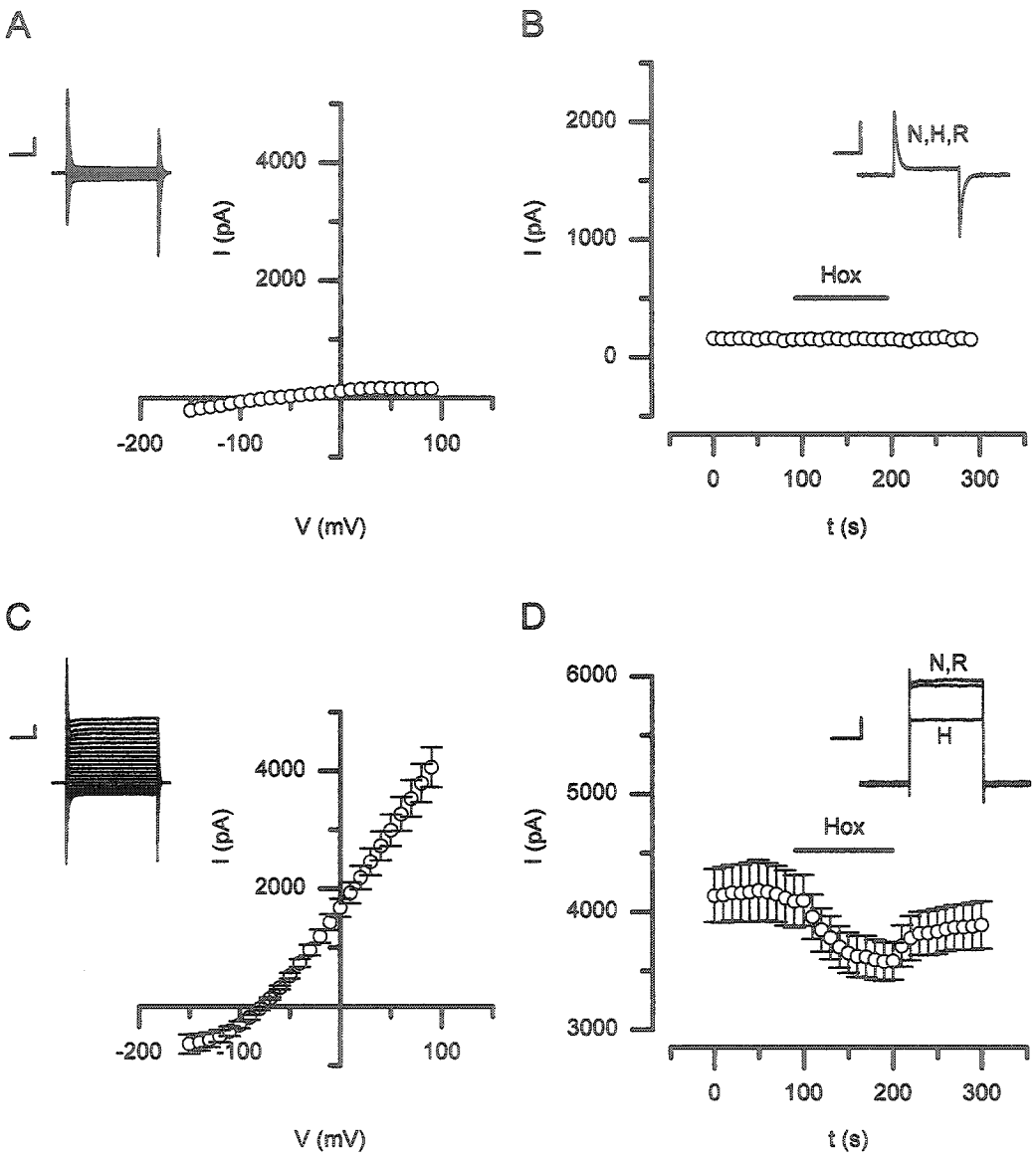
A
4000
2000
I (pA)
-200
-100
100
V (mV)
B
2000
1000
0
I (pA)
N,H,R
Hox
0
100
200
300
t (s)
C
4000
2000
I (pA)
-200
-100
100
V (mV)
D
6000
5000
4000
3000
I (pA)
N,R
H
Hox
0
100
200
300
t (s)

Figure 2. Effects of halothane, arachidonic acid and rotenone on THIK-1 currents. A, Halothane (5 mM) caused inhibition of the THIK-1 currents at +30 mV and occluded the response to hypoxia (n = 10). B, Arachidonic acid (AA, 5 μM; n = 5) caused potentiation of the THIK-1 current at + 30 mV. Hypoxia was still effective in the presence of AA, causing inhibition of the THIK-1 currents (see example in C). D, Example showing lack of effect of the complex I inhibitor, rotenone (1-5 μM) on the THIK-1 currents (n = 3).

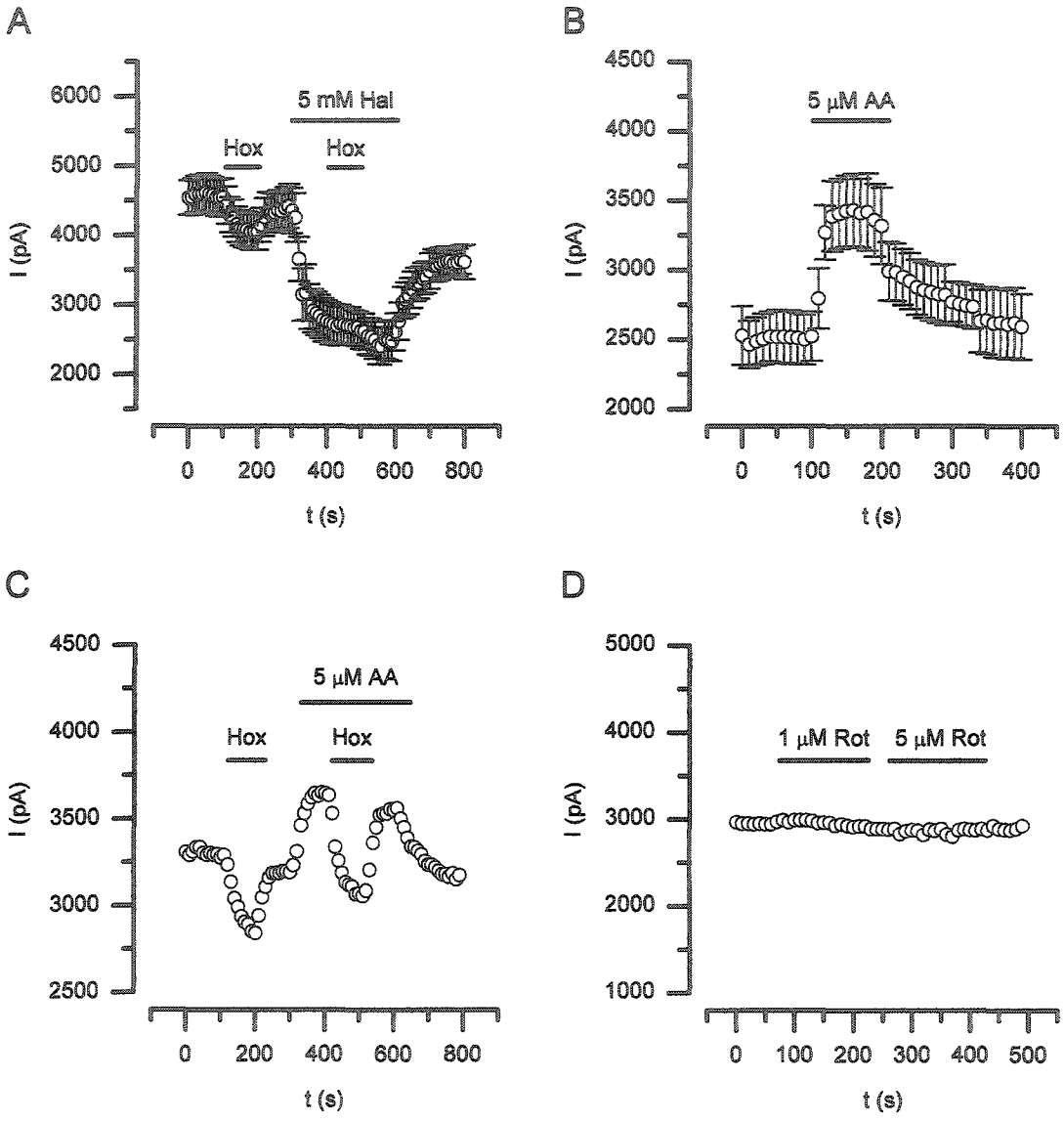
A
6000
5000
4000
3000
2000
I (pA)
5 mM Hal
Hox
Hox
0
200
400
600
800
t (s)
B
4500
4000
3500
3000
2500
2000
I (pA)
5 μM AA
0
100
200
300
400
t (s)
C
4500
4000
3500
3000
2500
I (pA)
5 μM AA
Hox
Hox
0
200
400
600
800
t (s)
D
5000
4000
3000
2000
1000
I (pA)
1 μM Rot
5 μM Rot
0
100
200
300
400
500
t (s)

Figure 3. Effects of hypoxia, halothane and arachidonic acid on the resting potential of HEK 293 cells expressing THIK-1 channels. A, Example traces showing the hypoxia-induced depolarization (~ 2mV) of the resting potential. B, Halothane also caused membrane depolarization and occluded the response to hypoxia. C, Arachidonic acid (AA) caused hyperpolarization but hypoxia still elicited membrane depolarization in the presence of AA. Note that in A-C, the resting potential is near E_K (~ -83 mV) in THIK-1 expressing cells, suggesting a predominance of these open K^+ channels at rest.

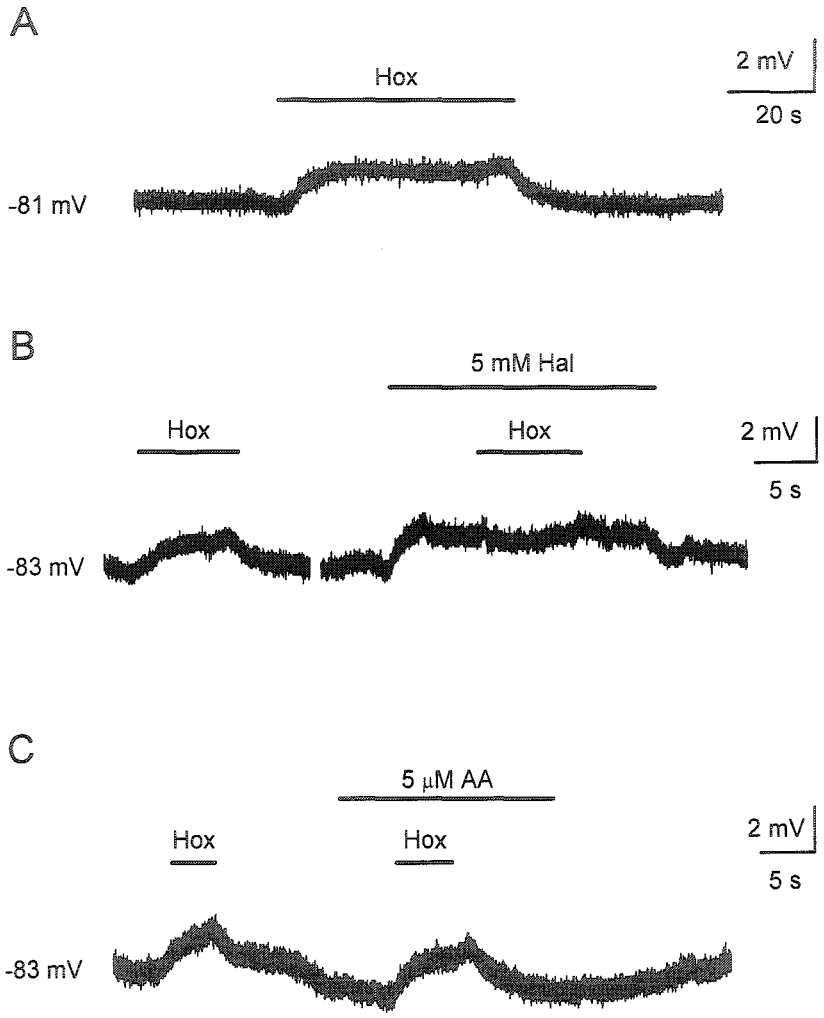
A
Hox
2 mV
20 s
-81 mV
B
5 mM Hal
Hox
Hox
2 mV
5 s
-83 mV
C
5 μM AA
Hox
Hox
2 mV
5 s
-83 mV

APPENDIX 2

Other Neurotransmitter Receptors Expressed by GPN neurons

A characterization of the receptors expressed by GPN neurons was extended to include the neurotransmitters acetylcholine (ACh), dopamine (DA) and serotonin (5-HT). Similar methods to those described in Chapter 4 of this thesis were used, except that the neurotransmitter was applied by pressure ejection from a multi-barrelled pipette.

RESULTS

The majority of neurons tested responded to 'puffs' of ACh (19/19), 5-HT (9/14) and DA (7/9), applied by pressure ejection. ACh, at a concentration of 50 μM, produced depolarization of all cells tested (not shown). Application of 50 μM 5-HT produced membrane depolarization (Fig. 1 A; n = 9), though in a few cases (n = 2), 5-HT produced membrane hyperpolarization (Fig. 1 B). Application of brief hyperpolarizing current

pulses before, during and after the application of 5-HT (Fig. 1 B, inset) revealed that the hyperpolarization was accompanied by a decrease in membrane conductance. The reversal potential of 5-HT-evoked current was ~ –30 mV (Fig. 1 C-D), suggesting that 5-HT modulated non-selective cation channels on GPN neurons.

Application of 100 μM DA produced depolarization (Fig. 2 A-D) in the majority of the cells (n = 7/9). However, it was accompanied by either a decrease (Fig. 2 B) or an increase (Fig. 2 D) in membrane conductance, suggesting that different mechanisms may be involved. Reversal potentials for DA-evoked current was ~ –40 mV (Fig. 2 E-F). As in the case of 5-HT, these data may indicate the presence of non-selective cation channels.

Furthermore, some GPN neurons exhibited spontaneous activity during current-clamp experiments. Exposure to a variety of blockers indicated that the spontaneous discharge was sensitive to the 5-HT_2 receptor antagonist, ritanserin (Fig. 3 C), and to the $5HT_3$ receptor antagonist (3-α-tropanyl)-3,5-dichlorobenzoate (MDL72222) respectively (Fig. 3 G). Since these drugs block different 5-HT receptor subtypes, more than one receptor appear to be involved. Application of the nicotinic blocker, mecamylamine, or the purinergic blocker, suramin, had no detectable effect on the discharge (Fig. 3 B, F).

DISCUSSION

GPN neurons were responsive to ACh, 5-HT and DA. Reversal potentials for 5-HT- and DA-evoked currents were found to be ~ –30 and -40 mV, respectively, suggesting the involvement of non-selective cation channels. The fact that all the neurons tested responded to ACh is interesting in two aspects. First, immunostaining carried out

in cultures, as well as nerve whole mounts, showed that the majority of GPN neurons were positive for the cholinergic marker, VAChT (see Chapter 3), suggesting that ACh is a neurotransmitter involved in cell-cell communication among these neurons. Second, chemoreceptor type I cells in the rat carotid body are a source of ACh (Zhang and Nurse, 2004), which could act on nearby terminals, assuming they express similar ACh receptors as the soma. In addition, GPN neurons responded to DA and 5-HT. There are two potential sources of these neurotransmitters close to GPN terminals, i.e. CB type I cells and petrosal neurons. Since these two cell types are important in chemosensory transmission it is possible that GPN neurons are part of a broader and more complex network involved in CB chemoreceptor function. Finally, since 5-HT receptor antagonists blocked the spontaneous activity elicited by some GPN neurons in culture, 5-HT may also be involved in the synaptic mechanisms that regulate interactions between neighbouring GPN neurons. Further experiments are needed to clarify these issues.

Figure. 1. 5-HT-evoked responses in GPN neurons. A-B are examples of different responses evoked during current-clamp recordings. A, Example of a cell that responded to 5-HT with a depolarization of the membrane potential, as seen in the majority of GPN neurons. B, Example of 5-HT induced membrane hyperpolarization accompanied by a decrease in conductance, as revealed by application of constant hyperpolarizing current pulses (B, inset). C, Shows an example of 5-HT-evoked currents that reversed at ~ –20mV under voltage-clamp; the voltage clamp protocol used is shown below the traces. D, Mean ± (s.e.m.) 5-HT-evoked currents at different voltages; note reversal potential of ~ –30 mV (n = 3).

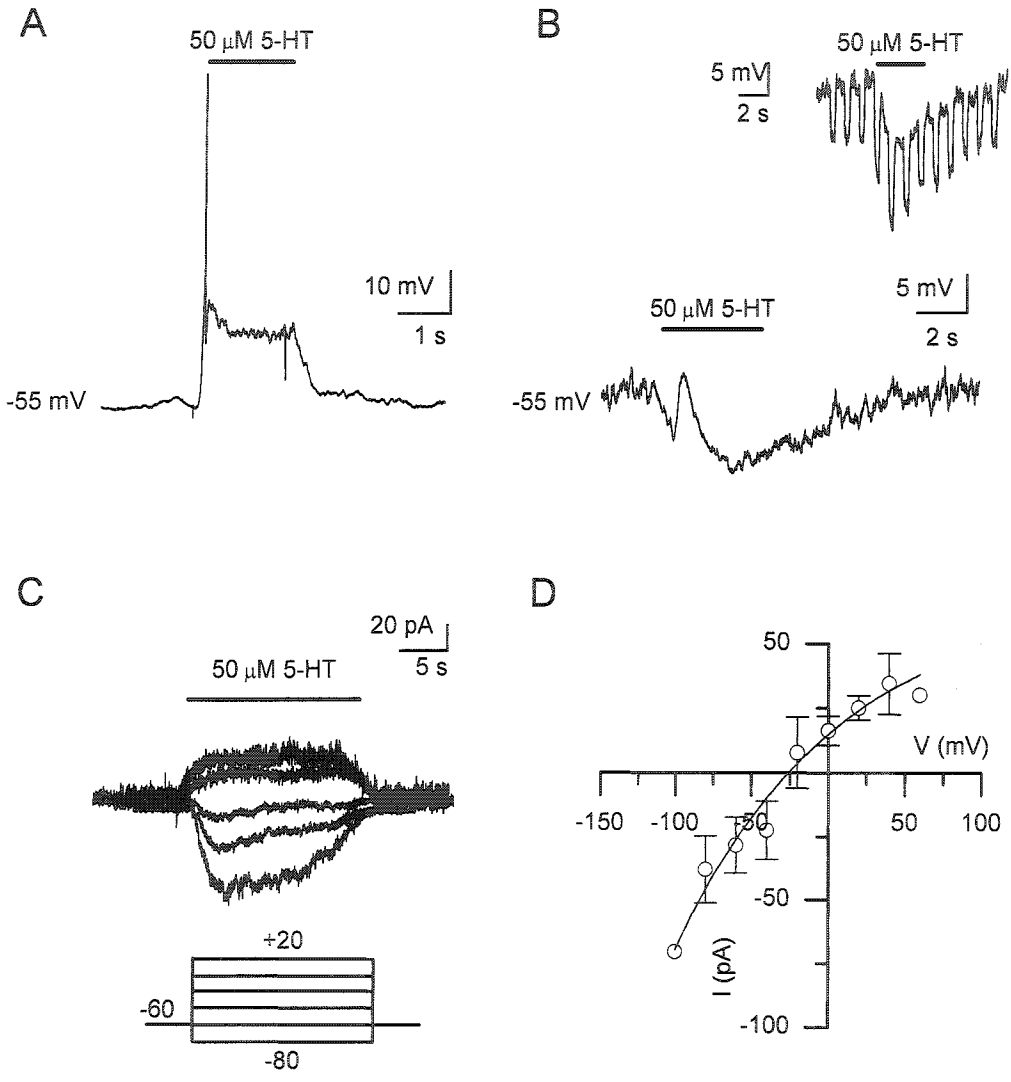
A
50 μM 5-HT
10 mV
1 s
-55 mV
B
50 μM 5-HT
5 mV
2 s
50 μM 5-HT
5 mV
2 s
-55 mV
C
20 pA
5 s
50 μM 5-HT
+20
-60
-80
D
50
V (mV)
-150
-100
-50
50
100
-50
-100
I (pA)

Figure. 2. DA–evoked responses in GPN neurons. A-D, Examples of different responses evoked during current-clamp recordings. A-D, Example of cells that responded to DA with a depolarization of the membrane potential accompanied by either a decrease in conductance (B), and an increase in conductance (D). E, Shows an example of DA-evoked current that reversed at ~ –20mV under voltage-clamp; the voltage clamp protocol is shown below the traces. F, Mean ± (s.e.m.) DA-evoked currents at different voltages; note reversal potential of ~ –40 mV (n = 3).

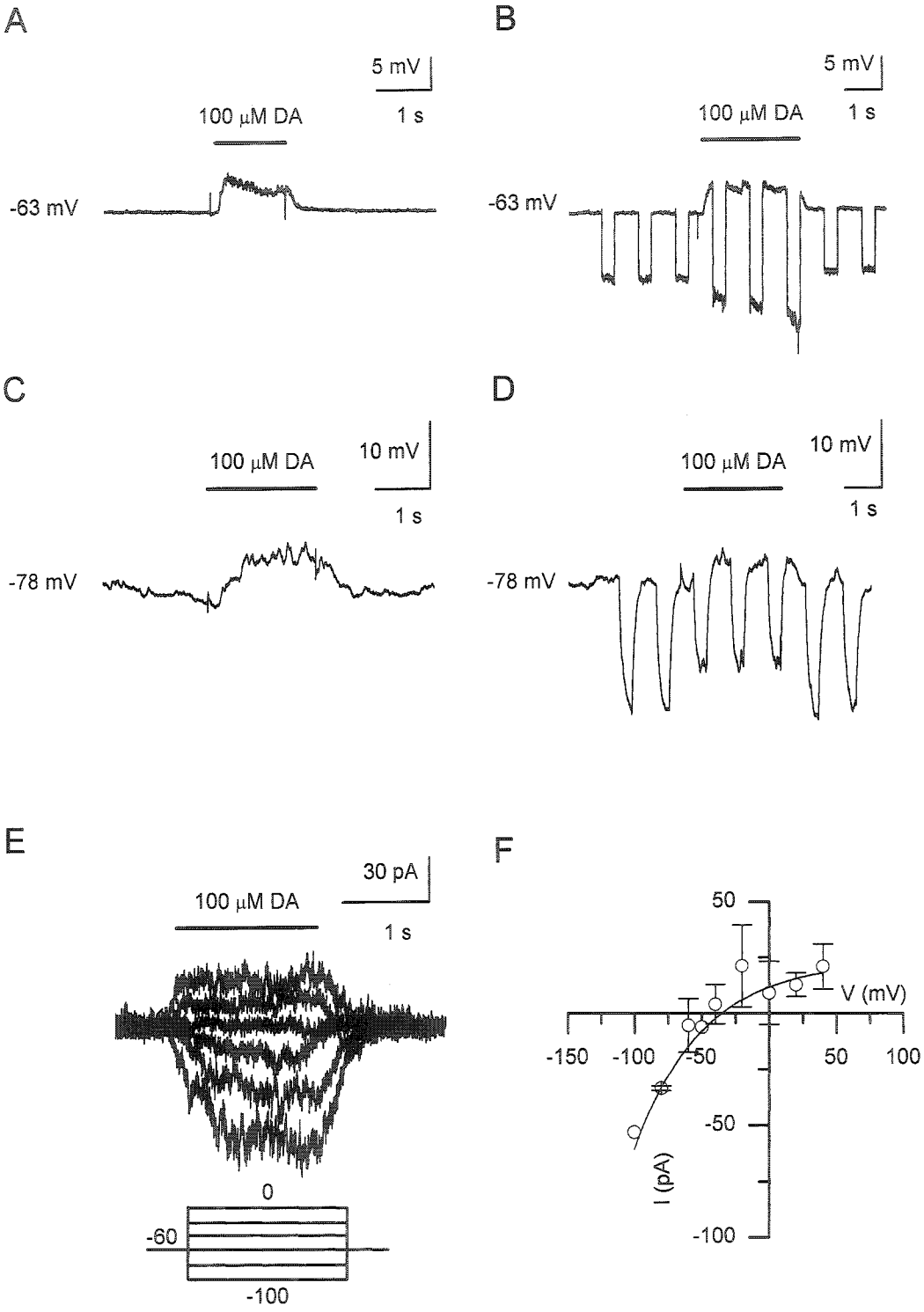
A
5 mV
100 μM DA
1 s
-63 mV
B
5 mV
100 μM DA
1 s
-63 mV
C
100 μM DA
10 mV
1 s
-78 mV
D
100 μM DA
10 mV
1 s
-78 mV
E
30 pA
100 μM DA
1 s
0
-60
-100
F
50
V (mV)
-150
-100
-50
50
100
-50
I (pA)
-100

Figure 3. Effects of pharmacological agents on spontaneously active GPN neurons. A-D, An example of the effect of the nicotinic antagonist mecamylamine, and a 5-HT_2 receptor blocker, ritanserin, on the same spontaneously active neuron. Only ritanserin appeared to inhibit activity. E-H, Example of the effect of the purinergic antagonist suramin, and a 5-HT_3 receptor blocker, MDL72222, on the same spontaneously active neuron. MDL72222 appeared to inhibit the spontaneous activity, while suramin did not seem to have any effect.

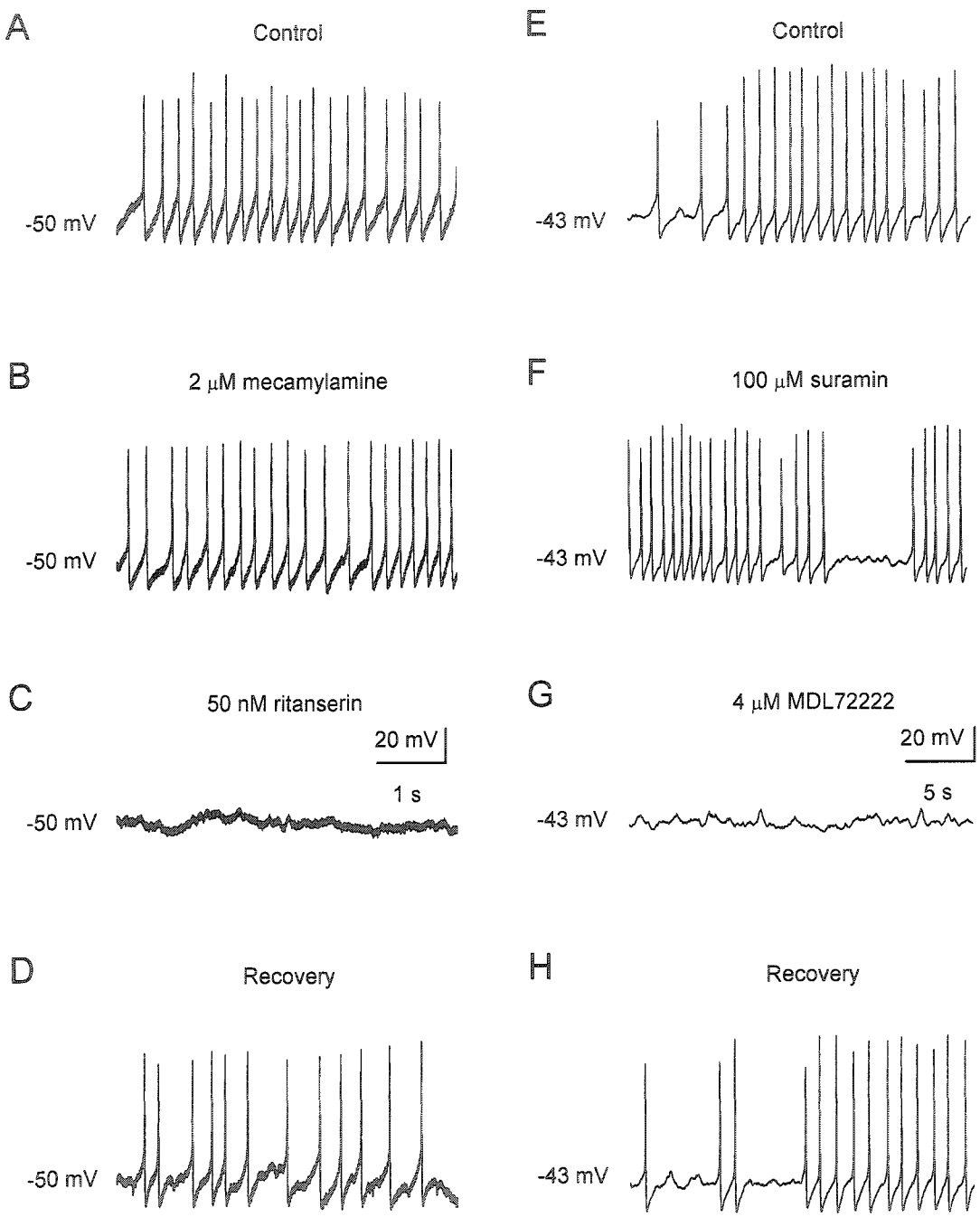
A
Control
-50 mV
E
Control
-43 mV
B
2 μM mecamylamine
-50 mV
F
100 μM suramin
-43 mV
C
50 nM ritanserin
20 mV
1 s
-50 mV
G
4 μM MDL72222
20 mV
5 s
-43 mV
D
Recovery
-50 mV
H
Recovery
-43 mV

APPENDIX 3

Is the O_2 sensor located in the mitochondria of GPN neurons?

INTRODUCTION

Oxygen-sensing is a fundamental biological process necessary for physiological adaptation of living organisms to variation in habitat and environment. These adaptations to a fall in PO_2 (hypoxia) involve a wide range of mechanisms that occur at different organizational levels in the body. Most O_2-sensitive systems described to date consist of a sensor that produces a mediator in response to changes in PO_2, which in turn alters the function of an effector. In many chemosensory systems currently known, modulation of K^+ channels during hypoxia is a common effector mechanism (López-Barneo *et al.* 2001, 2003). In GPN neurons, hypoxia inhibits a background K^+ conductance leading to depolarization of the neuronal resting potential (Campanucci *et al.* 2003a). We hypothesize that hypoxic depolarization in this cell type leads to Ca^{2+} influx and activation of nNOS, which in turn causes inhibition of CB chemoreceptors via NO release. Although the effector mechanisms have been intensely studied in a wide variety of cell types (López Barneo *et al.* 2001), the molecular identity of the oxygen sensor and its cellular location, as well as the signaling pathways that couple the sensor to the cellular response, are poorly understood.

Mitochondrial hypothesis of O_2-sensing

The mitochondrion, which consumes O_2 during oxidative phosphorylation and ATP synthesis, has long been considered as a potential site for O_2-sensing. During mitochondrial respiration, four electrons are transferred from NADH, through the electron transport chain (ETC) complexes, to O_2 at complex IV. This mechanism reduces

O_2 to H_2O and the resulting free energy change is conserved in the form of ATP synthesis. It has been estimated that 2 – 3 % of the O_2 consumed by mitochondria is incompletely reduced, yielding reactive oxygen species (ROS; Parsons *et al.* 1966). The mitochondrial hypothesis of O_2-sensing involves inhibition of mitochondrial respiration during hypoxia, leading to either a change in ROS generation or alteration of intracellular ATP/ADP ratio (Duchen and Biscoe, 1992). This hypothesis was supported by the fact that ETC inhibitors such as cyanide and azide, which inhibit complex IV, cause neurotransmitter release from carotid body (CB) O_2-sensitive type I cells (López-Barneo, 2001). More recently, mitochondrial inhibitors have been shown to mimic hypoxia in causing inhibition of background K^+ currents in rat type I cells (Wyatt and Buckler, 2004). On the other hand, an extra-mitochondrial, rotenone-sensitive biding site has been proposed as the O_2 sensor in these cells (Ortega-Sáenz *et al.* 2003). It has been suggested that one way for mitochondria to signal changes in PO_2 (within physiological range) is through changes in the redox state of the ETC or via effects on the generation of reducing equivalents (i.e., NADH) in the Krebs cycle (Chandel and Schumaker, 2000). Recent data suggest that ROS generated by mitochondria play a physiological role in the responses of the pulmonary vasculature to hypoxia (Chandel *et al.* 1998; Duranteau *et al.* 1998). However, the complexity of this system is demonstrated by the contradictory reports concerning the effect of hypoxia on ROS generation in pulmonary arteries. Hypoxia has been reported to cause both, a decrease (Archer *et al.* 1993; Weir and Archer, 1995) and an increase (Waypa *et al.* 2001, Waypa and Schumacker, 2002) in ROS generation, which is coupled to K^+ channel inhibition and subsequent vasoconstriction.

METHODS

Cell isolation techniques and electrophysiological recordings were carried out as described in Chapter 2 of this thesis.

PRELIMINARY RESULTS AND DISCUSSION

Lack of effect of rotenone on the GPN hypoxic response

Application of rotenone, a blocker of mitochondrial complex I, at concentrations of 1-5 μM, caused an inhibition of outward K^+ current at higher concentrations (Fig. 1 A). Fig. 1 B summarizes these data for a group of 5 distal GPN neurons. Fig. 1 C, 1 μM rotenone did not affect the reversible inhibition of the whole-cell outward current during hypoxia (n = 3 distal GPN neurons). Interestingly, when 5 μM rotenone was applied to proximal GPN neurons (n = 3), hypoxia partially reversed the inhibition caused by rotenone (Fig. 1 D). However, this effect was never observed in distal GPN neurons (Fig. 1 C), therefore its significance is presently unclear. These data suggest that complex I of the ETC is not involved in the GPN response to hypoxia. Further experiments with application of blockers that inhibit at different complexes are needed in order to clarify the role of mitochondria in O_2 sensing in GPN neurons.

Figure 1. Effects of rotenone alone and rotenone plus hypoxia in GPN neurons. A, Dose dependent inhibition of outward current by rotenone (0.1-5 mM), applied during a time series protocol (step to +30 mV). B, Dose response curve for rotenone inhibition of outward current (n = 5 distal GPN neurons). C, Effect of 1 and 5 μM rotenone on the hypoxic response in distal (C; n = 3) and proximal (D; n = 3) GPN neurons, respectively. Note, hypoxia (Hox) partially reversed the inhibition due to rotenone in proximal neurons (D); however in distal neurons (C), hypoxia caused further inhibition in the presence of rotenone. The reasons for these differences are unknown.

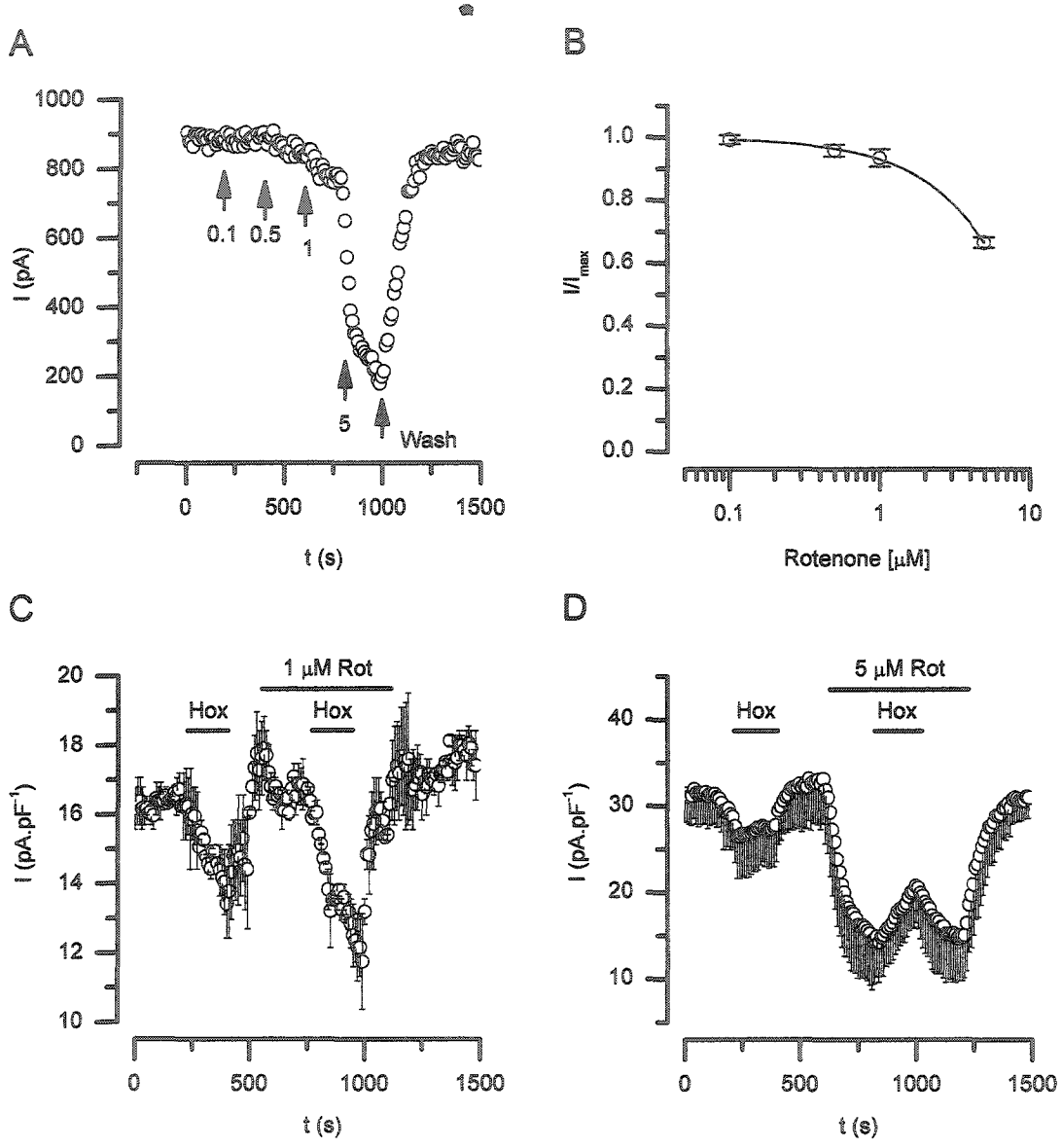
A
1000
800
600
400
200
0
I (pA)
0.1
0.5
1
5
Wash
0
500
1000
1500
t (s)
B
1.0
0.8
0.6
0.4
0.2
0.0
I/I_max
0.1
1
10
Rotenone [μM]
C
20
18
16
14
12
10
I (pA.pF⁻¹)
1 μM Rot
Hox
Hox
0
500
1000
1500
t (s)
D
40
30
20
10
I (pA.pF⁻¹)
5 μM Rot
Hox
Hox
0
500
1000
1500
t (s)

APPENDIX 4

Does hypoxia modulate Ca^{2+} channels in GPN neurons?

INTRODUCTION

Regulation of ion channels by oxygen tension was first demonstrated in the chemoreceptive type I cells of the carotid body, where K^+ channels are inhibited rapidly by hypoxia (reviewed by López-Barneo *et al.* 1998). More recently, native voltage-gated L-type Ca^{2+} channels in vascular smooth muscle and carotid body type I cells have also been shown to be regulated by hypoxia (Franco-Obregon and López-Barneo, 1996a,b; Franco-Obregon *et al.* 1995; Montoro *et al.* 1996; Summers *et al.* 2000, 2002). As described in Chapter 3 of this thesis, the O_2-sensitivity of GPN neurons is mediated by background K^+ channels that are inhibited by hypoxia, leading to depolarization and an increase in electrical excitability. Preliminary data obtained during recording of whole-cell currents from some GPN neurons in the presence of TTX (1 μM), showed that hypoxia augmented an inward current at step potentials ~ -25 mV. These data raise the possibility that a Ca^{2+} current is activated during hypoxic conditions. Ca^{2+} influx through voltage-dependent Ca^{2+} channels is a likely pathway for activation of nNOS, NO production, and subsequent inhibition of carotid body chemoreceptor function during hypoxia. Here, I obtained preliminary evidence that hypoxia augmented Ca^{2+}-channel current in GPN neurons, independent of its effects on K^+ channels. This represents another potential pathway for facilitating Ca^{2+} entry and nNOS activation in GPN neurons.

METHODS

Cell culture and electrophysiology. Methods are identical to those described in Chapter 2 and 3 of this thesis.

PRELIMINARY RESULTS AND SIGNIFICANCE

In physiological Ca^{2+} concentration (2 mM), the augmentation of an inward current during hypoxia was observed using ramp depolarizations (Fig. 1 A). This current, was activated in the presence of 1 μM TTX, but was inhibited by 200 μM Cd^{2+}, suggesting it was carried by Ca^{2+} channels. To date I have studied this effect in both populations of GPN neurons (Fig. 1 B), and these data suggest that hypoxia causes an augmentation of Ca^{2+} currents in these cells. The data are preliminary since Ca^{2+} currents were not adequately clamped in these experiments. In other cell types hypoxia has been shown to modulate Ca^{2+} currents causing both inhibition, as in the case of cardiac L-type (Fearon *et al.* 1999; 2000a,b) and T-type Ca^{2+} channels (Fearon *et al.* 2000c; reviewed by López-Barneo *et al.* 2001), or augmentation as observed in L-type Ca^{2+} channels in the rabbit carotid body type I cells (Summers *et al.* 1999; 2000). The latter seemed to required CO_2/HCO_3-buffered solutions since Montoro *et al.* (1996) observed a voltage-dependent inhibition of Ca^{2+} currents in the same rabbit carotid body preparation in Hepes-buffered solutions. In GPN neurons, the hypoxic inhibition of leak K^+ currents together with hypoxic activation of the Ca^{2+} current (proposed here) would be a powerful physiological mechanism for increasing intracellular Ca^{2+} and activating intracellular NOS, leading to NO synthesis during hypoxia. This would further allow NO synthesis

and release from GPN neurons to carry out its inhibitory effect on carotid body function during hypoxia.

Figure 1. Evidence for hypoxic augmentation of Ca^{2+} currents. A, Representative current traces elicited by ramp voltages from -60 to 0 mV. Note that hypoxia caused an increase in inward current (around ~ -25 mV) in the presence of 1 μM TTX, and this effect was abolished by adding 200 μM Cd^{2+}. B, Mean (± s.e.m.) current density for both populations of GPN neurons. Hypoxia caused a significant increase in the presumptive inward Ca^{2+} current. This point requires confirmation, however, since the Ca^{2+} current was not properly clamped in these experiments.

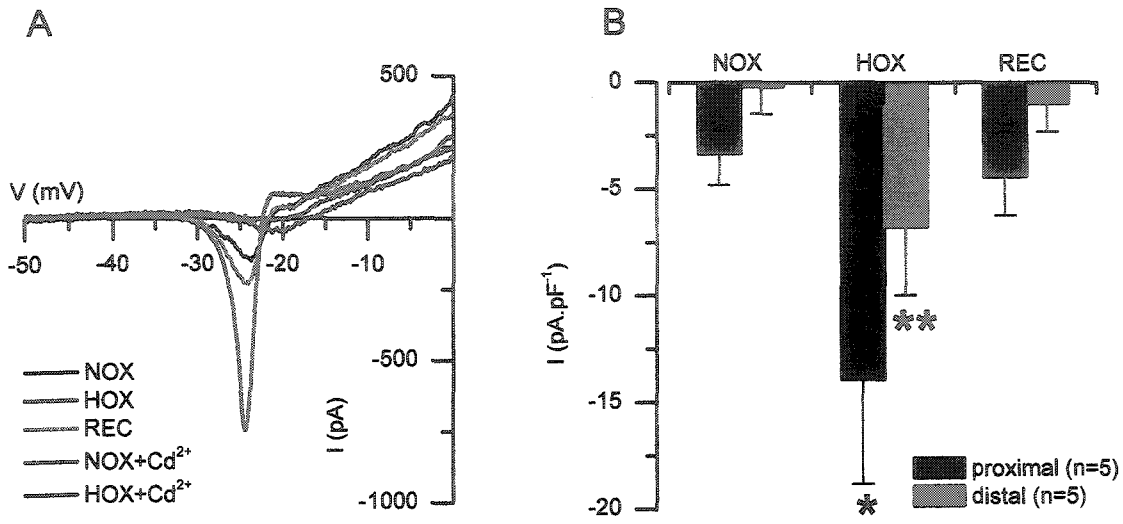
A
500
V (mV)
-50
-40
-30
-20
-10
-500
I (pA)
-1000
NOX
HOX
REC
NOX+Cd2+
HOX+Cd2+
B
NOX
HOX
REC
0
-5
-10
-15
-20
I (pA.pF-1)
**
*
proximal (n=5)
distal (n=5)